

**École polytechnique de Louvain**

# **Formation of high resolution images via Synthetic Aperture Radar embedded on satellite**

with Aerospacelab

Author: **Cyril WAIN**

Supervisor: **Luc VANDENDORPE**

Readers: **Christophe CRAEYE, Thomas FEUILLEN, Sumit KARKI**

Academic year 2019–2020

Master [120] in Electrical Engineering

# Acknowledgements

This work would probably never have been possible without the support and advice of many people.

First of all, my supervisor Prof. Luc Vandendorpe for his recommendations, his interest in my research, his guidance throughout the academic year but also for all his courses which I followed with attention and which motivated me to pursue in the field.

Then Mr. Thomas Feuillen for his numerous advices, his high availability, his huge support as well as his very good knowledge of the topic which allowed me to answer a good number of questions.

I would also like to thank the company Aerospacelab for having proposed this topic and for having challenged me to think about the physical implementation of the theoretical model. Especially, I would like to thank Mr. Sumit Karki and Mr. Thomas Francois for their multiple displacements and the many fruitful discussions we have had during the year.

Also, many thanks to Prof. Christophe Craeye for dedicating time to read and assess this work.

More indirectly, I would like to thank the European Space Agency (ESA) for the development of the course "Echoes in space [1]" which allowed me to learn a lot about the field of Earth observation via Synthetic Aperture Radar (SAR).

Finally, I would like to thank in particular my family, who have been of unfailing support, who have always pushed me to persevere and without whom I would not have been able to complete these 5 years of studies. I conclude by thanking my friends for their precious support throughout my years of study.

# Abstract

Today, Earth observation systems have become the main source of information in the fight against global warming. Previously reserved for governmental agencies (due to the colossal amounts of money required), the development of these systems is starting to become accessible to private companies. Indeed, the emergence of small satellites such as CubeSats has greatly reduced the cost of development of such systems. In recent years it has therefore been possible to observe the emergence of new companies dedicated to the trade of Earth observation information.

One of the indispensable tools for Earth observation is the Synthetic Aperture Radar (SAR). This is an imaging radar that allows high-resolution images to be acquired through specific processing of the data received by the radar. This tool has many advantages, such as being able to carry out day and night observations or being independent of weather conditions (which is not the case with optical systems).

This master thesis describes the global functioning of SAR, but also studies, develops and comments different algorithms allowing the acquisition of high-resolution images (the model developed here allows to reach a resolution of 1m x 1m). In order to improve the comprehension of the system but also to validate certain hypotheses, a simulator of SAR data and the processing of these data have been implemented in Python. Finally, the physical characteristics required for the realization of the studied system are also discussed.

The aim of this work is therefore to help new companies such as Aerospacelab to acquire a good understanding of the functioning of SAR, to be aware of the physical specifications required to build such a tool and show the benefits of it. The idea is to encourage them to carry out further research on the topic and to develop such systems themselves in the future. Indeed, the deployment of SAR systems on small satellites is opening up new applications that are very useful in the fight against global warming.

# Contents

<b>Acknowledgements</b>	i
<b>Abstract</b>	ii
<b>Nomenclature</b>	ix
<b>1 Introduction</b>	1
<b>2 State of the art</b>	4
2.1 History of SAR . . . . .	4
2.2 Current SAR performances and specifications . . . . .	11
2.3 Future Missions . . . . .	13
<b>3 Fundamental knowledge</b>	15
3.1 What is RADAR? . . . . .	15
3.2 Electromagnetic waves . . . . .	16
3.2.1 Wavelength . . . . .	16
3.2.2 Frequency . . . . .	17
3.2.3 Propagation's speed . . . . .	17
3.2.4 Polarization . . . . .	17
3.2.5 Phase of the wave . . . . .	17
3.2.6 Coherence . . . . .	18
3.3 Electromagnetic spectrum . . . . .	18
3.4 Radar bands . . . . .	20
3.5 Radar equation . . . . .	24
3.6 Doppler effect . . . . .	27
3.7 Active remote sensing systems . . . . .	28
3.8 Radar detection and ranging . . . . .	29
3.9 Radar imaging . . . . .	30
3.10 Imaging geometry . . . . .	31
3.10.1 Geometry nomenclature . . . . .	31

3.11	Radar imaging effects . . . . .	33
3.11.1	Foreshortening . . . . .	33
3.11.2	Layover . . . . .	33
3.11.3	Radar shadowing . . . . .	34
3.12	Scattering mechanisms . . . . .	35
3.13	Real aperture radar . . . . .	36
3.13.1	Operation principle . . . . .	36
3.13.2	Azimuth resolution . . . . .	36
3.13.3	Range resolution . . . . .	37
3.14	Pulse compression . . . . .	38
3.14.1	How does it works? . . . . .	39
3.14.2	Increased range resolution . . . . .	40
<b>4</b>	<b>The Principle of SAR</b>	<b>41</b>
4.1	Synthetic Aperture Radar Imaging . . . . .	41
4.2	Geometry of SAR . . . . .	42
4.3	Increased Azimuth resolution . . . . .	43
4.4	Range resolution . . . . .	44
4.5	SAR modes . . . . .	45
4.6	Applications . . . . .	46
4.6.1	Polarimetry . . . . .	46
4.6.2	Interferometry . . . . .	48
4.6.3	Time series . . . . .	50
<b>5</b>	<b>Model Development</b>	<b>51</b>
5.1	Notations . . . . .	51
5.2	Geometrical description . . . . .	52
5.3	Signal model . . . . .	53
5.3.1	Transmitted signal . . . . .	53
5.3.2	Received signal . . . . .	54
5.4	RawData simulation . . . . .	57
5.4.1	Simulation-specific notations . . . . .	57
5.4.2	Simulation development . . . . .	57
5.4.3	Choice of parameters . . . . .	62
5.4.4	Results . . . . .	63

<b>6</b>	<b>Image processing algorithms</b>	<b>65</b>
6.1	Matched filter . . . . .	66
6.1.1	Results . . . . .	67
6.2	Image focusing . . . . .	69
6.2.1	Range Migration . . . . .	73
6.2.2	Results . . . . .	74
6.3	Validation and Comparison . . . . .	77
<b>7</b>	<b>Practical design</b>	<b>83</b>
7.1	Data size . . . . .	83
7.2	Number of operations . . . . .	84
7.3	Choice of physical parameters . . . . .	87
7.4	System limitations . . . . .	88
7.4.1	Optimal Frequency . . . . .	88
7.4.2	Pulse Repetition Frequency (PRF) . . . . .	89
7.4.3	Sampling frequency . . . . .	90
7.4.4	Extending Range . . . . .	91
<b>8</b>	<b>Conclusion</b>	<b>92</b>
8.1	Summary of contributions . . . . .	92
8.2	Further research directions . . . . .	93
	<b>Bibliography</b>	<b>95</b>

# List of Figures

3.1	Electromagnetic wave [24]	16
3.2	Electromagnetic spectrum [25]	18
3.3	Radar bands [28]	20
3.4	side-looking geometry [34]	31
3.5	Geometry nomenclature [35]	31
3.6	Range of a radar [1]	32
3.7	Foreshortening [36]	33
3.8	Layover [36]	33
3.9	Radar Shadowing [1]	34
3.10	Radar imaging effects (modified from [1])	34
3.11	Specular reflexion [1]	35
3.12	Surface scattering [1]	35
3.13	Double bounce [1]	35
3.14	Volume scattering [1]	35
3.15	Azimuth resolution [39]	36
3.16	Range resolution [39]	37
3.17	LFM pulse before and after application of Matched filter [41]	40
4.1	Doppler beam sharpening [42]	42
4.2	Geometry 3D of SAR [43]	42
4.3	Relative target speed	43
4.4	Doppler shift across the aperture (inspired from [44])	43
4.5	Increased Azimuth resolution via SAR [1]	44
4.6	Strimap mode [47]	45
4.7	ScanSAR mode [47]	45
4.8	Softlight mode [47]	45
4.9	Polarimetry modes (modified from [1])	47
4.10	Interferogram of a volcano [50]	49
4.11	Time series over a deforested area	50
5.1	System's geometry	52

---

## LIST OF FIGURES

5.2	Digital representation of the system geometry . . . . .	58
5.3	Digital representation of the system geometry boundaries . . . . .	59
5.4	Structure of the raw data . . . . .	61
5.5	Input and output of the Raw data simulation . . . . .	63
6.1	Trade-off between the algorithms (modified from [51]) . . . . .	65
6.2	Matched filter operation on an area made up of a single target. . . . .	67
6.3	Matched filter operation on an area made up of four targets . . . . .	68
6.4	Range Cell Migration effect (modified from [53] and [54]) . . . . .	73
6.5	Range Migration operation effect . . . . .	74
6.6	Image Focusing operation on an area made up of four targets . . . . .	75
6.7	Matched filter operation on an area made up of four targets with threshold . . . . .	75
6.8	Comparison of the result obtained with and without performing the Range Migration operation . . . . .	76
6.9	Area used for testing the resolution in the azimuth direction . . . . .	77
6.10	Area used for testing the resolution in the range direction . . . . .	77
6.11	Area recovered via Matched filtering operation (azimuth direction) .	78
6.12	Area recovered via Matched filtering operation (range direction) .	78
6.13	Area recovered via Image Focusing operation (azimuth direction) .	78
6.14	Area recovered via Image Focusing operation (range direction) . .	78
6.15	Area recovered via Matched filtering operation (azimuth direction) .	79
6.16	Area recovered via Matched filtering operation (range direction) .	79
6.17	Area recovered via Image Focusing operation (azimuth direction) .	80
6.18	Area recovered via Image Focusing operation (range direction) . .	80
6.19	Image Focusing test on a landscape (modified from [1]) . . . . .	81
6.20	Image Focusing test on a airplane graveyard (modified from [55]) .	82
7.1	Data size evolution for different areas . . . . .	84
7.2	Data size evolution for different resolutions . . . . .	85

# Nomenclature

## Chapter 2: State of the art

<i>ALOS</i>	Advanced Land Observing Satellite
<i>DEM</i>	Digital Elevation Model
<i>DLR</i>	German Aerospace Center
<i>ERS</i>	European Remote Sensing
<i>ESA</i>	European Space Agency
<i>GMES</i>	Global Monitoring for Environment and Security
<i>InSAR</i>	Interferometric Synthetic Aperture Radar
<i>JERS</i>	Japan Earth Resources Satellite
<i>NASA</i>	National Aeronautics and Space Administration
<i>NISAR</i>	NASA-ISRO Synthetic Aperture Radar
<i>RADAM</i>	Radar of the Amazon
<i>RAF</i>	Royal Air Force
<i>SAR</i>	Synthetic Aperture Radar
<i>SIR</i>	Shuttle Imaging Radar
<i>SRTM</i>	Shuttle Radar Topography Mission
<i>UN</i>	United Nations

## Chapter 3: Fundamental knowledge

<i>GPS</i>	Global Positioning System
------------	---------------------------

<i>GSM</i>	Global System for Mobile Communications
<i>HF</i>	High Frequency
<i>LFM</i>	Linear Frequency Modulation
<i>MEADS</i>	Medium Extended Air Defense System
<i>NATO</i>	North Atlantic Treaty Organization
<i>RADAR</i>	RAdio Detection And Ranging
<i>RAR</i>	Real Aperture Radar
<i>UHF</i>	Ultra High Frequency
<i>VHF</i>	Very High Frequency
<i>Wi – Fi</i>	Wireless Fidelity
<i>WSR</i>	Weather Surveillance Radar

#### **Chapter 4: Principle of SAR**

*D – InSAR* Differential Interferometric SAR

<i>HH</i>	Horizontally sent – Horizontally received
<i>HV</i>	Horizontally sent – Vertically received
<i>TOPS</i>	Terrain Observation with Progressive Scan
<i>VH</i>	Vertically sent – Horizontally received
<i>VV</i>	Vertically sent – Vertically received

# Chapter 1

## Introduction

Nowadays, global warming of the planet is an undisputed reality. It is simply the biggest environmental problem of our time. It has impacts on health, food production, safety, the economy and many other aspects of our lives. This global change is extremely complex: it is characterized by large-scale spatial changes over long periods of time. As a result, it is necessary to study the phenomena not on a regional but on a global scale (as an example poor air quality at a local level is not necessarily due to local conditions).

By using Earth observation techniques from space, it is possible to monitor global environmental variations. Indeed, space has the advantage of providing data with regular, uniform and global coverage. It also provides data that are reliable in terms of time and allows observation of remote regions that are generally undersampled by traditional methods. Therefore, Earth observation from space can provide scientists with images and maps of global change that could not be obtained using terrestrial technologies and is considered as the optimal tool in the fight against climate change [2, 3]. Here are a few examples of applications realized by space-based Earth observation systems:

- Identification of oil leaks in the Ocean.
- Monitoring the evolution of deforestation, biodiversity and wildlife.
- Studying the melting of ice by observing the evolution of glaciers.
- Managing natural resources such as energy, water and agriculture to prevent famines.
- Contributing to the fight against the spread of disease and other health risks.
- Managing the expansion of large cities to make urbanization more in tune with social, economic and ecological issues.

Earth observation systems are mainly divided into two categories: optical and radar systems. Each of these two types of sensors has its own advantages and disadvantages, and its own areas of application. Optical satellites are excellent for gathering information because of their very high resolution. However, optical sensors are highly dependent on lighting and weather conditions. Radar imaging systems, on the other hand, do not offer the same high resolution but have the advantage of being completely independent of lighting and weather conditions. In addition, it is still possible to obtain very good resolution via Synthetic Aperture Radar satellites which have higher resolution radar. SAR satellites can therefore ensure that observations are made every time a new visit is made, which makes it possible to accurately monitor and detect environmental changes. For this reason, SAR systems will generally be preferred to optical sensors for ground-based observations from space [4].

Until recently, the availability of SAR images was limited by the small number of SAR systems in orbit due to the significant costs associated with this infrastructure. Today, following the trends of Space 4.0, this situation is beginning to change. New companies such as Aerospacelab are starting to design smaller satellites allowing them to reduce costs, use state of the art technology and be able to replace them on a regular basis. It is now possible to imagine a constellation of small satellites allowing worldwide coverage and offering frequent revisions.

**Contribution:** The aim of this thesis is to introduce the operating principle of SAR systems to Aerospacelab and to study a system that can be implemented on a small satellite while still providing a fairly good resolution (1m x 1m). In this interest, a python simulator will be created allowing the generation and processing of data for a system whose specificities have been entered in the simulator. This will give a first idea of the results that could be obtained by such a system and what requirements this system will have to satisfy.

In this master thesis, **chapter 2** will review the events and discoveries that have contributed to the development of Synthetic Aperture Radars. Then, the current and future performances of SAR will be discussed in order to be able to evaluate the performances that will be obtained by the system studied during the course of the thesis.

Then, in **chapter 3**, all the knowledge necessary for a good understanding of this thesis will be established. The electromagnetic spectrum, the principle of active remote sensing systems, radar imagery, scattering phenomena, etc. will be described. This chapter will finally discuss the limits of a classical radar system (Real Aperture radar).

**Chapter 4** will introduce the principle of Synthetic Aperture Radar. It will explain how this system improves resolution. The geometry of the system will also be reviewed and illustrated. The principle of polarimetry, interferometry and times series will be covered in order to show the wide range of applications that can be realized by SAR systems.

The development of the mathematical model will be discussed in **Chapter 5**. Expressions of the transmitted and received signals will be presented and will then be used to design a python simulator to generate SAR data.

**Chapter 6** will discuss the processing of the data received by the satellite. Two main algorithms will be studied: Matched Filtering and Image Focusing. These two algorithms will be implemented in python and will be applied to the data generated in the previous chapter. It will then be possible to compare the different results obtained and draw conclusions.

Finally, the performances and specificities (memory space and computing power) of the studied system will be discussed in **chapter 7**. From these conclusions it will be possible to investigate the limits of the system.

# Chapter 2

## State of the art

### 2.1 History of SAR

Radar satellite remote sensing has a long and prosperous tradition on an international scale. Starting with SeaSat in the late 1970s, numerous missions contributed to a vast range of data, improving environmental and Earth system sciences. Since the 1990s and 2000s, very successful satellite missions were launched and provided large amounts of data to scientists, commercial users and public authorities. In this section, we are going to discover the various discoveries and missions that have played a major role in the history of radar satellite remote sensing.

#### First airborne mapping radar (1943)

Until 1940, all the radar systems were ground-based. This is partly a consequence of the fact that large amounts of power were required but, also, because large antennas were needed. This meant that they were transmitting very long wavelengths (about many tens of metres). The next advance was then how do you get one of these radar systems onto an aircraft? Indeed, at that time, if you had an antenna larger than about 1.5 metres, it would not have been possible to fit it onto the aircraft. In order to respond to this issue, it was therefore necessary to develop a system making it possible to create signals of shorter wavelengths and being less costly in terms of energy.

This system was invented by the British in 1940 and is called the cavity magnetron. This was the first system that was capable of generating short wavelengths (about 10 centimetres wavelengths) in a consistent high-energy fashion. This therefore allowed the installation of radar systems on aircraft. As a consequence of that, the first airborne radar system was born.

The British built such a system (called radar H2S) and decided to equip their bomber with it in order to provide them with a ground mapping for navigation and night bombing. On January 30, 1943, H2S radar was used for the first time by RAF bombers and became the first ground mapping radar to be used operationally. Later versions of H2S reduced the wavelength, first to 3 cm and then 1.5 cm at which wavelength the system was capable of detecting rain clouds [1].

Therefore, unfortunately, we can notice that it is impossible to detach the evolution of radar remote sensing from a story that involves military instrumentation and development. Mostly in secret and largely used in the context of wartime.

### **First civilian airborne mapping (1967)**

Some of the earliest broad-scale applications of radar remote sensing occurred in regions where persistent cloud cover limits the acquisition of imagery in the optical portion of the spectrum. The first such large-scale civilian application of airborne imaging radar was performed in 1967. It has resulted in images used to produce a mosaic of a  $20,000 \text{ km}^2$  ground area of the Darien Province in Panama. This region had never been photographed or mapped in its entirety before because of persistent (almost perpetual) cloud cover and inaccessible tropical forest. The success of this project led to the application of radar remote sensing throughout the world [5].

### **RADAM (1971)**

In 1971, a  $500,000 \text{ km}^2$  survey of Venezuela was carried out. This project resulted in improved border definitions with its neighbouring countries. It also permitted a systematic inventory and mapping of the country's water resources, including the discovery of the previously unknown source of several major rivers.

In the same year, Project Radam (Radar of the Amazon) was begun. This project consisted of a reconnaissance survey of the Amazon and the adjacent Brazilian northeast. This proved to be a huge mapping project of  $8,500,000 \text{ km}^2$ . At that time, it was the largest radar mapping project ever undertaken. It was used for geological analysis, timber inventory, transportation route location and mineral exploration, as well as a number of other applications. Such information is essential to planning sustainable development in such ecologically sensitive areas [5].

## First satellite radar (1978)

Radar in space didn't happen until the 1970s. In 1973, the Skylab mission was launched. This station was equipped with a small radio altimeter that was used to demonstrate that you could use radar systems in space, but it wasn't an imaging system.

Indeed, the first imaging system in space as well as the first civilian spaceborne imaging synthetic aperture radar was the Seasat satellite launched in June 1978. Seasat flew a microwave altimeter and a multi-beam scatterometer (L-band system) and, as its name suggests, was optimised for looking at the ocean surface.

Even though the system failed after about four months due to a technical issue, the SeaSat instrument clearly defined a niche role for active microwave instruments in studying the ocean at a range of scales. During its brief 110-day lifetime, SeaSat collected more information about the oceans than had been acquired in the previous 100 years of shipboard research. It established satellite oceanography and proved the viability of imaging radar for studying our planet. SeaSat data also demonstrated that fish catches and ocean conditions are correlated, which has resulted in more efficient fishing [6].

Following its incredible success and the usefulness of the results, it has given birth to many satellites and remote sensing instruments on Earth (and other planets) that track changes in the oceans, land and ice. Real-time satellite data are now being provided to commercial users through the Fleet Numerical Oceanographic Center.

## Radar Shuttle Missions (1981)

The success of the SeaSat mission prompted the first flight of a side-looking SAR on the Shuttle. The Shuttle was seen as an opportunity to progressively develop and fly increasingly more complex radar systems for short missions, allowing the hardware to be returned to Earth for reuse on follow-on missions.

In 1981, the first shuttle imaging radar was flown in space. In the time frame of the early 1980s and early 1990s, NASA developed and launched a total of three SAR technology demonstration missions. They were designated as SIR missions which stand for Shuttle Imaging Radar. The first one was called SIR-A. It carried an L-band antenna. This mission was so successful that, in 1984, this L-band system returned to space in a shuttle mission, which was called SIR-B. Based on these two shuttle missions NASA developed the idea to deploy also a C-band antenna in the space shuttle payload bay. At the same time, the German Aerospace Center (DLR) wanted to develop an X-band synthetic aperture radar.

NASA and the Germans have therefore teamed up to also deploy an x-band antenna in order to have, for the first time, all three frequencies in space: X-band, C-band and L-band. It took 10 years to develop the system and the shuttle campaign called SIR-C/X-SAR, the third campaign, was flown in 1994. There were 2 missions, each lasted eleven days in April and October 1994 [7].

### A radar orbits Venus (1990 – 1994)

The concept of remote sensing radar is also of great interest in the exploration of planets. Indeed, the extreme conditions (dust storm, perpetual rain, opaque clouds of sulfuric acid, ...) present on some of them prevents the study of these planets by optical devices.

The Magellan probe to Venus becomes the first interplanetary synthetic aperture radar system. It orbited the planet and gradually built up a highly detailed image of the surface. The thick carbon dioxide atmosphere doesn't allow visible light to penetrate, so we can't observe the surface using the visible part of the spectrum. However, the atmosphere is transparent to the 13 cm radio waves used by the radar imager [8].

### ERS (1991 – 2000)

European Remote Sensing (ERS) satellite becomes the European Space Agency's first Earth-observing satellite and carries the first long-term satellite radar imager. The choice of C-band has been made because it's the best for ocean imaging. Indeed, in the 1980s, it was believed that the radar will be used only for oceanographic applications. However, after the launch of ERS-1, it became clear that land monitoring should be studied too. ERS-1 was developed to carry out a 3-year mission. So, in 1995, ESA launched ERS-2. But, in fact, ERS-1 has been used for during one decade [9].

Then, during a time, ESA had 2 systems in space. It was then thought that it was a good idea to use these two systems to perform interferometric applications. This would allow measuring small ground displacements from space. Indeed, in 1993, Didier Massonnet, with co-authors Rossi, Carmona and Adragna demonstrate that you can do interferometry with spaceborne radars. This concept was proven for the first time during the last three days of the October 1994 SIR-C/X-SAR mission. They then used ERS radar to measure the displacement of the Earth's surface caused by the Landers earthquake in California. ERS satellites were therefore the first satellites to perform interferometry.

## Shuttle Radar Topography Mission (2000)

The tremendous success of the first three space shuttle missions (carrying radar antennas in their payload bay) SIR-A, SIR-B, SIR-C/X-SAR led to the idea to fly an interferometric space shuttle mission. The concept had already been tested during the last three days of the October 1994 SIR-C/X-SAR mission. When, during three repetitive days, controlled repeat orbits were flown off.

SRTM (Shuttle Radar Topography Mission) was a joint NASA-DLR research effort that flew a single pass radar interferometric imaging system. The SRTM mission was in fact the first fixed baseline single-pass spaceborne InSAR technology system with wide-swath ScanSAR and dual frequency (C-band and X-band) coverage as well as with dual-polarisation capability. The mission objective was to obtain single-pass interferometric SAR imagery to be used for DEM (Digital Elevation Model).

It took 6 years until February 2000, when the shuttle radar topography mission took place. After only eleven days, the whole planet was topographically mapped until 60° north and south (representing nearly 80% of the land masses) which was the most norther orbit that the space shuttle could reach. SRTM proved that radar remote sensing is capable, operationally, to map the Earth's topography in a very high geometric resolution [10].

## TanDEM-X (2010 – 2014)

Following the incredible success of the mission SRTM (in which the German Aerospace Center participated through the development of the X-band antenna), it was decided by the German government to support the development of two X-band satellites that would fly in parallel to acquire X-band interferometric datasets.

In June 2007, TerraSAR-X, a high resolution (3m) imaging radar operating at X-band, was launched. In June 2010, an identical satellite was also launched and subsequently flew in “tandem” with the first satellite. This close formation orbit (the satellites get as close as 150m) allows for single-pass radar interferometry. This will ultimately provide a high-resolution vertical surface model of the entire land surface of the world, with a horizontal posting of 12m and a vertical accuracy of 2m, far outperforming the SRTM data in both resolution and coverage [11].

## Sentinel 1 (2014)

Based on the great success of the C-band radar satellite in the 1990s with ERS-1 and ERS-2, it was decided by ESA to launch further C-band radar satellites. In the same time, ESA participated in the development of the Copernicus program (which is coordinated and managed by the European Commission) aimed at developing European information services based on satellite Earth Observation and in situ (non-space) data. Copernicus's goal is then to provide vast amounts of global data in order to help service providers, public authorities and other international organisations to improve the quality of life for the citizens of Europe. The information services provided are freely and openly accessible to its users.

As part of the Copernicus program, ESA has therefore developed new satellites. These are called Sentinels. The first one, Sentinel-1, was launched in 2014 followed by Sentinel-1b which was launched in 2016. They both share the same orbital plane with a 180° orbital phasing difference. This allows the mission to provide an independent operational capability for continuous radar mapping of the Earth with enhanced revisit frequency, coverage, timeliness and reliability for operational services and applications requiring long-time series. These 2 sentinels represent then a big shift in the paradigm of using space-spaced radar systems. They are acquired in an unprecedented geometric resolution and thanks to these 2 satellites in space ESA have a global coverage every 5 to 6 days [12].

Therefore, the Sentinel's mission ensures continuity of C-band SAR data to applications in maintaining key instrument characteristics such as stability and accurate well-calibrated data products. This mission allowed to enable the development of new applications and met the evolving needs of GMES, such as in the area of climate change and associated monitoring.

## ICEYE-X1 and Capella-Denalu (2018)

As it can be noted, prior to 2014, the majority of SAR missions were primarily government projects and were not that widespread. One reason for this is the extremely high cost of such missions. At that time, the use and development of SAR applications was therefore limited by the scarcity of SAR imagery [13].

However, in recent years, the development of small satellites called CubeSats has revolutionised the field of space but also of Earth observation. Indeed, unlike large satellites, they offer major advantages in terms of development costs and development time. Moreover, due to their small size, it is possible to launch several of them in a single rocket launch. It is consequently possible to imagine large constellations of small satellites in order to greatly improve the speed of revisit, which would make it possible to detect changes with better temporal resolution. In summary, these small satellites make it possible to combine the temporal resolution of GEO satellites with the spatial resolution of LEO missions. All of these advantages have made the commercial solution feasible. Independent companies such as Capella or ICEYE have started to trade Earth observation information and thus to develop small SAR satellites [14, 15].

On 12 January 2018, ICEYE sent its first model, the ICEYE-X1, into space. It is the first commercial satellite and also the first satellite weighing less than 100kg to carry a SAR. ICEYE sent a second satellite, ICEYE-X2, on 3 December 2018. In the same launcher were 64 small satellites including DENALI, the first small satellite of the Capella company (Denali was the first small US satellite radar). In spite of their small size, these satellites allow to obtain a very good resolution of  $1m \times 1m$ . The future objective of these two companies is to build their own constellation and thus provide revisits almost every hour. There is no doubt that this new type of satellite will revolutionize the SAR field and lead to the emergence of new applications (e.g. road traffic monitoring) [16, 17].

## 2.2 Current SAR performances and specifications

Before developing a new system, it is important to find out about the performances and specifications of current SAR systems. In order to have a global view, in this section, it will be possible to observe the characteristics of a large satellite corresponding to a government mission but also the characteristics of a small satellite built by a private company. Since this Master thesis focuses mainly on the Stripmap mode (see section 4.5) only the specifications associated with this mode will be provided.

Regarding the large satellite, the choice has been made on the Sentinel-1. This choice can be explained by the fact that, today, it is one of the satellites whose data are the most used. This is partly a consequence of the wide availability of data collected under the Copernicus Program. Moreover, this satellite continues to prove its performance and reliability since its deployment in 2014. The specifications of this satellite can be consulted at the Table 2.1.

Parameters	Stripmap value
Altitude of the satellite	693 km
Resolution	5m × 5m
Swath length	80 km
Swath width	80 km
Radar band	C
Polarization	VV, HH, HV, VH
Carrier frequency of the pulse	8.18 GHz
BandWidth of the pulse	100-300 MHz
Physical antenna size	12.3m × 0.82m
Angular spread in the azimuth direction	0.23°
Spacecraft weight	2200 kg
Spacecraft dimensions	3.4m × 1.3m × 1.3m
Look angle of the radar	30°
Period of pulse sampling	3.33 ns
Pulse Repetition Frequency	1-3 KHz
Pulse width	5-100 μs
Orbit repeat cycle	12 days
Downlink X-band	520 Mbits/s
RF peak power	4100 W

Table 2.1: Sentinel-1 specifications [18]

Concerning the small satellite, preference was given to the ICEYE-X2. At present it is one of the only small satellites in operation that achieves such good resolution as large satellites and it is considered to be the future of SAR instruments. The specifications of this satellite can be seen at the Table 2.2.

Parameters	Stripmap value
Altitude of the satellite	570 km
Resolution	3m × 3m
Swath length	50 km
Swath width	30 km
Radar band	X
Polarization	VV
Carrier frequency of the pulse	9.65 GHz
BandWidth of the pulse	100-300 MHz
Physical antenna size	3.2m × 0.4m
Angular spread in the azimuth direction	0.44°
Spacecraft weight	85 kg
Spacecraft dimensions	0.5m × 0.6m × 0.8m
Look angle of the radar	30°
Period of pulse sampling	?
Pulse Repetition Frequency	4-6 KHz
Pulse width	?
Orbit repeat cycle	18 days
Downlink X-band	140 Mbits/s
RF peak power	4000 W

Table 2.2: ICEYE-X2 specifications [19]

As explained, the performance shown is for Stripmap mode. However it is important to note that in Spotlight mode (see section 4.5) the ICEYE-X2 is able to reach a resolution of 0.5m which is impressive for a satellite of this size. Unfortunately the author has not been able to find any information about the period of pulse sampling  $T_s$  and the pulse width  $T_c$  of this model.

All of these data will allow the comparison of the specifications obtained for the system developed during this master thesis with real instruments that are currently operational and that provide excellent results. Hence, this will give an idea of the feasibility and consistency of the parameters obtained for the developed system.

## 2.3 Future Missions

Already in the pipeline, there is a very exciting earth exploration designed by ESA, it's called Biomass. This is a P-band system (70 cm wavelength). It is specifically design to map the above-ground carbon stored in the tropical forests for which high wavelength is needed to penetrate the forest canopy. The Earth Explorer Biomass will provide global maps of the amount of carbon stored in the world's forests and how this changes over time, mainly through absorbing carbon dioxide, which is released from burning fossil fuels.

Biomass will also provide essential support to UN treaties on the reduction of emissions from deforestation and forest degradation. Forest type and forest cover worldwide can be detected by today's satellites, but Biomass will take the information to the next level. Due for launch in 2021, the satellite will carry the first P-band synthetic aperture radar, able to deliver accurate maps of tropical, temperate and boreal forest biomass. The global mass of trees is not obtainable by ground measurement techniques. Observations from this new mission will also lead to better insight into rates of habitat loss and, therefore, the effect this may have on biodiversity in the forest environment. Now, looking at the European Copernicus program, they have already decided for the upcoming decades to continue their series of sentinels. So already in the planning are Sentinel-1c and Sentinel-1d.

Due to the great success of TerraSar-x and Tandem-x mission which is the state of the art, the best interferometric system flying in space, the German Aerospace Center is being interested in continuing this successful twin mission with another frequency. It will be an L-band system, the project is therefore called Tandem-L. To ensure regular observations with short repeat intervals, Tandem-L will employ cutting-edge radar technology based on the latest digital beamforming techniques which allow for the mapping of ultra-wide image swaths with high azimuth resolution. The goal of Tandem-L will be to interferometrically map large parts of the Earth's landmass up to two times per week. Tandem-L will allow a large number of applications such as the systematic monitoring of deformations of the Earth's surface on a millimeter scale for the investigation of earthquakes and risk analysis, the quantification of glacier motion and melting processes in the polar regions, the fine scale measurement of variations in the near-surface soil moisture as well as observations of the dynamics of ocean surfaces and ice drift [1].

We can ask ourselves, what happened to NASA ? It can be observed that there is a long gap since February 2000 when the SRTM was flying. The emphasise of NASA has rather changed to multi-sensor systems based on optical system and atmospheric remote sensing. But, today, NASA is back on track.

They plan to launch in the near future a NASA L-band system called NISAR which will work in combination with the Japanese ALOS. Indeed, the Japanese also have great experience in the field. They started with an L-band system called JERS-1 in the 1990s and then continued these L-band time series with ALOS-1 and ALOS-2 (2006 and 2014 respectively) [1].

Many countries have also decided to embark on the SAR adventure such as India, China, Argentina and many others which are now in the process of launching radar satellites. In addition to countries and government agencies, there is also the emergence of private companies such as ICEYE and Capella. As a reminder, these companies are building smaller satellites, allowing a great reduction in costs and an increase in the rate of development. These smaller satellites thus always carry the most recent technologies and can easily be replaced. Over the next few years, these companies wish to achieve a constellation of 18 and 36 satellites respectively. With such constellations the revisit rates will decrease until approaching 6 hours at the end of 2020 [20, 21].

This growing establishment of spaceborne sensors, with different characteristics such as the frequency band, will increase the potential of radar remote sensing to contribute to many scientific endeavours. In the future many follow-on missions will guarantee a continuous flow of global data coverage and even an increase in the variety of wavelengths, which will provide us greater information content.

# Chapter 3

## Fundamental knowledge

The previous chapter showed the growing interest in radars during these last decades; interest which comes mainly from the latter's ability to overcome the shortcomings of optical remote sensing systems and complement the information collected by such systems.

During this chapter, it will first be explained what is really hidden behind the word radar. This will help to understand how it can provide information that would be impossible to obtain with optical systems. In addition, the operating principle of systems similar to those encountered in the previous chapter will be described in detail.

### 3.1 What is RADAR?

The acronym Radar stands for **R**Adio **D**etection **A**nd **R**anging. It describes a system which illuminates a portion of space with an electromagnetic wave and receives the waves reflected by the objects therein, which makes it possible to detect their existence and to determine certain of their characteristics. These characteristics are manifold: it can be the horizontal position of objects, their altitude, their speed and sometimes their shape. The determination of this data allows the radar to inform the user, but also to eliminate a large number of unwanted objects in order to keep only the interesting "targets" [22].

In order to fully understand the operation of a radar, it is therefore imperative to know what an electromagnetic wave is and to understand how it interacts with its environment.

## 3.2 Electromagnetic waves

The electromagnetic wave is a model used to represent electromagnetic radiation. It is important to clearly distinguish electromagnetic radiation, which is the phenomenon studied, and the electromagnetic wave, which is one of the representations of the phenomenon. Another quantum (or corpuscular) representation takes into account the existence of the photon (small lump of energy) [23].

This is the Scottish scientist James Clerk Maxwell, who in the 1860s and 1870s, developed a scientific theory (validated experimentally a few years later by Henri Hertz) to explain electromagnetic waves. He noticed that electrical fields and magnetic fields can couple together to form electromagnetic waves. He summarised this relationship between electricity and magnetism into what is now referred to as “Maxwell’s Equations”. According to these equations, a variation of the electric field creates a magnetic field (which varies over time) and a variation of the magnetic field creates an electric field (which also varies over time). As a result, unlike mechanical waves, electromagnetic waves do not require a medium to propagate, so they can propagate in vacuum. The electric and magnetic fields of the wave oscillate in directions perpendicular to each other and the direction of propagation of this wave is perpendicular to the plane formed by these 2 directions. The electromagnetic wave is therefore called a transverse wave.

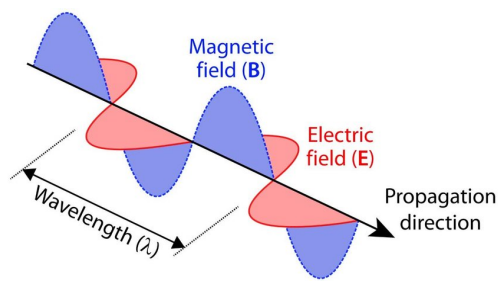


Figure 3.1: Electromagnetic wave [24]

In radar remote sensing, this radiation is often described with the help of the wave model. Indeed, it is very successful in describing and designing systems which aim at diffracting light into a spectrum for analysis. In order to fully understand the associated phenomena, we have to familiarize ourselves with the key vocabulary that is used to describe electromagnetic waves.

### 3.2.1 Wavelength

The waves have crests and troughs similar to those of ocean waves. The distance between crests is the wavelength. The wavelength is thus the spatial dimension over which it repeats itself. The shortest wavelengths are just fractions of the size of an atom, while the longest wavelengths scientists currently study can be larger than the diameter of our planet!

### 3.2.2 Frequency

The number of these crests that pass a given point within one second is described as the frequency of the wave. One wave or cycle per second is called a Hertz (Hz).

### 3.2.3 Propagation's speed

The propagation speed is identical for all electromagnetic waves and is therefore equal to the speed of light (because light is an electromagnetic wave), that is to say an approximate speed of  $3 \cdot 10^8$  [m/s]. This speed varies slightly depending on the medium in which the wave propagates, but in general this variation is so small that it is neglected and we consider this speed as constant. In radar imaging context, this approximation is quite suitable so we don't have to worry too much about that small change in velocities through the atmosphere. However, in some cases as for altimeters, because you are trying to measure distances of a few centimetres, you have to take into account the change in the velocity.

There exists a relation connecting these first three quantities which is valid for any electromagnetic wave:

$$c = f \cdot \lambda \quad (3.1)$$

where  $c$  is the speed of light,  $f$  and  $\lambda$  are respectively the frequency and the wavelength of the considered wave.

### 3.2.4 Polarization

Another property of electromagnetic radiation is, because it is a transverse oscillation, that it has polarisation. Polarisation is a measurement of the electromagnetic field's alignment. In the figure above, the electric field (in red) is vertically polarised. Think of throwing a Frisbee at a picket fence. In one orientation it will pass through, in another it will be rejected. This is similar to how sunglasses are able to eliminate glare by absorbing the polarised portion of the light. In terms of polarisation, it can become more complex because the wave can actually do a spiral like a corkscrew and then we talk about circular polarisation.

### 3.2.5 Phase of the wave

One other key property of electromagnetic waves is the ability to describe the cycle that the wave is in, so at what point in the cycle is this wave. The wavelength, the frequency, the speed, the polarisation may all be identical but the location of where the peaks and the troughs are may be slightly different. That property is

called the phase of the wave. The measurement of the phase difference between 2 waves is a key property that can be measured in a radar system.

### 3.2.6 Coherence

Another important feature of electromagnetic waves is what is called the coherence. Coherence is a property of two waves that allows them to combine together. The peaks and troughs might actually cancel each other out or multiple peaks might add together to make a bigger wave. Typically, this only happens when you have waves that are of exactly the same wavelength and frequency. In a radar system, that is fine because the system is transmitting his own waves and it can fix it to a particular frequency or wavelength. Then, we can be quite confident that the waves will be coherent, and they will combine together in constructive or destructive ways. The coherence of a wave is really important for when we look at the construction of a synthetic aperture radar and also when we look at radar interferometry.

## 3.3 Electromagnetic spectrum

Across the electromagnetic spectrum, there are typically labels that are given to each of the bands in order to take into account the different physical properties of the waves that compose them.

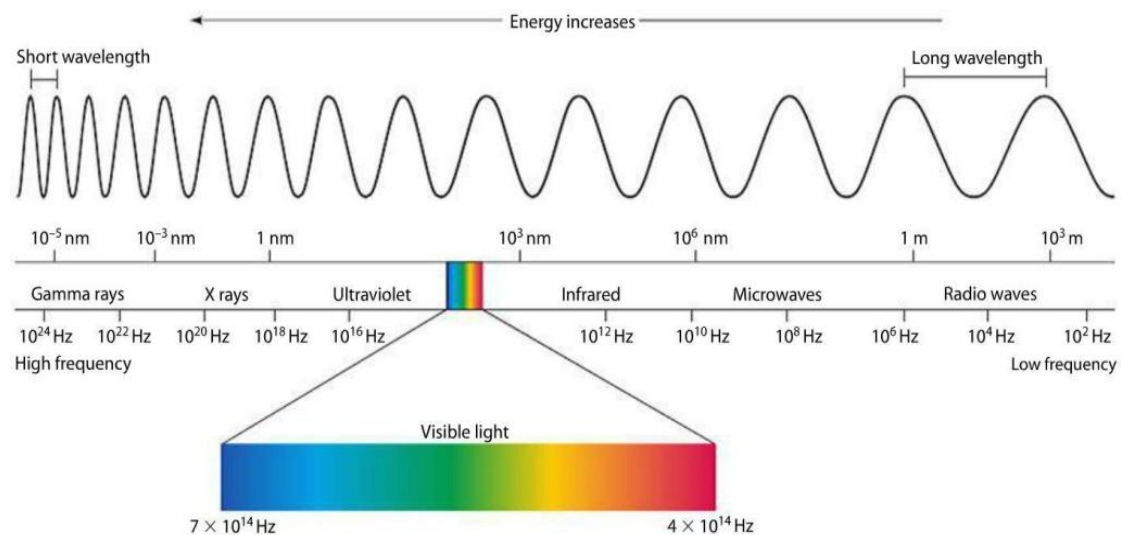


Figure 3.2: Electromagnetic spectrum [25]

## CHAPTER 3. FUNDAMENTAL KNOWLEDGE

---

The one that most of the people are familiar with is the visible part of the spectrum. That is the part of the spectrum that our eyes are more sensitive to. This is the region of hundreds of nanometres in terms of wavelength. It is also where the sun peeks in its emitted radiation. So, the sun peaks in the hundreds of nanometres and our eyes are sensitive to that and that kind of makes sense that human has developed eyes that are sensitive to where most of the radiation is to see.

Beyond the blue end, one get into the ultraviolet, we heard of ultraviolet radiation largely in the context of getting a suntan or getting sunburned and with too much exposure potentially skin cancer and that is because the ultraviolet electromagnetic radiation is got much more energy. Beyond that, one get into the X-rays and ultimately the gamma rays where we are going to shorter wavelengths, higher frequencies and greater energy in those waves. As a result, because of that increased energy, they typically are more dangerous to human beings. Indeed, these waves are “ionising,” meaning these that they have such a high energy that they can knock electrons out of atoms. Exposure to these high-energy waves can alter atoms and molecules and cause damage to cells in organic matter. These changes to cells can sometimes be helpful, as when radiation is used to kill cancer cells.

If we go to the visible part of the spectrum and go beyond the red part, we get into the near-infrared part. On earth and in earth observation, the radiation belonging to this part, is mostly coming in from the sun. Then, if we go to longer wavelengths, in the range of two microns, we are looking at admitted radiation from the earth’s surface. Indeed, surfaces which have a physical temperature on the region of 300 Kelvin are emitting radiation in this range. This can be picked up with thermal imaging cameras or sensors on satellites optimised for looking at thermal wave bands. If we go to even longer wavelengths, we come to a part of the electromagnetic spectrum which is into the millimetre wavelengths. In this region of the spectrum, water vapour actually absorbs so much of the radiation that it has limited use for applications in the field of earth observation.

When we go to even longer wavelengths, so in the range of centimetre wavelength, we are into the microwave part of the spectrum. From here, it starts to be possible of seeing through the atmosphere and even more, seeing through clouds. That is because the water droplets that make up clouds are a lot smaller than the centimetre size wavelengths of the microwaves. As you get to longer microwaves, wavelengths are about 20-25 centimetres and it is what our mobiles and GPS systems are using.

Going even farther, we are getting into the domain of the radio part of the electromagnetic spectrum. It is long wavelengths that can travel a greater distance and it is mostly for this reason that they are used in the context of radio communications (hence the name...).

Following the scientific convention, radio and microwaves are usually described in terms of frequency [Hertz], infrared and visible light in terms of wavelengths [meters], and X-rays and gamma rays in terms of energy [electron volts]. This goal of this convention is to allow the convenient use of units that have numbers that are neither too large nor too small.

Finally, the civil and military frequency bands are allocated internationally within the World Radiocommunication Conference with the participation of international organisations such as NATO. However, within a country, sovereign institutions can take over frequency bands for the exclusive use of the military or police forces. However, these institutions are under increasing pressure from industrialists to the extent that the new civil technologies (GSM, Wi-Fi, etc.) have an increasing spectral occupation, but offering a very large financial profit. It is therefore time for cooperation between the various players and for cohabitation (not always very successful) so as to limit interference between the different applications. The most suitable frequency from an application point of view is therefore not always available and it is often necessary to find a compromise [26].

### 3.4 Radar bands

Radar systems transmit electromagnetic waves that are in the range of the microwaves [5 Mhz – 130 Ghz]. It is this frequency band which is used since most objects reflect microwaves and then can be detected by a radar system performing in this band. The frequency of the microwaves used depends on the radar application [27].

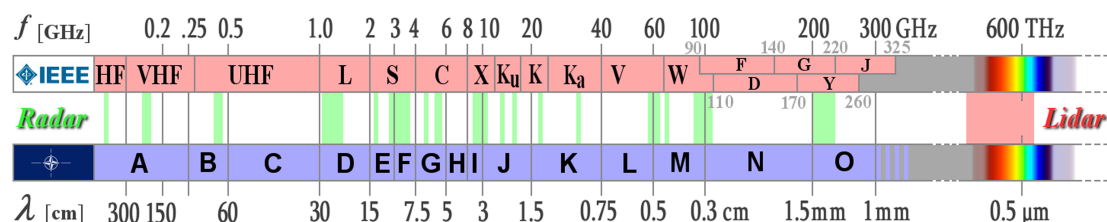


Figure 3.3: Radar bands [28]

The choice of frequency depends on the application requirements. Indeed, different frequency means different antenna size, range and resolution.

Regarding the minimum antenna size, it is proportional to the wavelength and then inversely proportional to the frequency. Airborne applications are often limited in the size of antenna that can be used, which will dictate a higher frequency and lower wavelength choice.

The ability of the radar to focus the radiated and received energy in a narrow region is also dependent on both antenna size and frequency choice; a larger antenna allow the beam to be more tightly focused. Therefore, a higher frequency also allows the beam to be more tightly focused, for a given antenna size.

Another consideration is the range of the radar system which is also influenced by the choice of frequency. Higher frequency systems are usually of lower power due to electronic circuit limitations and experience greater atmospheric attenuation (due to their shorter wavelength). The ambient electrical noise that can odd operation of analog circuitry also becomes more pronounced at higher frequencies. Most of the radar signal absorption and scattering is due to oxygen and water vapour. Water vapour, in particular, has high absorption in the “K” band. When this was discovered, the band was divided into Ka, for “above” and Ku for “under,” the frequencies where radar operation is limited due to water vapour absorption. At higher frequencies in portions of the millimetre band, oxygen causes similar attenuation through absorption and scattering.

It is also necessary to know the generic size of what one wishes to observe since only the objects whose typical size is at least of the order of magnitude of the wavelength are visible by the radar.

Finally, the radar operating frequency also has an effect on Doppler frequency measurements. Indeed, the Doppler frequency shifts are proportional to both the relative velocity and the radar frequency [29].

Radar systems are then generally designated by the wavelength or frequency band in which they operate. This makes it possible to quickly understand for what type of application the radar has been developed.

## A- and B- Band (HF- and VHF- Radar)

These bands correspond to frequencies below 300 MHz. These have been used for a very long time. They were the cutting edge of radio technology at the start of the Second World War. Today, they are mainly used for very distant surveillance radars which are called "transhorizon" radars. It is easier to obtain very high power at these low frequencies, and their attenuation is lower in the atmosphere. However, their resolution is lower than at higher frequencies and they require huge antennas to obtain a beam which can give a suitable angle and azimuth. These frequencies are also used in telecommunications. The bandwidth available for radars is therefore limited. They have been popular again since the advent of stealth planes, their shapes not affecting low frequencies as much [27].

## Band C (radar UHF)

Frequencies from 300 MHz to 1 GHz are used for the detection and tracking of satellites but also ballistic missiles over long trajectories. These radars therefore act as long-range surveillance and for the acquisition of fire data (e.g. MEADS extended medium-range air defence systems).

## Band D (band radar L)

These frequencies of 1 GHz to 2 GHz are preferred for radars of range up to 400 km. They can emit high power pulses with large bandwidth and compressed. Due to the curvature of the Earth, the maximum detection range is limited at low altitudes and targets close to the ground disappear under the radar horizon relatively quickly. In the area of air traffic management, long-range radars for air corridors use these frequencies. To remember their use in the classic nomenclature, it suffices to think that L band is for Large and Long range antenna.

## Bands E and F (band radar S)

The atmospheric attenuation of the E and F bands is slightly higher than in the previous band and radars using these frequencies must therefore have greater power to obtain an equivalent range. For example, the MPR radar, from its name in English Medium Power Radar, uses a pulse of 20 MWatts. Since precipitation is starting to be observed with these bands, it is used in weather radars, generally in tropical and subtropical regions. Indeed, the attenuation is relatively negligible even in the presence of high precipitation rates which allows us to see beyond the first storms. This is no longer true with the higher frequencies of weather radars used in more northerly latitudes. Special airport weather surveillance radars

operating in this band have a detection range which is generally around 100 km. However, S-band weather radars, like the US Meteorological Service's WSR – 88D, have a range of more than 250 km.

### **Band G (band radar C)**

These frequencies, located between 4 GHz and 8 GHz, are used by several mobile battlefield radars for aerial surveillance and fire control of short and medium range missiles. The resolution being proportional to the frequency for the same antenna diameter, this band makes it possible to obtain good resolution with a reduced antenna and easy to move. These frequencies are also used by weather radars in more northern regions, such as Canada and northern Europe, due to the much lower antenna and transmitter costs. Precipitation causes attenuation in these frequencies if their hourly rate is high. Strong thunderstorms therefore partially or totally block the view. However, this phenomenon can be offset by a denser network of radars with partially overlapping coverage areas and from different points of view.

### **Bands I and J (band radar X and Ku)**

These bands are between 8 GHz and 12 GHz and therefore require an even smaller antenna. This is the reason why they are so popular for systems requiring a light radar system and whose range is limited. However, due to their short wavelength, these waves are strongly attenuated by precipitation, even light. These bands are also common in civil and military maritime radars. They allow the use of small inexpensive antennas with an interesting range and good accuracy. Generally, these are slotted or plate waveguide antennas (patch antennas) which are protected by a radome. Finally, synthetic aperture radars (SAR) for civil and military cartography by plane or satellite most often use these frequencies.

### **Band K (radar K and Ka)**

In this band, the frequencies range from 18 GHz to 40 GHz, atmospheric absorption is therefore important and causes attenuation of the radar beam. This has the effect of limiting the distance resolution and range. K-band radars are therefore limited to the very short range of very high accuracy and a very fast scanning rate. Surface radars use very short pulses of a few nanoseconds at these frequencies. They can thus follow the movements of vehicles on the tarmac and airport runways, their resolution making it possible to visualise the silhouette of the vehicles.

## Band V

The frequencies are in the 40-75 GHz window, so the attenuation becomes critical. Even the water vapour in the air causes the signal to scatter. The range of radars using the V-band is therefore only two metres and is limited to motion detection.

## Band W

This band is located just before the border between microwaves and infrared, the frequencies there are between 75 GHz and 110 GHz. This frequency range has two modes. This is due to the strong attenuation caused by oxygen molecules ( $O_2$ ). Around 75 GHz, the attenuation is maximum, while at 96 GHz it is minimum. Recent radars used for parking, blind spot coverage and speed control in some luxury cars use a frequency of 75 GHz to 76 GHz. Oxygen attenuation immunises them from interference from other frequencies.

## 3.5 Radar equation

In most applications, the radar should be designed to meet specific performance requirements. These requirements include the maximum range, range resolution, maximum velocity, velocity resolution, covered field of view in the angular space, and many other additional demands. In order to know how to achieve these requirements, it is essential to introduce the *radar equation*. This reflects the influence of physical phenomena on the radiated power, the propagation of the wave, and up to the reception of the reflected signal. This *radar equation* is then used to estimate the performance of a radar system [30].

When high-frequency energy is radiated from an isotropic antenna, it propagates uniformly in all directions. Then, areas of equal power density form concentric spherical surfaces ( $A = 4\pi R^2$ ) around the antenna. As the radius of the sphere increases, the same amount of energy is scattered over a larger spherical surface. In other words, in a given direction, the power density decreases as the distance from the transmitter increases. The formula for calculating the power density  $S_t$  for an omnidirectional system is therefore as follows:

$$S_t = \frac{P_t}{4\pi R_0^2} \quad (3.2)$$

where  $P_t$  is the transmitted power [W] and  $R_0$  is the antenna-to-target distance [m].

If, for the same transmit power, the antenna only transmits over a portion of the sphere, then the power density increases in the direction of transmission. This characteristic is called antenna gain. This gain is a consequence of the concentration of the transmitted power in only one direction. The formula for calculating the power density  $S_g$  in the direction of maximum gain is given by:

$$S_g = S_t \cdot G \quad (3.3)$$

where  $G$  is the antenna gain [-].

The detection of a target does not depend solely on the power density at its position. It also depends on how much of the energy reflected from the target is returned in the direction of the radar's receiving antenna. In order to determine the value of this reflected power, it is necessary to know the radar cross-section  $\sigma$  of the target. This value, which is difficult to determine, depends on several parameters. First of all, it is logical to consider that the larger the area illuminated by the signal, the greater the reflected power. Then, beyond the size, the capacity of an object to reflect the waves depends on its shape, the composition of its surface and the nature of the materials used. This translates into the following example: an Airbus will be easily detectable, whereas it will be almost impossible to detect a stealth aircraft. When it reaches its target, the reflected power  $P_r$  is therefore expressed as follows:

$$P_r = \frac{P_t}{4\pi R_0^2} \cdot G \cdot \sigma \quad (3.4)$$

In a simplified way, we can consider the target as a transmitter of the reflected signal. The reflected power  $P_r$  can therefore be considered as if it were a power emitted by the target. Since the propagation conditions of the signal are identical on the outward and return paths, we can reuse the same development to determine the power density  $S_r$  reaching the location of the radar receiving antenna:

$$S_r = \frac{P_r}{4\pi R_1^2} = \frac{P_t \cdot G \cdot \sigma}{(4\pi)^2 R_0^2 R_1^2} \quad (3.5)$$

with  $R_1$  the distance between the target and the receiving antenna.

At the receiving antenna, the received power  $P_e$  is dependent on the power density  $S_r$  at the receiving site and the effective antenna aperture  $A_e$ . The effective antenna aperture arises from the fact that an antenna suffers from losses. Therefore, the received power at the antenna is not equal to the input power. Most of the time, the efficiency of the antenna  $K_a$  is around 0.6 to 0.7. Applied to the geometric antenna area  $A$ , the effective antenna aperture is equal to  $A \cdot K_a$ . As a consequence

of what the expression of the received power is the following:

$$P_e = S_r \cdot A e = \frac{P_r}{4\pi R_1^2} = \frac{P_t \cdot G \cdot \sigma \cdot A \cdot K_a}{(4\pi)^2 R_0^2 R_1^2} \quad (3.6)$$

If we consider the transmitting antenna and the receiving antenna as a single antenna ( $R_0 = R_1 = R$ ) and express the gain in terms of wavelength ( $G = \frac{4\pi A K_a}{\lambda^2}$ ), then the expression of the received power becomes:

$$P_e = \frac{P_t \cdot G^2 \cdot \sigma \cdot \lambda^2}{(4\pi)^3 R^4} \quad (3.7)$$

Solving for range R, we obtain the classic radar equation:

$$R = \sqrt[4]{\frac{P_t \cdot G^2 \cdot \sigma \cdot \lambda^2}{(4\pi)^3 P_e}} \quad (3.8)$$

Let  $P_{e,min}$  be the minimum necessary signal power for radar detection. Any signal of lower power cannot be detected because it is drowned out by the receiver noise. This minimum power signal  $P_{e,min}$  is therefore the signal that allows the radar to reach its maximum detection range  $R_{max}$ :

$$R_{max} = \sqrt[4]{\frac{P_t \cdot G^2 \cdot \sigma \cdot \lambda^2}{(4\pi)^3 P_{e,min}}} \quad (3.9)$$

It is important to note that when developing this radar equation, we considered ideal propagation conditions (without losses). However, in practice, propagation is affected by many losses that can considerably reduce the radar's effectiveness. The main ones are internal attenuations in the transmitter and receiver circuits, losses due to fluctuations of the equivalent surface and, of course, atmospheric losses encountered during the propagation of the electromagnetic wave. A loss factor L must therefore be added to the equation:

$$R_{max} = \sqrt[4]{\frac{P_t \cdot G^2 \cdot \sigma \cdot \lambda^2}{(4\pi)^3 P_{e,min} \cdot L}} \quad (3.10)$$

Finally, we realise that this equation makes it possible to quickly visualise the influence of the characteristics of a radar system on its detection range [31].

## 3.6 Doppler effect

Another important phenomenon concerning electromagnetic waves is that their echo may, in some cases, have a different frequency from that of the emitted wave. This variation occurs when the distance between the antenna and the target varies over time. This phenomenon is described by the *Doppler effect*.

In order to understand this phenomenon, we need to think of a wave emitted at a given frequency towards a moving observer, or vice versa. The wavelength of the signal is constant but if the observer gets closer to the source, he moves towards the successive wave fronts and thus perceives more waves per second than if he had remained stationary, thus an increase in frequency. In the same way, if the observer moves away from the source, the wave fronts will reach it with a delay that depends on the speed at which it moves away, thus a decrease in frequency. We speak of a shift towards blue for a nearer approach and towards red in the case of a farther away approach, referring to the light spectrum. The same applies to all ranges of electromagnetic waves including the waves used by radars. In mathematical terms, the variation in frequency  $f_D$  can be expressed by:

$$f_D = \frac{2V_r}{\lambda} \quad (3.11)$$

where  $V_r$  is the source-observer relative velocity [m/s] and  $\lambda$  is the wavelength [m].

The radial velocity component is used because the frequency variation is due to the relative displacement between the source and the observer. The tangential component of real velocity does not imply distance or approach and therefore cannot be perceived. Thus, a radar that probes the atmosphere can only perceive the radial component of its speed by the Doppler effect. To know its complete speed, its angular position between each sounding must be noted, which gives the tangential component.

$$f_D = \frac{2V \cdot \cos(\alpha)}{\lambda} \quad (3.12)$$

where  $V$  is the speed of the target and  $\alpha$  is the angle formed between the radar-target axis and the actual target motion axis.

It is important to note that the  $f_D$  measurement is relatively small compared to the wavelength for usual velocities measured by a radar. For a continuous-wave radar, the frequency difference can be made by mixing the transmitted and returned waves, which causes a beat that can be measured [32].

However, in the case of a pulse radar this is not possible. Indeed, the direct measurement of  $f_D$  is most of the time too weak to be measured by the instruments.

In this case, the phase difference between successive pulses is used because, if the target moves relative to the radar between two pulses, the wave will have to travel a longer path which will result in a phase difference  $\phi$ . The maximum phase shift that one can have between two identical waves is  $360^\circ$  before the two overlap again:

$$\phi = -\frac{2R \cdot 2\pi}{\lambda} \quad (3.13)$$

where  $R$  is the radar-to-target distance.

We know that the radial speed  $V_r$  is equivalent to  $\frac{d(R)}{dt}$  and that the phase shifter  $\phi$  is connected to  $f_D$  via  $f_D = \frac{1}{2\pi} \cdot \frac{d(\phi)}{dt}$ . Then we can express the Doppler frequency variation  $f_D$  as:

$$|f_D| = \frac{2V_r}{\lambda} = \frac{2V_r \cdot f_t}{c} \quad (3.14)$$

where  $f_t$  is the transmitted frequency and  $c$  is the speed of the light.

### 3.7 Active remote sensing systems

Radars are active remote sensing systems. Unlike passive systems, it means that we have control over the illumination of the target area. We can illustrate this difference by comparing the sense of hearing of humans to that of bats. Our ears are only used passively, we are just picking up the signals that come from around us and we are detecting that. And the quality of what we hear depends on the ambient noise of our environment. However, if we were a bat, we would actually transmit a signal from our mouth and we would actively listen for the echoes that come back. This is exactly what we do with a radar system, so we are actively transmitting our own signal and waiting for the echoes to come back. This is really useful because it gives us a complete control over the illumination of the target. It means that we can define the wavelength and frequency of the signal that we send out. We can also control the polarisation, so we can decide to transmit vertically polarised or horizontally polarised waves. That kind of control is really useful because the system is no longer relying on solar illumination from the Sun. It means that we can make measurements during the daytime and also during the night time. We are not dependent on the sunlight. We are just generating our own signal to illuminate the area.

A second advantage of active systems is that, since we can choose the frequency of the transmitted signal, we can characterise them so that they only see what we want. We can therefore, for example, opt for a signal whose wavelength is much greater than the size of the water drops ( $\lambda$  of the order of a few centimetres), which

will allow the system to see through clouds and rain. In a way, this will make the system weather independent. It can therefore be noted that it is possible to assign many different tasks to radars. However, in order to make the right choice of radar specifications, we also need to have a good understanding of how the microwaves interact with the earth's surface.

One of the most important things to consider is that it is actually the properties of the earth's surface that are on a scale of a chosen wavelength that mostly influences the signal that we will get back to our radar system. Looking at surface roughness for example, what we are interested in is then the surface roughness on a scale of our wavelength. This can be the small wind ripples on the ocean surface or it can be the texture and roughness of an agricultural. The dielectric properties of the material also have an influence. And, for most applications that have an interest in earth observation, it is the liquid water content of the material that will have the biggest influence on the dielectric properties. This therefore makes it possible to distinguish between different plantations. How much the dielectric properties influence the energy which is scattered, it doesn't change the direction in which that energy is scattered. The key properties of the earth's surface that determine in which direction the energy is scattered is the roughness and also the orientation of the surface. The orientation is important because we are transmitting polarised waves. Polarised waves have an orientation and, as they meet other objects that may be oriented in different ways, then the interaction will be quite different. The slope direction or the individual scattering objects like twigs or branches in a tree may have a particular orientation that means that the interaction of the polarized waves may be different as a consequence of the different orientation of the target [1].

Finally, one of the key things about a radar system is that we measure the time delay. The key things that a radar is exceptionally good at is measuring how long it takes for the echo to come back.

### 3.8 Radar detection and ranging

The principle by which the radar can determine the distance to a target is quite simple. Consider a pulse transmitted towards the target at  $t = 0$ . This pulse will propagate through the medium at the speed of light  $c$  until it encounters the target at a distance  $R$ . Then, a certain part of the pulse will be reflected back towards the radar and will reach the radar at  $t = \tau$ . Knowing the travel time of the pulse as well as its speed, we can determine the distance between the radar and the target

in the following way:

$$R = \frac{\tau c}{2} \quad (3.15)$$

The presence of the factor 2 is due to the fact that  $\tau$  is the propagation time of the pulse for a round trip and thus for a distance equivalent to  $2R$ .

### 3.9 Radar imaging

Imaging radar is an application of radar which is used to create two-dimensional images, typically of landscapes. Unlike optical sensors, imaging radar provides its own light to illuminate an area on the ground and take a picture at radio wavelengths (wavelengths on the order of a few centimetres to a metre). In order to take such a picture, an antenna and a digital computer storage to record it is then needed. In a radar image, one can see only the energy that was reflected back towards the radar antenna. The radar moves along a certain path and the area illuminated by the radar (the footprint) is moved along the surface in a swath, building the image. In the radar image, each pixel corresponds to the radar backscatter for the corresponding area on the ground: very bright pixels correspond to a high backscatter while dark pixels correspond to a low backscatter [33].

The most classic application of radar is to determine the position and movement of highly reflective objects (such as ships or aeroplanes) by emitting a radiowave signal and then studying the direction and delay of the reflected signal. Radar imagery, on the other hand, produces images of objects or landscapes by recording the intensity of the reflected signal in order to determine the amount of scattering. Different intensities of backscatter produce pixels of different brightness, which in the end produces a 2D image.

Several techniques have been studied in order to produce such images. Most of them are based on the Doppler effect caused by the movement of the observed targets but also on the principle of repeatedly changing the viewing angle from which the target is observed. Over the years, these methods have been continuously improved and provide increasingly higher resolution images. The main applications of Radar Imaging are the mapping of the Earth and other planets, surface topography, agricultural monitoring, ice patrol, etc.

## 3.10 Imaging geometry

One way to intuitively understand the difference between optical and radar imaging systems is to compare the ability of the eyes and ears to determine the direction. The eyes, which operate at wavelengths of the order of hundreds of nanometres, can differentiate very fine details. Ears, on the other hand, operate at wavelengths of centimetres to metres and are not very good at determining direction, and radar systems are very similar to that. There is, however, one way to overcome that: by looking obliquely.

Indeed, as we have just seen, radars are very good at measuring time. The antenna sends out pulsed microwaves and detects the time it takes for the echoes to return back to the antenna. However, if the radar transmitted its pulses just below it, on a flat surface, most radar-target distances would be identical and echoes would then have the same travel time. Therefore, it would not be possible to determine the direction using time measurement.

But, by adopting a side-looking geometry and transmitting the pulses obliquely, the radar system is able to resolve distinct targets on the ground by detecting a different time delay for each of the targets, since the time delay is then approximately correlated with distance along the ground (in the range direction). So, in that way, it is possible to get over the fact that the directional ability of the radar system is very poor.

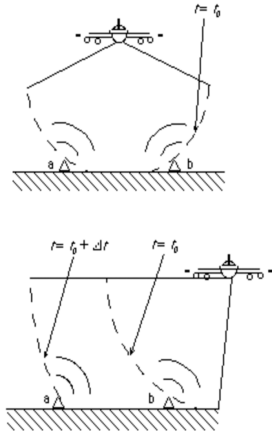


Figure 3.4: side-looking geometry [34]

In order to have an overall understanding of the system, it is important to understand the vocabulary that is used to describe its geometry. In addition, this knowledge will be crucial in understanding what is actually observed by a radar imaging system but also in understanding how the waves interact with the surface.

**Nadir** is the direction under a certain location. In the context of radar imagery, this location refers to the point just below the aircraft or satellite. More specifically, it corresponds to the vertical direction from the point under consideration to the direction of the force of gravity. The direction away from Nadir is called the zenith.

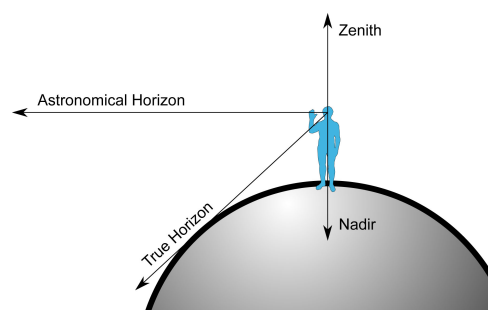


Figure 3.5: Geometry nomenclature [35]

*Azimuth* is the direction of the flight path of the aircraft or satellite. It can therefore be considered as the line of flight. In an image, azimuth is also known as along-track direction, since it is the relative along-track position of an object within the antenna's field of view following the radar's line of flight.

*Range* is the dimension of a radar image perpendicular to the flight path. In the context of radar remote sensing, we differentiate slant range and ground range. The slant range is the distance from the radar to the target, and the ground range is the projection of this distance onto the earth's surface.

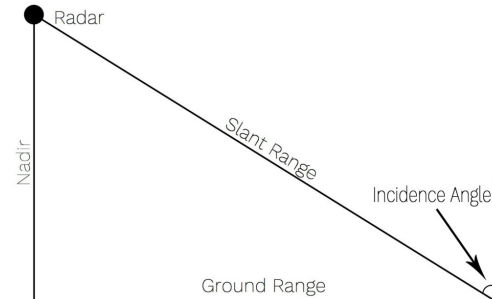


Figure 3.6: Range of a radar [1]

*Swath* is a term which roots come from the agricultural field in which it describes the width of a scythe. The analogy was then made with remote sensing radar. In this context, the width of the swath corresponds to the area of the ground surface that is illuminated by the sensor instrument.

In the context of satellite radar imagery, the swath refers to the area of the Earth's surface illuminated by the radar. In this case, the swath width corresponds to the width of the strip in the direction of the range. However, in this context, there is also a longitudinal component corresponding to the movement of the sensor in the direction of the azimuth.

*Incidence angle* is the angle defined by the incident radar beam and the normal to the intercepting surface. In general, the intensity of the backscatter decreases as the angle of incidence increases. The angle of incidence changes across the band of the radar image; it increases from near range to far range.

In the case of satellite radar imagery, the change in the incidence angle for flat terrain across the imagery band tends to be quite small, usually of the order of several degrees. In the case of an inclined surface, the local incidence angle is defined as the angle between the incident radar beam and a line normal to that surface.

## 3.11 Radar imaging effects

As explained previously, the radar system is looking to the side. This geometry has unique effects on the way objects appear in the radar image. This provides very interesting technical analyses, but it can also lead to problems of image distortion in certain spatial configurations. These problems result from the typical geometric relationship between the sensor and the observed area. In this section, we will look in more detail at different spatial configurations that induce distortions in the radar image. Specifically, we will focus on the effects called : Foreshortening, Layover and radar shadowing.

First, in order to understand these different effects, it is useful to explain the meaning of an elevation displacement. This phenomenon corresponds to a displacement of an element, from its initial position towards the nadir point (towards the sensor). This effect is particularly important when the element in consideration is located close to the nadir point. The displacement therefore increases as the angle of incidence decreases. Topographic features that can cause this type of displacement are, for example, mountains or tall buildings.

### 3.11.1 Foreshortening

Foreshortening is the spatial distortion by which a slope of land facing the radar illumination appears compressed compared to its true appearance, the slope then appears flattened in the direction of the radar. Foreshortening is a special case of elevation displacement. The effect is therefore more pronounced for steep slopes and for radars that use small incidence angles.

### 3.11.2 Layover

The Layover corresponds to an extreme form of Foreshortening in which the echo coming from the top of an element arrives before the echo corresponding to the base of this element. The image of such an element appears as falling towards the radar. Layover effects on a radar image look then very similar to effects due to foreshortening. As with foreshortening, layover is most severe for small incidence angles, at the near range of a swath, and in mountainous terrain [37].

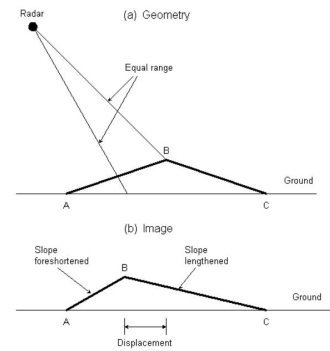


Figure 3.7: Foreshortening [36]

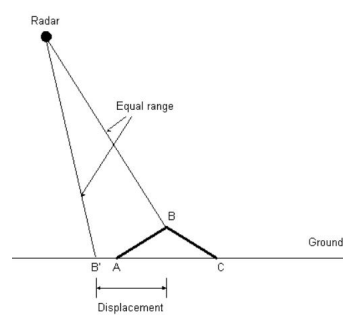


Figure 3.8: Layover [36]

### 3.11.3 Radar shadowing

Radar shadowing refers to the absence of radar illumination due to the presence of a reflecting or absorbing element. The shape and quantity of these radar shadows depend on several factors: the radar viewing direction, the angle of incidence, the altitude of the platform, and the topography of the observed area. The size of these shadows increases with the angle of incidence. The direction of these shadows can serve as a good indicator of the direction of illumination of the radar but also provides information about the topography and height of the features causing the shadows. However, the shadows mask certain areas and it is therefore not possible to obtain information about them since no echoes return from these areas. Satellite-borne radars, having a low angle of incidence, tend to produce less radar shadow.

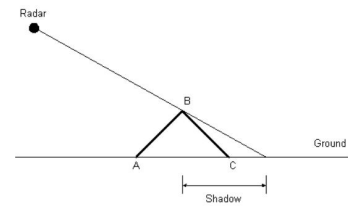


Figure 3.9: Radar Shadowing [1]

All of these 3 effects can be observed in the figure 3.10.

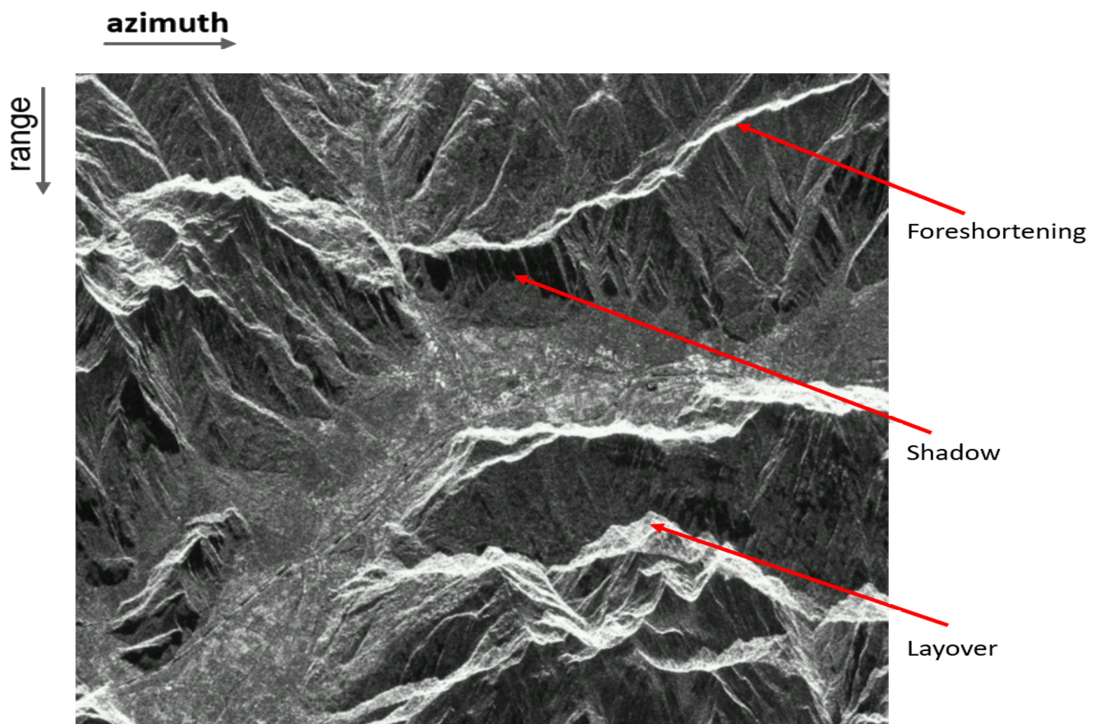


Figure 3.10: Radar imaging effects (modified from [1])

## 3.12 Scattering mechanisms

In addition of being able to locate the different elements present in the illuminated area, SAR systems are also able to differentiate between these elements. In order to fully understand how this works, it is mandatory to have a good understanding of the different types of scattering that can occur on the Earth's surface.

### *Specular Reflexion*

When the pulse encounters a smooth, flat surface at the scale of its wavelength, almost all of its energy is dispersed in a specular direction. Areas with these characteristics appear very dark in the image since the radar receives almost nothing from this position. This is why smooth water surfaces (river, lake, ...), parkings and roads always appear very dark on radar images.

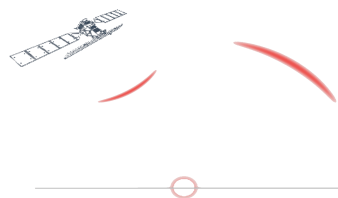


Figure 3.11: Specular reflexion [1]

### *Surface Scattering*

When the pulse hits a somewhat rough surface, some of its energy is scattered towards the sensor. Whether a surface is considered slightly or strongly rough depends on the wavelength, angle of incidence and spatial resolution of the system.

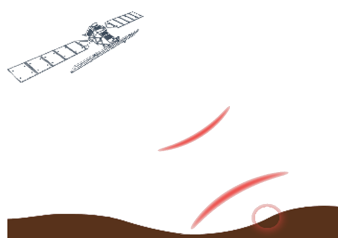


Figure 3.12: Surface scattering [1]

### *Double bounce*

When the pulse successively encounters two relatively smooth surfaces perpendicular to each other, its echo is of great intensity. This is due to the multiple transmission of energy towards the sensor. This type of phenomenon occurs mainly on buildings and other artificial structures. This explains why echo intensities from cities are always higher than those from the countryside.



Figure 3.13: Double bounce [1]

### *Volume Scattering*

When the pulse encounters a 3D object, the energy is repeatedly scattered in several directions before some of this energy is returned to the sensor (=multiple bounces). This phenomenon occurs for example in snow, in the canopy and in vegetation in general.

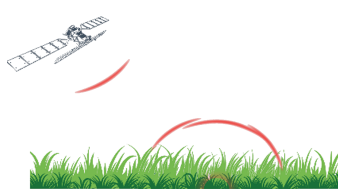


Figure 3.14: Volume scattering [1]

## 3.13 Real aperture radar

Now that the background knowledge required to understand a radar system has been established and the concept of radar imagery is well understood, it is time to describe how a radar imaging system works. Most radar systems are based on the same operating principle. Therefore, in this section, we will describe the operation of Real Aperture Radar (RAR) which is a relatively basic system and will therefore serve as a good basis for understanding more advanced systems.

### 3.13.1 Operation principle

The principle of Real Aperture Radar is to direct a narrow beam of energy perpendicular to the flight path of the carrier platform (aircraft or spacecraft) using a real physical aperture antenna. This energy pulse is emitted by the radar antenna, and the relative intensity of the reflections is then used to produce an image of a narrow band of terrain.

Reflections from areas at greater distances arrive at the radar after a proportionally longer time, which is then projected in the range direction of the image with an amplitude corresponding to the backscatter intensity. Before transmitting a new pulse, the radar steps forwards a small distance in order to image a new strip of terrain. Finally, all of the side-by-side image strips will be assembled to reconstruct the direction of the azimuth [38].

### 3.13.2 Azimuth resolution

Azimuth resolution  $\rho_A$  describes the ability of an imaging radar to separate two closely spaced elements in the direction parallel to the sensor's motion.

The situation is illustrated in Figure 3.15 First, consider that buildings *A* and *B* are simultaneously in the radar beam. In this case, for almost all impulses, they will both cause a reflection and their echoes will be received at the same time by the radar. It will therefore not be possible for the radar to distinguish building *A* from building *B*. Building *C*, which is further in the azimuth direction, is not illuminated by the first beam (the one that illuminated *A* and *B*). The echo from building *C* will therefore only be received by the radar if the radar realises a forward motion. However, following this movement, the first 2 buildings are no longer illuminated and therefore the echo emitted by building *C* will be recorded

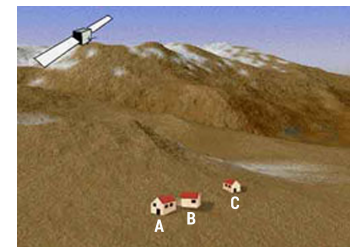


Figure 3.15: Azimuth resolution [39]

separately. In this example, after reconstruction of the different scenes, the radar will image 2 elements instead of 3. It is therefore understandable that for a real aperture radar, two targets along the radar path can only be separated if the distance between them is greater than the width of the radar beam. The beam width is therefore considered to be the azimuth resolution, which is also dependent on the slant range to the target for these systems.

For all types of radars, the beam width is a constant angular value with distance. For a one-antenna system with a given wavelength  $\lambda$ , the azimuth beam width  $b$  depends on the physical length  $l$  of the antenna in the horizontal direction according to :

$$b = \lambda/l \quad (3.16)$$

Then to obtain the azimuth resolution, multiply this value by the slant distance  $R$  between the antenna and the illuminated area.

$$\rho_A = b \cdot R = \frac{\lambda R}{l} \quad (3.17)$$

It quickly becomes apparent that real aperture radars do not provide fine resolution from orbital altitudes.

In order to improve the azimuth resolution of these radars, a longer antenna or a shorter wavelength must be chosen. However, as we have already seen, using a shorter wavelength generally results in greater attenuation of clouds and the atmosphere, which reduces the ability of the radars to image in all weather conditions.

### 3.13.3 Range resolution

The range resolution  $\rho_R$  is the minimum distance between two elements so that they can always be distinguished by the radar. In order for the radar to be able to distinguish between them, their echoes must necessarily be received at different times.

The figure 3.16 is intended to illustrate the situation. In this example, we consider the transmitted signal to be a single pulse of duration  $L$  [s]. The signals  $P_A$  and  $P_B$  reflected by the buildings will therefore also be of length  $L$ . In order for the radar to be able to distinguish the two echoes, they must not

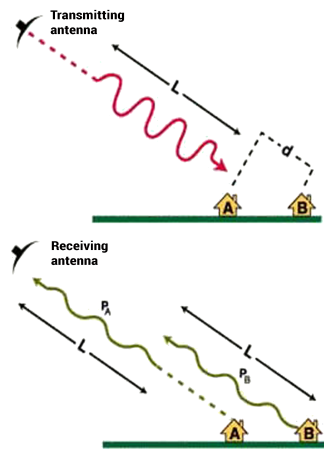


Figure 3.16: Range resolution [39]

overlap. Given that building  $B$  is at an oblique distance  $d$  from building  $A$ , the time difference between the arrival of the initial signal and the arrival of  $P_B$  at position  $A$  is therefore  $\frac{2d}{c}$  (with  $c$  the speed of light since it is an electromagnetic wave). It is then obvious that in order to prevent the two echoes from overlapping, the following inequality must be respected:  $\frac{2d}{c} > L$ .

The range resolution in the oblique direction is therefore given by :

$$\boxed{\rho_R = \frac{c \cdot L}{2}} \quad [\text{m}] \quad (3.18)$$

And the range resolution projected on the ground is therefore:

$$\boxed{\rho_R = \frac{c \cdot L}{2\sin(\phi)}} \quad [\text{m}] \quad (3.19)$$

where  $\phi$  is the angle of incidence.

### 3.14 Pulse compression

As demonstrated in the previous section, when the emitted signal corresponds to a constant pulse of length  $L$ , the resolution range depends strongly on its length. To obtain a very fine resolution, one could therefore imagine emitting an extremely short pulse. However, this is not a practical solution.

Indeed, as can be seen from the radar equation, the maximum distance travelled by the pulse is proportional to the fourth root of the transmitted power; however, the equipment needed to transmit a very short and high energy pulse is difficult to build (especially in embedded systems due to voltage power limitations due to arc effects, max 40 kV in general). Shortening the length of the pulse will therefore reduce the range of the radar, which is quite annoying when it comes to satellite radar imagery. We notice that range and resolution are two requirements in opposition to each other: to get a fine resolution, a short pulse is needed, but to reach a long-range the pulse must be long enough to have enough energy.

This is why most long-range radar systems use the pulse compression or chirp approach. This is an alternative method of pulse compression using frequency modulation. In this approach, instead of sending a short pulse at a constant frequency, a long pulse is sent out with a modulated frequency.

### 3.14.1 How does it works?

The modulation used for pulse compression is the linear frequency modulation (LFM). It corresponds to an increase of the pulse frequency from  $f_0$  to  $f_0 + B$  during the chirp duration  $\tau_p$ . The expression of the transmitted signal  $S_t(t)$  is therefore as follows:

$$S_t(t) = A \cdot \exp[j2\pi(f_0 + \alpha t)t] \cdot \text{rect}\left[\frac{t}{\tau_p}\right] \quad (3.20)$$

where  $A$  is the amplitude of the signal,  $f_0$  the carrier frequency and  $\alpha$  the frequency rate of the chirp modulation ( $\alpha = \frac{B}{2\tau_p}$ ). The term *rect* corresponds to the *rectangular function* which is defined as follows:

$$\text{rect}(t) = \begin{cases} 1 & \text{if } t \in [0, 1] \\ 0 & \text{elsewhere} \end{cases} \quad (3.21)$$

When an echo is received from an element at distance  $R$ , the received signal  $S_r(t)$  corresponds to the signal transmitted attenuated by a factor  $\sigma$  and with a delay  $\tau = \frac{2R}{c}$ . The expression of this signal is therefore given by :

$$S_r(t) = \sigma \cdot A \cdot \exp[j2\pi(f_0 + \alpha(t - \tau))(t - \tau)] \cdot \text{rect}\left[\frac{t - \tau}{\tau_p}\right] \quad (3.22)$$

In order to recover the useful information, a matched filter is performed between the transmitted signal and the received one. As a reminder, the matched filtering operation is defined as :

$$S_{MF}(t) = \int_{-\infty}^{\infty} S_r(u) \cdot S_t^*(u - t) du \quad (3.23)$$

By replacing the terms with their respective expression, we obtain:

$$\begin{aligned} S_{MF}(t) &= \int_{-\infty}^{\infty} \text{rect}\left[\frac{u - \tau}{\tau_p}\right] \cdot \exp[j2\pi(f_0 + \alpha(u - \tau))(u - \tau)] \\ &\quad \cdot \text{rect}\left[\frac{u - t}{\tau_p}\right] \cdot \exp[-j2\pi(f_0 + \alpha(u - t))(u - t)] du \end{aligned} \quad (3.24)$$

After simplifications, the output of the matched filter is approximately [40] :

$$S_{MF}(t) = \frac{\sin(\pi\alpha\tau_p(t - \tau))}{\pi\alpha\tau_p(t - \tau)} \cdot \exp\left[-j\frac{4\pi R}{\lambda}\right] \quad (3.25)$$

We notice that the expression corresponds to a cardinal sinus. We then understand the name *pulse compression* since we have gone from a long pulse to a cardinal sinus (see figure 3.17).

### 3.14.2 Increased range resolution

The width of the cardinal sine of the Equation 3.25 is  $\frac{1}{\alpha \cdot \tau_p}$  where the term  $\alpha \cdot \tau_p$  corresponds to the bandwidth  $B$  of the transmitted signal:

$$W_{sinc} = \frac{1}{\alpha \cdot \tau_p} = \frac{1}{B} \quad [s] \quad (3.26)$$

Following the same reasoning as in the Section 3.13.3, the new range resolution  $\rho_R$  (in the oblique direction) is given by:

$$\boxed{\rho_R = \frac{c}{2B}} \quad [m] \quad (3.27)$$

And the range resolution projected on the ground is then given by:

$$\boxed{\rho_R = \frac{c}{2B \sin(\phi)}} \quad [m] \quad (3.28)$$

where  $\phi$  is the incidence angle.

This resolution is independent of the pulse duration. Then, with the *pulse compression* method, it is possible to achieve much finer resolutions while maintaining a large range.

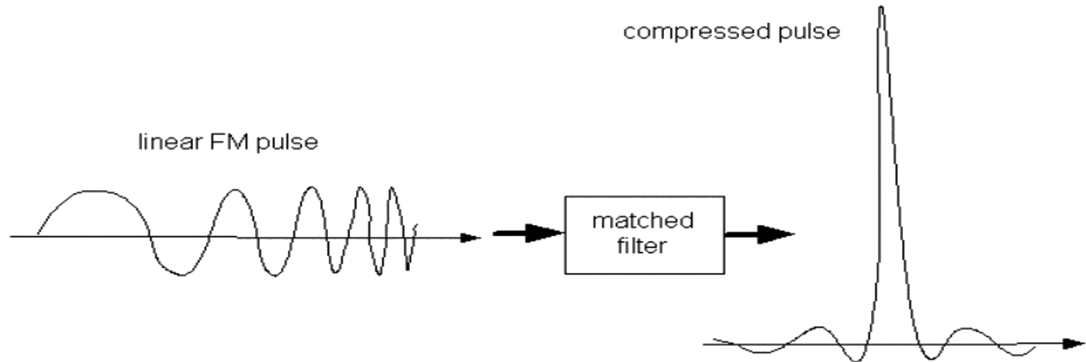


Figure 3.17: LFM pulse before and after application of Matched filter [41]

# Chapter 4

## The Principle of SAR

As discussed in the previous chapter, the wavelengths used in radar imaging are of the order of a few centimetres to a metre. Since these wavelengths are much longer than those used by optical and near-infrared types of remote sensing, radar imagery requires much larger systems in order to be able to get the same level of detail on the Earth's surface. For example if, with a conventional radar imaging system, we would like to get a resolution of about ten metres in the azimuth direction then we would need an antenna that is in the region of a few kilometres long. However, it is pretty infeasible to make such an antenna and then put it into space. This is the reason why systems such as the one seen in the previous chapter (the real aperture radar) have poor azimuth resolution.

### 4.1 Synthetic Aperture Radar Imaging

There exists a method for solving the problem just mentioned. This method is called *aperture synthesis*. The principle behind aperture synthesis is simply using lots of small antennas (which are individually very poor in determining a direction) together in a consistent way which allows simulating a larger antenna. However, making a huge antenna by sticking hundreds of small antennas together would not change the problem. So the idea is to use a single small antenna but to use it a hundred times by changing its position after each measurement session. Then, by storing and processing all the data that comes back together, we can then emulate an antenna which is as if it was one kilometre long, but using a small antenna. This is the principle of aperture synthesis, we are synthesising a one-kilometre-long antenna with a small antenna, but using it multiple times over the kilometer. Radars using this method are therefore called *Synthetic Aperture Radar (SAR)*.

One way to think about how a synthetic aperture radar works is to think of the principle of *Doppler beam sharpening*. This is a method of processing the backscattered signal from on-board radars into a higher-resolution image. It uses the Doppler information contained in the signal returning from targets to give a better azimuth resolution than the antenna's own resolution. The radar antenna of an aircraft or satellite is so small (relative to the wavelength used) that the radar energy propagates over a wide area (usually several degrees wide in a direction orthogonal to the direction of the platform) making the radar's ability to determine the direction of the signal very poor. To improve this capability, this method takes advantage of platform motion in that targets in front of the platform return an increased Doppler signal (slightly higher in frequency) and targets behind the platform return a downgraded Doppler signal (slightly lower in frequency). The amount of offset varies with the angle forward or backward from the orthonormal direction. Knowing the speed of the platform, the return of the target signal is placed in a specific angle "bin" that changes over time. The signals are integrated over time and thus the radar "beam" is synthetically reduced to a much smaller aperture. Specifically (and based on the ability to distinguish the smallest Doppler shifts), the system can have hundreds of very "tight" beams simultaneously. This technique therefore greatly improves the angular resolution.

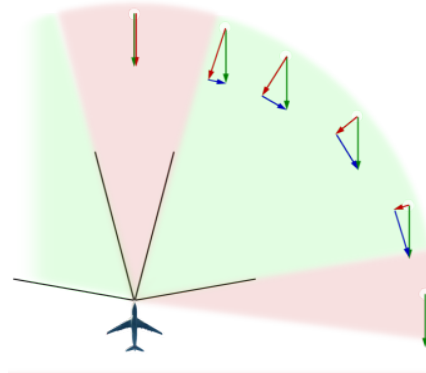


Figure 4.1: Doppler beam sharpening [42]

## 4.2 Geometry of SAR

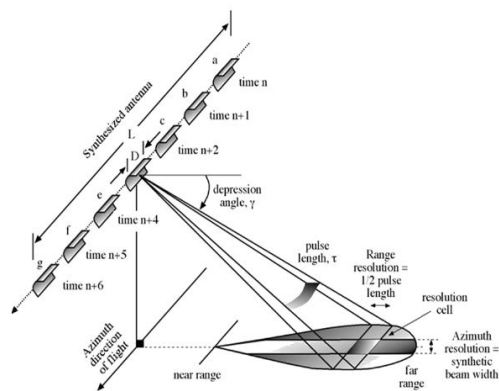


Figure 4.2: Geometry 3D of SAR [43]

The geometry of the system therefore corresponds to a small antenna of size  $D$  which performs a sequence of measurements of a region during a certain part  $L$  of its orbit. The width of the area illuminated by this antenna is  $W = \frac{R\lambda}{D}$  (where  $R$  is the distance between the radar and the centre of the illuminated area.). An element on the ground is therefore visible by the radar for a maximum length of  $W$ . This is why the synthetic aperture  $L$  will be maximum of length  $W$ .

### 4.3 Increased Azimuth resolution

The principle of SAR is therefore to improve azimuth resolution. As explained, this is achieved by simulating a large antenna (using radar displacement) and then applying the Doppler Beam sharpening principle to the collected data set.

First we will express the Doppler frequency associated with the system geometry. In this context, the source (the radar) is moving at a speed  $V$  and the target is fixed. As described in the Equation 3.11, the Doppler frequency is given by:  $f_d = \frac{2V_r}{\lambda}$ . By observing the figure 4.3, we can easily deduce the expression of the relative velocity:  $V_r = V \cdot \sin(\theta/2)$ . The angle included in the sinus is relatively small so the expression can be simplified as follows:  $V_r = \frac{V\theta}{2}$ . By replacing  $V_r$  by its expression in the Doppler frequency equation, we obtain:

$$f_d = \frac{2v_r}{\lambda} = \frac{V\theta}{\lambda} \quad (4.1)$$

The next step is to determine the change of Doppler shift across the aperture.

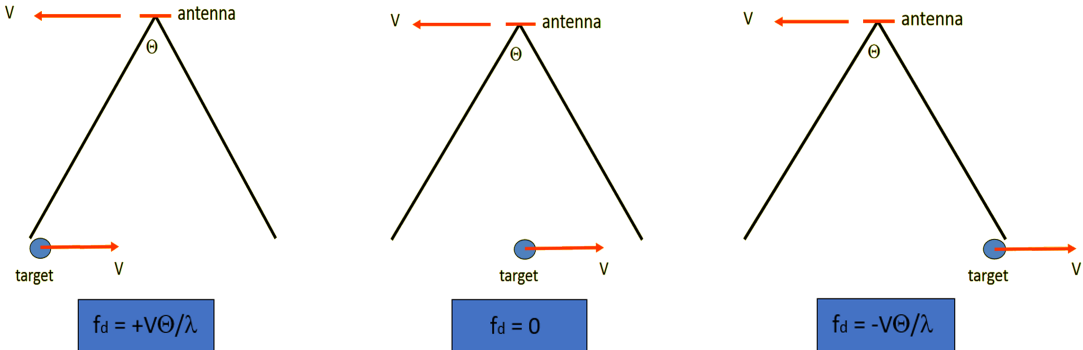


Figure 4.4: Doppler shift across the aperture (inspired from [44])

Regarding the figure 4.4 it can be deduced that the variation of the Doppler shift through the aperture is of:  $\frac{2V\theta}{\lambda} = 2f_d$ . Therefore, the Azimuthal Bandwidth of the SAR is given by:  $B = 2f_d$ .

In signal processing, it is known that if an electrical system has a bandwidth  $B$ , then it can resolve a signal that has a time length of  $\Delta t = \frac{1}{B}$  [45].

The time interval that can be resolved is then given by:

$$\Delta t = \frac{1}{B} = \frac{1}{2f_d} = \frac{\lambda}{2V\theta} = \frac{D}{2V} \quad (\text{as } \theta = \lambda/D) \quad (4.2)$$

To obtain the spatial interval, one only has to multiply the temporal interval by the speed  $V$  of the radar. The resolution in the azimuth direction  $\rho_A$  can thus be expressed as:

$$\boxed{\rho_A = V \cdot \Delta t = \frac{D}{2}} \quad (4.3)$$

Therefore we notice that SAR allows obtaining an incredible resolution in azimuth with a small antenna size. Moreover, the smaller the antenna, the finer the resolution will be. This property may seem counter-intuitive at first because, as we have seen, the smaller the antenna is, the wider the beam will be (for a given wavelength). However, this property becomes clearer when we notice that a wide beam induces the fact that an element will be visible for a longer period of time, which means that the synthetic aperture will be longer and will therefore allow obtaining a finer resolution. Also, unlike the azimuth resolution obtained with a system such as RAR (Equation 3.17), the resolution obtained via SAR is independent of the slant range distance, wavelength and altitude of the platform. Therefore, the same system onboard an aircraft or satellite should have the same resolution. There is no other remote sensing system with the same property [46]. It is now understandable why SAR have become the indisputable reference systems in on-board radar imagery. The figure 4.5 illustrates and summarises very well the solution applied by SAR in order to obtain a high resolution in azimuth.

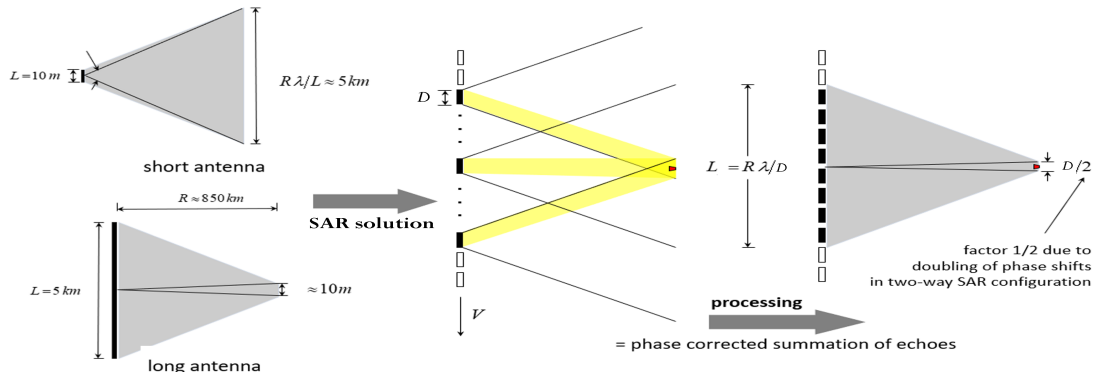


Figure 4.5: Increased Azimuth resolution via SAR [1]

## 4.4 Range resolution

As systems always seek to achieve the best possible resolution, SAR systems also apply the pulse compression principle described in the Section 3.14.2.

The pulse emitted by the SAR therefore corresponds to a chirp and the range resolution  $\rho_R$  obtained is as follows:

$$\boxed{\rho_R = \frac{c}{2B\sin(\phi)}} \quad (4.4)$$

## 4.5 SAR modes

Today's SAR systems are capable of operating in different imaging modes.

The most basic mode is called **Stripmap**. In this mode, the radar beam is fixed on a strip, allowing a continuous strip to be imaged. The system thus scans a swath whose width is the width of the radar beam and whose length is the path taken by the carrier. In this case, the azimuth resolution obtained corresponds to that of the equation.

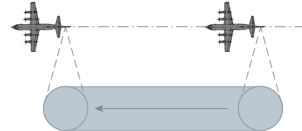


Figure 4.6: Stripmap mode [47]

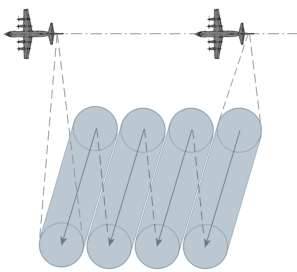


Figure 4.7: ScanSAR mode [47]

If one wishes to produce an image on a wider strip, there is the **ScanSAR** mode. In this mode, the antenna is directed to different angles of elevation corresponding to several sub-bands. As the aircraft or satellite moves, the sounding swath will take the form of a series of zig-zag strips parallel to each other. Each sub-band is illuminated by several pulses, but these are of shorter duration than in the Stripmap mode, so the azimuth resolution is degraded.

If an even higher azimuth resolution is desired than with the Stripmap mode, the **Spotlight** mode is used. In this mode, the antenna beam is directed to a fixed point in order to illuminate a given area. The illumination time of a region is therefore much longer, which results in a very long synthetic aperture and therefore a better resolution. This mode therefore does not image continuous bands but rather individual areas along the radar's flight path.

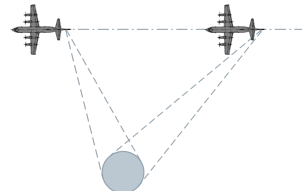


Figure 4.8: Spotlight mode [47]

There are also other imaging modes such as TOPS, Interferometric Wide Swath or still Wave Mode. They each have different advantages and disadvantages, but it is important to note that there are fundamental limitations to SAR. Improving azimuthal resolution leads to a degradation in bandwidth and vice versa [48].

## 4.6 Applications

SAR systems have many distinct applications: they can map the Earth, identify oil spills in the ocean, study the evolution of deforestation, monitor agricultural land to predict famine, or track maritime traffic. All these applications are carried out using different techniques, each of which uses different characteristics of the signals received. In this section we will describe the 3 main techniques which are called Polarimetry, Interferometry and Time Series.

### 4.6.1 Polarimetry

Polarimetry is a technique that consists of measuring, processing and interpreting the state of **polarisation** of an electromagnetic wave. As seen in the Section 3.2.4, polarisation is a characteristic of transverse waves, so it can be used to characterise the pulses transmitted and received by the radar. The state of polarisation of the echo can be related to the geometric characteristics of the observed surface such as shape, roughness, orientation, or to intrinsic surface properties such as moisture, salinity, and density.

As explained previously, the radar is an active remote sensor, so it can control the polarity of the pulse it transmits and receives. There are 4 possible configurations. The first two correspond to the case where the radar transmits with a certain polarisation and receives echoes with the same polarisation, these are the HH and VV configurations (the first letter corresponds to the transmitted polarity and the second to the received polarity) and we then speak of Co-Polarisation. The last 2 configurations correspond to the case where the radar receives echoes with a polarisation orthogonal to the transmitted one, these are the HV and VH configurations and we then speak of Cross-Polarisation.

This technique makes it possible, for example, to choose the colours of the radar images. Indeed, as seen in the Section 3.12, the plants react in the form of volume scattering and this phenomenon often tends to generate a depolarisation of the pulse. By comparing the intensity perceived in HH mode and HV mode, we can deduce the proportion of echoes that have kept or changed their polarisation and thus deduce whether the echoes come from an element corresponding to vegetation or not. We can therefore imagine imposing the color green for elements whose backscatter HV/HH ratio is important. The phenomenon of Double bounce also produces (most of the time) a depolarisation of the wave. In order to differentiate the echoes coming from an element from a double bounce to one coming from a volume scattering, one must then compare the phases obtained in co-polarisation and cross-polarisation mode. Indeed, a phase difference can often be noticed

between the 2 modes in the case of a volume scattering but much less frequently in the case of a double bounce [1].

By comparing the intensity and phase shift of the echoes for different polarisation modes, it is therefore possible to obtain a great deal of information concerning the composition of the elements present on the observed surface.

In the figure 4.9, it is possible to observe the radar images obtained for the same area but using different modes of polarisation. In particular, it can be seen that water appears darker in the case of cross-polarisation. This is due to the fact that the water produces a single bounce and therefore does not generate depolarisation, the intensity perceived by the cross-polarisation is therefore lower than in the case of co-polarisation.

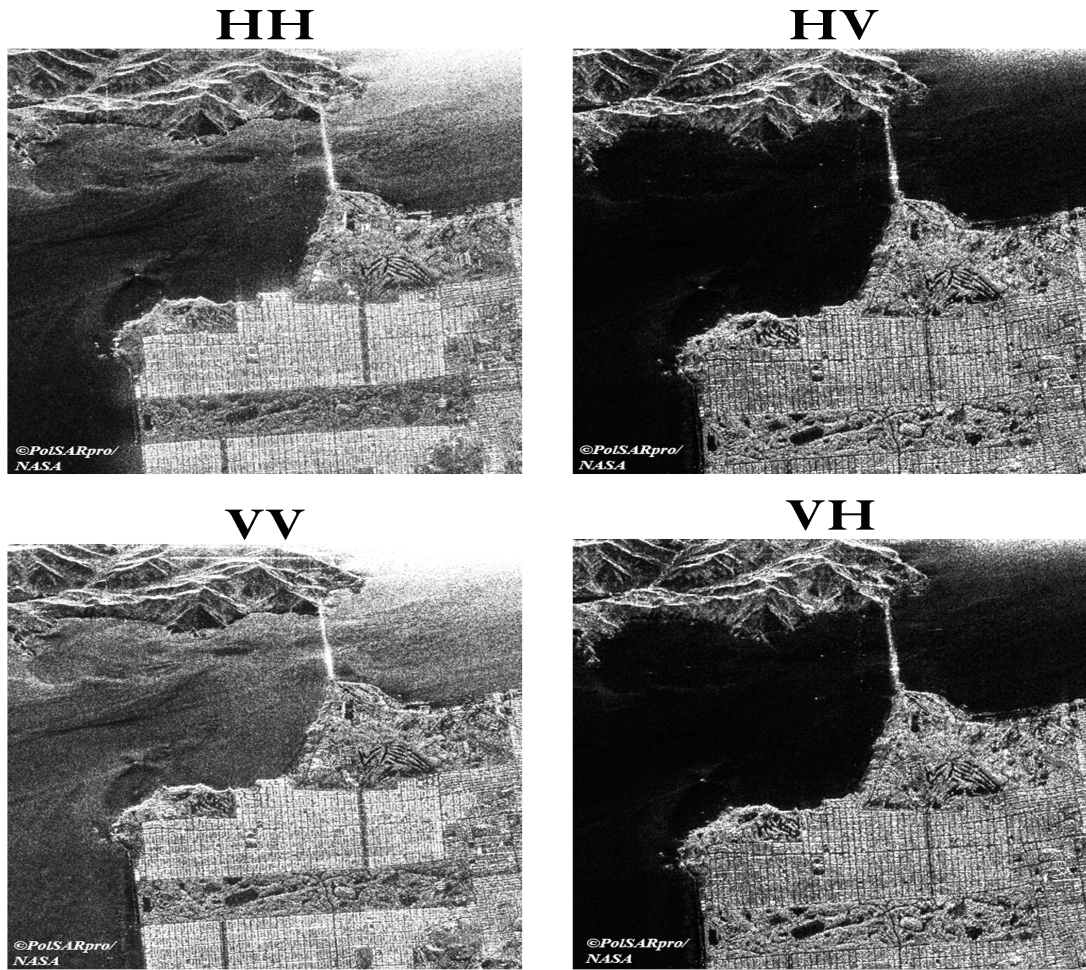


Figure 4.9: Polarimetry modes (modified from [1])

### 4.6.2 Interferometry

Radar interferometry is one of the most remarkable things that can be achieved with a radar system. This technique makes it possible to produce digital elevation models (DEM). Radar polarimetry works by studying the polarisation state of the echo. Concerning radar interferometry, it works by studying the **phase** of the received echoes.

So first we may ask how to determine the phase of the received signal. To do so, we can again (see Section 3.7) make an analogy with our ears. If we had only one ear, we would not be able to determine the direction from which the sound comes. However, with the help of our two ears, we can determine the phase difference of the perceived sound between our two ears and thus determine the direction from which the sound is coming from. Radar systems do the exact same thing except that instead of using two ears, two receiving antennas are used. These 2 antennas can be on the same platform (as in the case of the SRTM, see Section 2.1), we then speak of mono-static mode. The 2 antennas can also be on 2 separate platforms located on 2 slightly different orbits (as in the case of the TandemX mission, see Section 2.1), we then speak of bi-static mode. A third possibility is to use a single antenna that slightly modifies its orbit during its rotation with the earth and thus produce an image of the same area during its second pass.

As we have already explained, radar systems are very good at determining distance but rather bad at determining direction. However, if both antennas measure the phase of the echoes then it becomes possible to determine the direction accurately. Therefore, by combining distance and direction information, it is possible to determine the 3D position of the elements and thus produce DEMs.

When making several phase measurements of the same area at different times, it can be observed that in some cases a phase difference between two echoes from the same position may appear. These phase differences are usually observed on objects whose geometry varies over time. These phase differences are caused, for example, by trees moving because of the wind or by the movement of waves on water surfaces. The method of measuring phase differences between two images is called **differential interferometry** (D-InSAR) [49].

The term **coherence** is used to describe the similarity in phase and amplitude between two echoes coming from a given position. The coherence measurement is therefore an indicator of the quality of the phase determined by the two systems. A high coherence means that one can be confident about the quality of the measurement performed, but if the coherence is low then one cannot be sure of the accuracy

of the measurement performed. Coherence is also a means of obtaining information about the land cover type. Indeed, it is known that areas with a low coherence correspond to vegetation while areas with a very high coherence correspond to artificial constructions such as buildings.

Interferometry and more precisely differential interferometry is a powerful tool in the field of geology and geography. The melting of glaciers, or the deformation of land caused by earthquakes are examples of what can be observed using this technique.

The figure 4.10 corresponds to the interferogram of a volcano. The deformation results from changes in the volume of a shallow chamber. The accumulation of magma in this chamber results in the inflation, or expansion, of the volcano, while the release of magma from the chamber results in deflation or contraction.

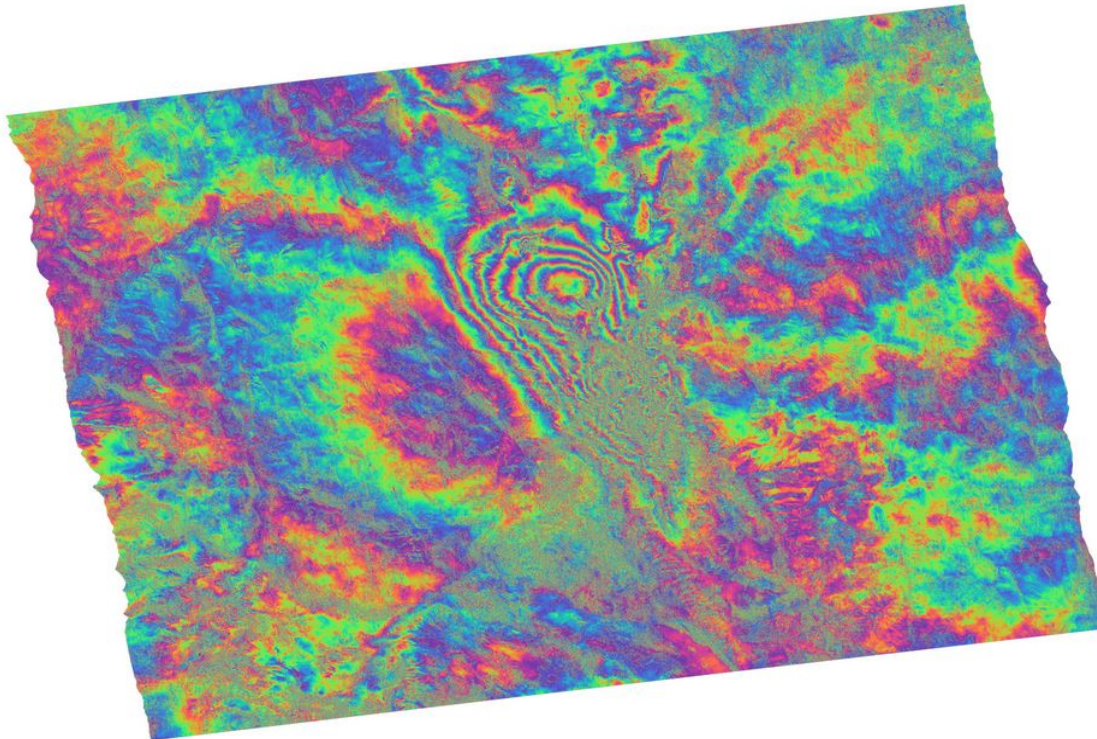


Figure 4.10: Interferogram of a volcano [50]

### 4.6.3 Time series

One of the methods frequently used in remote sensing for observing the Earth's surface is the Time series method. This method consists of collecting over time radar images in order to observe potential changes in topography or simply to observe seasonal characteristics.

This method is also widely used in optical remote sensing. However, as already explained, radars have the advantage that they operate day and night and are not disturbed by the presence of clouds. This is therefore very advantageous in winter where there is a lot of cloud cover or in tropical areas where there is almost perpetual cloud cover.

These image collections can be made over short periods of time (say one year) as well as over long periods of time. Over a short period of time, one can thus study the evolution of the vegetation of a forest or the behaviour of an agricultural field across the different seasons. Over a long period of time, it is for example possible to study the deforestation of tropical forests or to study the amount of ice surface that has disappeared.

By observing the amount of change in an area, it is then possible to classify different types of land cover. Indeed, we know that a forest will change less significantly over the course of a year than an agricultural field, which varies enormously over a year. This classification can therefore be done blindly and further increases the amount of information that can be extracted from remote sensing sensors [1].

In the figure 4.11, it is possible to observe the impact of deforestation in a region of the Amazon between 2007 and 2010. We know the size of a pixel, so it is enough to calculate the number of white pixels in the image on the right to know the area of forest that has been felled during the three years.

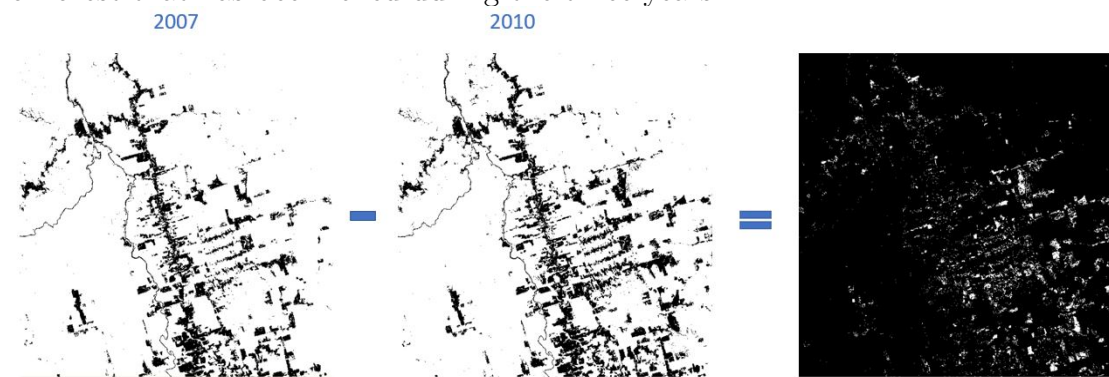


Figure 4.11: Time series over a deforested area

# Chapter 5

## Model Development

In the previous sections, the theoretical basis for developing a good understanding of how a SAR operates has been established. The attention will now be turned on the design of such a system and it will be explored a way to further enhance its ability to produce high-resolution images. This chapter will focus on the development of the model used by the system designed within the framework of this master thesis. The signal processing will be described in the next chapters.

### 5.1 Notations

This section gathers and defines all the parameters used in the development of the model.

Synthetic aperture length	$L$
Physical antenna length	$l_a$
Physical antenna height	$h_a$
Position of the target in the range direction	$x$
Position of the target in the azimuth direction	$y$
Width of the ground swath	$X$
Along-track beamwidth	$D$
Ground distance from the nadir point to the illuminated area	$X_{start}$
Minimal slant range for a target in the illuminated area	$R_0$
Altitude of the satellite	$H$
Speed of the satellite	$V$
Look angle of the radar	$\Theta$
Angular spread of the radar beam in the azimuth direction	$\phi$
Angular spread of the radar beam in the range direction	$\alpha$

Carrier frequency of the radar	$f_0$
Bandwidth of the chirp	$B$
Wavelength	$\lambda$
Time duration between 2 chirps	$T_p$
Time duration of a chirp	$T_c$
Time duration between 2 samples	$T_s$
Minimal delay for a target in the illuminated area	$\tau_{min}$
Time delay of the echo	$\tau$

## 5.2 Geometrical description

In order to fully understand the model it is essential to have a good representation of the system geometry (shown in the figure 5.1). Indeed, this allows a quick visualization of the system boundaries.

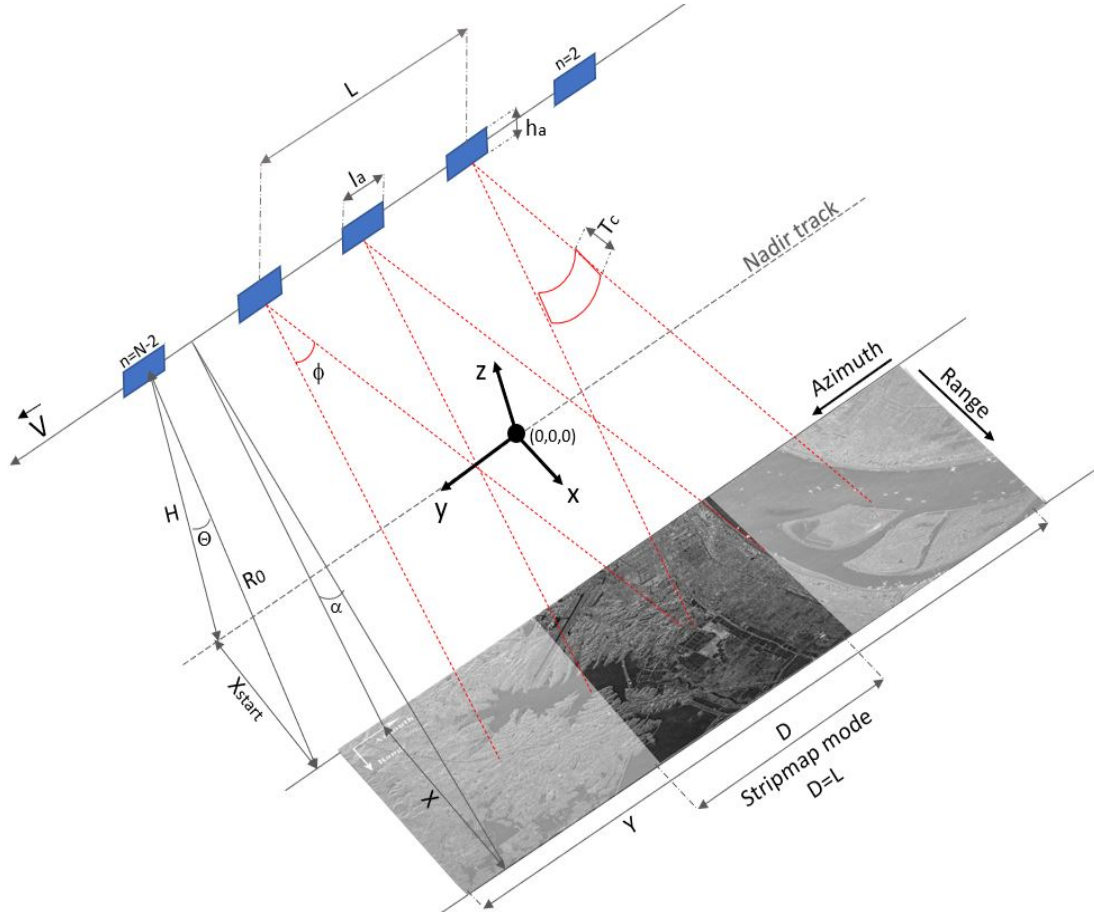


Figure 5.1: System's geometry

The area illuminated by the radar at a time  $t$  is represented by the dark grey area, it is  $D$  long and  $X$  wide. The value of the parameters  $D$  and  $X$  is limited by the size of the physical antenna ( $l_a, h_a$ ) and the wavelength  $\lambda$ . Indeed, using the geometry of the system (observable in the figure 5.1) and knowing that  $\phi = \frac{\lambda}{l_a}$  and  $\alpha = \frac{\lambda}{h_a}$ , we obtain the following expressions:

$$D = 2 \cdot R_0 \cdot \tan\left(\frac{\phi}{2}\right) \iff D \simeq \frac{R_0 \lambda}{l_a} \quad (5.1)$$

$$X = H \cdot \tan(\Theta + \alpha) - X_{start} \iff X = H \cdot \tan\left(\Theta + \frac{\lambda}{h_a}\right) - X_{start} \quad (5.2)$$

It is also important to note that in Stripmap mode, the length of the synthetic aperture  $L$  is equal to the length  $D$  of the surface illuminated by the radar:  $L = D$ .

## 5.3 Signal model

The objective here is to obtain a model that allows high-resolution images to be produced. After reading the section 3.14, it is obvious that the modulation used is the *LFM* (also called chirp modulation) for its ability to provide high resolution in the range direction.

### 5.3.1 Transmitted signal

The transmitted signal  $S(t)$  will consequently correspond to a chirp. Depending on the application for which it is intended, it will have a certain carrier frequency  $f_0$  and according to the desired resolution it will have a bandwidth  $B$ . The expression of the transmitted signal is then as follows:

$$S(t) = \exp\left[j2\pi \int_0^t \left(f_0 - \frac{B}{2} + \frac{B}{T_c}t\right) dt\right] \cdot \text{rect}\left[\frac{t}{T_c}\right] \quad (5.3)$$

$$\iff S(t) = \exp\left[j2\pi \left(\left(f_0 - \frac{B}{2}\right)t + \frac{B}{2T_c}t^2\right)\right] \cdot \text{rect}\left[\frac{t}{T_c}\right] \quad (5.4)$$

The term *rect* corresponds to the rectangular function. Here it is intended to limit the pulse duration to  $T_c$  and is defined as :

$$\text{rect}(t) = \begin{cases} 1 & \text{if } t \in [0, 1] \\ 0 & \text{elsewhere} \end{cases} \quad (5.5)$$

### 5.3.2 Received signal

The signal  $R(t)$  received by the antenna, at a given position, corresponds to the sum of the signals coming from different targets  $c_j$  present in the illuminated area  $\mathbb{A}$ . Each target is characterized by the triplet  $(\alpha_j, x_j, y_j)$ <sup>1</sup> and the number of targets present in the observed area is given by the variable  $K : \{c_1, c_2, \dots, c_K\} \in \mathbb{A}$ . Since the signal from a target  $t_j$  reaches the radar after a delay<sup>2</sup>  $\tau_j[n]$ , the equation for the received signal can be written as:

$$R(t) = \sum_{j=1}^K \alpha_j S(t - \tau_j[n]) \quad (5.6)$$

A window needs to be added to this expression in order to determine whether the target of interest is located within the area illuminated by the radar at time  $t$ . If not, the target should be ignored. Keeping the marker fixed in the figure 5.1, the azimuthal position of the radar at time  $t$  is given by:  $Vt - \frac{L}{2} - \frac{Y}{2}$ . In order for the target to be within the area illuminated by the radar, the azimuth distance between the radar and the target must be at most  $\frac{L}{2}$ . This condition can be written as follows:

$$-\frac{L}{2} \leq y - Vt + \frac{L}{2} + \frac{Y}{2} \leq \frac{L}{2} \quad (5.7)$$

The window associated with this condition and following the same definition as the Equation 5.5 can be expressed as follows:

$$\text{rect} \left[ \frac{y - Vt + L + \frac{Y}{2}}{L} \right] \quad (5.8)$$

The Equation 5.6 then becomes:

$$R(t) = \sum_{j=1}^K \alpha_j S(t - \tau_j[n]) \cdot \text{rect} \left[ \frac{y - Vt + L + \frac{Y}{2}}{L} \right] \quad (5.9)$$

In order to image the entire area with high resolution in azimuth, the radar moves and takes measurements at different positions. The distance between two positions is given by  $V T p$  and the time taken to reach a position  $n$  is given by  $n T p$ .

---

<sup>1</sup>where  $\alpha$  represents the amplitude of the backscatter after application of the radar gain,  $x$  the position in the range and  $y$  the position in azimuth.

<sup>2</sup>is the time for one pulse to reach the target and return. It depends on the position  $n$  of the radar and the position  $(x_j, y_j)$  of the target. Its expression can be observed in the Equation 5.15.

Then, the expression of the received signal depends on the location of the radar and is expressed as follows:

$$R(t) = \sum_{n=0}^{N-1} \left( \sum_{j=1}^K \alpha_j S(t - \tau_j[n] - nT_p) \cdot \text{rect} \left[ \frac{y - Vt + L + \frac{Y}{2}}{L} \right] \right) \quad (5.10)$$

Once the signal is received, it is converted back to baseband to facilitate processing. The expression of the received baseband signal  $R_{BB}(t)$  is given by :

$$R_{BB}(t) = \sum_{n=0}^{N-1} \left( \sum_{j=1}^K \alpha_j S(t - \tau_j[n] - nT_p) \cdot \exp[-j2\pi f_0 t'] \cdot \text{rect} \left[ \frac{y - Vt + L + \frac{Y}{2}}{L} \right] \right) \quad (5.11)$$

The time parameter  $t$  can be expressed discretely using the parameters  $T_s$  and  $T_p$  :

$$t = nT_p + iT_s + \tau_{min} \quad (5.12)$$

Similarly, the time parameter  $t'$  can be expressed as :

$$t' = iT_s + \tau_{min} \quad (5.13)$$

The term  $R_{BB}(t)$  will now be written in its discrete form:  $R_{BB}[n, i]$ . By replacing the time parameters  $t$  and  $t'$  by their respective expressions, the expression 5.11 becomes :

$$R_{BB}[n, i] = \sum_{j=1}^K \alpha_j \cdot S(iT_s + \tau_{min} - \tau_j[n]) \cdot \exp[-j2\pi f_0(iT_s + \tau_{min})] \cdot \text{rect} \left[ \frac{y - V(nT_p + iT_s + \tau_{min}) + L + \frac{Y}{2}}{L} \right] \quad (5.14)$$

The expression of the delay  $\tau_j[n]$ , which corresponds to the time taken by the pulse to reach the target at position  $(x_j, y_j)$  and then return, is given by :

$$\tau_j[n] = \frac{2}{c} \cdot \sqrt{H^2 + (X_{start} + x_j)^2 + \left( y_j - V \cdot nT_p + \frac{L+Y}{2} \right)^2} \quad (5.15)$$

By replacing  $S$  by the expression of the transmitted signal and inserting the expression of the delay into the Equation 5.14, the latter becomes :

$$\begin{aligned}
 R_{BB}[n, i] = & \sum_{j=1}^K \alpha_j \cdot \exp \left[ -j \frac{4\pi f_0}{c} \sqrt{H^2 + (X_{start} + x_j)^2 + \left( y_j - VnT_p + \frac{L+Y}{2} \right)^2} \right] \\
 & \cdot \exp \left[ j \frac{\pi B}{T_c} \left( iT_s + \tau_{min} - \frac{2}{c} \sqrt{H^2 + (X_{start} + x_j)^2 + \left( y_j - VnT_p + \frac{L+Y}{2} \right)^2} \right) \right] \\
 & \cdot \exp \left[ -j\pi B \left( iT_s + \tau_{min} - \frac{2}{c} \sqrt{H^2 + (X_{start} + x_j)^2 + \left( y_j - VnT_p + \frac{L+Y}{2} \right)^2} \right) \right] \\
 & \cdot \text{rect} \left[ \frac{iT_s + \tau_{min} - \frac{2}{c} \sqrt{H^2 + (X_{start} + x_j)^2 + \left( y_j - VnT_p + \frac{L+Y}{2} \right)^2}}{T_c} \right] \\
 & \cdot \text{rect} \left[ \frac{y - V(nT_p + iT_s + \tau_{min}) + L + \frac{Y}{2}}{L} \right]
 \end{aligned} \tag{5.16}$$

It can be noticed that the model of the received signal  $R_{BB}[n, i]$  is an additive model on the different targets and that it corresponds to a product of three exponentials with a time and a space window. From this expression, it can also be observed that the received signal for a given target depends on the amplitude of its backscatter  $\alpha_j$  and on the delay<sup>3</sup>  $\tau_j[n]$  taken by the pulse to reach this target and return.

---

<sup>3</sup>expressed here as:  $= \frac{2}{c} \sqrt{H^2 + (X_{start} + x_j)^2 + \left( y_j - VnT_p + \frac{L+Y}{2} \right)^2}$

## 5.4 RawData simulation

The objective of this master thesis is to characterize a system allowing to obtain a resolution of 1m x 1m in the Stripmap mode (see Section 4.5). In order to validate the theoretical models, it is necessary to test them through simulations. However, in order to be able to perform such simulations, it is essential to have radar imaging data on which to test the model. There are many platforms where data can be obtained free of charge, in particular the ESA's Copernicus site, which makes data acquired by the Sentinels available, but these data are obtained via a system that does not necessarily correspond to the specific requirements (different altitude, different antenna, SAR mode, etc.). Possessing a data simulator, allowing the generation of radar imagery data produced by a system whose characteristics are set by the user, would therefore be an extremely useful tool in the validation process of a theoretical system. In this section, it will be explained how to realize such a data simulator.

### 5.4.1 Simulation-specific notations

In this section the different notations specific to data simulation are gathered and described, in addition to those in the Section 5.1.

Number of discrete positions $n$ crossed by the radar	$N$
Number of samples taken at each position $n$	$I$
Width of the area covered by the radar	$X$
Along-track length of the area covered by the radar	$Y$
Resolution of the image in the range direction	$\Delta x$
Resolution of the image in the azimuth direction	$\Delta y$
Number of pixels in the azimuth direction	$P_L$
Number of pixels in the range direction	$P_l$

### 5.4.2 Simulation development

A first step in data production is to digitally reproduce the geometry in which the real system operates. To do this, it is first necessary to construct the area that will be observed by the radar. This area will be of length  $Y$  and width  $X$ . The value of the parameter  $Y$  simply depends on the actual length of the area which the user wants to image. On the other hand, the value of the parameter  $X$  (which represents the width of the ground swath) depends on the height  $h_a$  of the physical antenna as shown in Eq 5.2. Also, since the system is designed to operate in Stripmap mode,  $D = L$  is considered (as explained in Section 5.2). The numerical adaptation of the real system geometry can be seen in the figure 5.2.

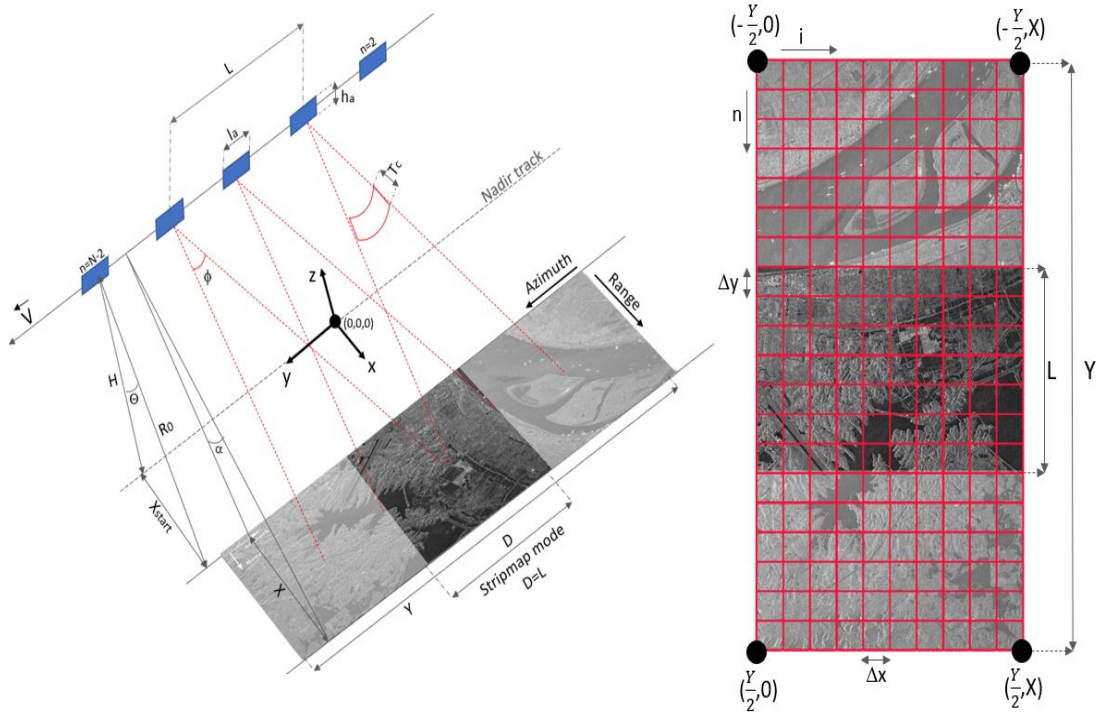


Figure 5.2: Digital representation of the system geometry

For reasons of time and computing power, in this thesis, the focus will be on the realization of 2D images. In this case there is no notion of elevation in the landscape. As a reminder, the goal here is to simulate data received by a system with given specifications (altitude, frequency, ...). As previously explained, the backscatter has different properties (amplitude, phase, polarization) that are specific to each target. It is therefore extremely difficult to simulate all of these behaviors for a entire area. So for demonstration purposes, in this master thesis, in order to simulate the backscatter, a 2D image will be selected to represent the observed area and the pixel value will be considered as the backsacatter of the corresponding target. The simulated raw data will not correspond to real radar data since the solution is not very physical, but it will still give an idea of the different operations performed and will allow the testing of the algorithms that will be discussed in this chapter.

In order to know the physical dimensions of a pixel, the length and the width of the imaged area have to be divided by the number of pixels of the respective dimensions of the picture. Thus, we have :

$$\Delta y = \frac{Y}{P_L}$$

and

$$\Delta x = \frac{X}{P_l}$$

where  $P_L$  is the number of pixels in the azimuth direction and  $P_l$  is the number of pixels in the range direction of the image.

It is obvious that the resolution will be limited by the parameters  $\Delta y$  and  $\Delta x$ . The higher the number of pixels in the picture, the better the resolution could be.

Next, the reference framework in which the system evolves must be established. This will allow to simulate the movement of the radar and thus determine the part of the image illuminated for a certain position  $n$  of the radar. The marker is placed in such a way that it is at mid-length in the azimuth direction and in  $X_{start}$  in the range direction. The y-azimuth position of a target can take a value between  $-\frac{Y}{2}$  and  $\frac{Y}{2}$ . The x-range position of a target can take a value between 0 and  $X$ . For better understanding, this reference marker is also shown in the figures 5.2 and 5.3.

It is now possible to express the position of the radar over time. The first step is to determine its initial position. The width of the radar beam in the azimuth direction is  $L$ , so the radar will acquire signals from any target at an azimuth range to the left and right of  $\frac{L}{2}$  or less. Targets at  $(-\frac{Y}{2}, x)$  are therefore visible to the radar as soon as it reaches the azimuth position  $y = -\frac{Y}{2} - \frac{L}{2}$ . In contrast, targets located in  $(\frac{Y}{2}, x)$  will no longer be detected by the radar when it reaches the position  $y = \frac{Y}{2} + \frac{L}{2}$ .

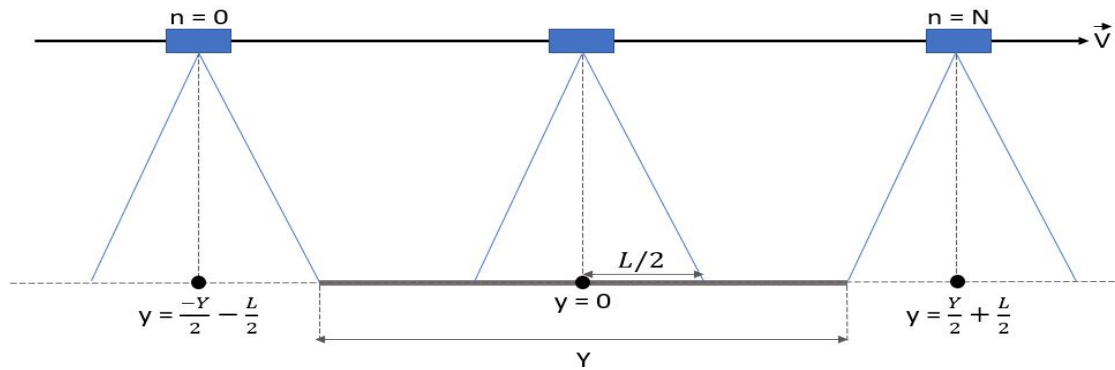


Figure 5.3: Digital representation of the system geometry boundaries

However, determining if a target is observable or not by the radar does not depend on its position in the range. All targets in the range  $[X_{start}, X_{start} + X]$  are observable for all positions of the radar (if their position in  $y$  allows it). In this simulation, the data are therefore performed for a single landscape band. To observe a larger area, the radar only needs to change its orbit slightly and then combine the different bands (or modify  $h_a$ ).

Raw data consists of matrix structures. Here, since the elevation is not taken into account, the matrix will be two-dimensional. Each dimension represents a temporal component. The azimuth component represents the time elapsed between each satellite position. In this dimension, each pixel will represent a time duration  $T_p$ . The range component represents the sampling time of the received signal at a certain position  $n$  of the radar. In this dimension, each pixel will represent a time duration  $T_s$ . The dimension of the matrix will be  $N \times I$ . The value of these 2 parameters can be determined as follows:

As explained above, the initial and final position of the radar (which images a certain area of length  $Y$ ) are respectively given by  $y = -\frac{Y}{2} - \frac{L}{2}$  and  $y = \frac{Y}{2} + \frac{L}{2}$ . The total distance covered by the radar is therefore  $Y + L$ . Since the speed of the radar is  $V$ , the time required to cover this distance is  $\frac{Y+L}{V}$ . The value of parameter  $N$  can be determined by the following expression :

$$N = \frac{Y + L}{V \cdot T_p}$$

Regarding parameter  $I$ , it represents the number of samples taken at a certain position  $n$ . However, for a position  $n$ , the radar receives the signals from all the targets present in the area illuminated by the radar. It receives them at slightly different times so it is necessary to sample over a longer period of time than  $T_c$  (corresponding to the duration of the a pulse). It is possible to determine the maximum time difference between the arrival of the first and last echo. Indeed, this time difference is given by :

$$\tau_{max} - \tau_{min} = \frac{2}{c} \sqrt{H^2 + (X_{start} + X)^2 + (L/2)^2} - \frac{2}{c} \sqrt{H^2 + X_{start}^2} \quad (5.17)$$

Therefore, knowing that the radar starts listening at time  $t$  corresponding to the time at which it will receive the echo from the nearest target, the total sampling time is  $T_c + \tau_{max} - \tau_{min}$ . The value of parameter  $I$  can thus be expressed as:

$$I = \frac{T_c + \tau_{max} - \tau_{min}}{T_s} \quad (5.18)$$

The figure 5.4 illustrates the structure of the output of the operation carried out to produce the raw data.

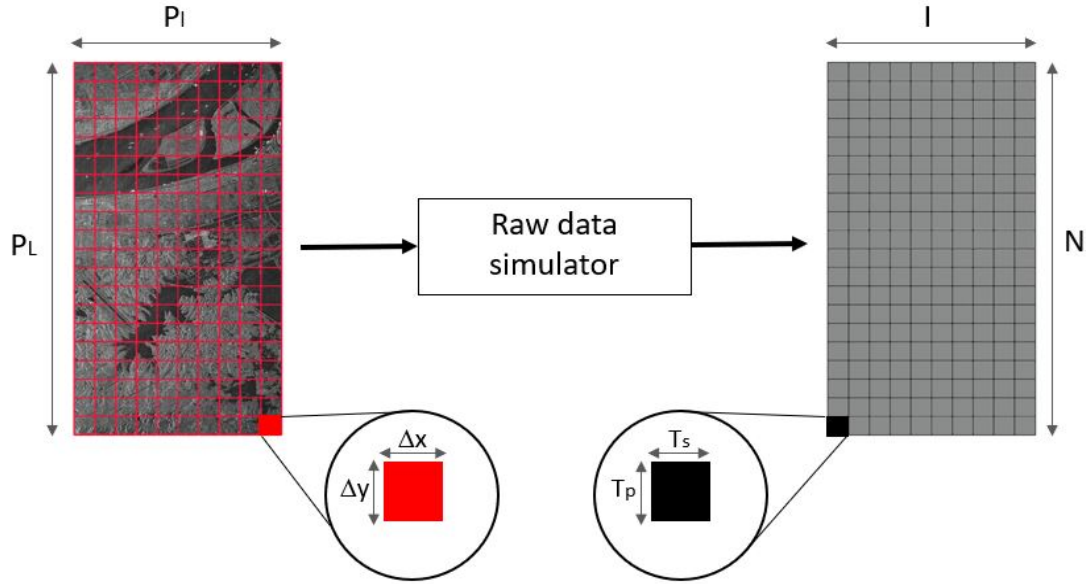


Figure 5.4: Structure of the raw data

### Signal model

The equation used to generate the raw data is the Equation 5.16 since it corresponds to the received signal (without approximations) to which the baseband operation has already been applied.

The expression used to generate the raw data can therefore be written in the following way:

$$RawData[n, i] = R_{BB}[n, i] \quad (5.19)$$

It can be noticed that the computational complexity of the Equation 5.16 is very large. Indeed, it is necessary to perform the operation for each potential target  $(x,y)$  but also for each element  $(n,i)$ ; the range of these variables can be very large and the computation time can quickly become huge. A solution is to perform matrix calculation. However each target  $(x,y)$  has its own delay and has an impact on several elements  $(n,i)$ . It was therefore decided to create an  $N \times I$  matrix and then generate the raw data by adding the  $N \times I$  matrix obtained for each pair  $(x,y)$ . This reduces the number of loops to two instead of four.

### Resolution limitations

By looking closely at the structure of raw data, two new resolution limitations can be observed.

The first one concerns the azimuth resolution. In this direction, one pixel represents a duration of  $T_p$ . Knowing that the speed of the radar is  $V$ , the azimuth resolution limitation  $\Delta a$  is given by :

$$\boxed{\Delta a = V \cdot T_p} \quad (5.20)$$

The second limitation relates to the slant range resolution  $\Delta sr$ . In this direction, one pixel represents a duration of  $T_s$ . The speed of propagation of the wave is the speed of light and the measured duration corresponds to a round trip. Hence, the limitation of the slant range resolution  $\Delta sr$  is given by :

$$\boxed{\Delta sr = \frac{cT_s}{2}} \quad (5.21)$$

In order to convert this resolution in the direction of the range, it is necessary to project the distance corresponding to  $cT_s$  in the range direction. Hence, the resolution in the range  $\Delta r$  can be expressed this way:

$$\boxed{\Delta r = \frac{cT_s}{2\sin(\phi)}} \quad (5.22)$$

where  $\phi$  is the angle of incidence.

#### 5.4.3 Choice of parameters

In order to start the simulation and thus generate the raw data, it is necessary to select the physical parameters of the system being simulated. Most of them have an impact on the final resolution.

Equations 4.4 and 4.3, which correspond to the limitations of resolution due to physical constraints, allow to set some parameters: To reach the desired resolution of  $1m \times 1m$ , Eq 4.4 requires that the pulse bandwidth  $B$  must be of 150MHz while Eq 4.3 requires that the length of the real aperture must be 2m.

For the same resolution, the limitations corresponding to equations 5.20 and 5.22 allow to set 2 other parameters: the pulse sampling frequency and the Pulse Repetition Frequency (*PRF*). Indeed, the Eq 5.20 imposes that  $T_p$  is equal to  $\frac{1}{V}$  which implies that the *PRF* is equal to  $V$  and the Eq 5.22 imposes that  $T_s$  is equal to  $\frac{2\sin(\phi)}{c}$  which implies that  $f_s$  is equal to  $\frac{c}{2\sin(\phi)}$ .

The set of system parameters established for the generation of the data are gathered in the following table:

Signification	Parameters	Value	Units
Speed of light	$c$	$3 * 10^8$	m/sec
Altitude of the satellite/radar	$H$	550	Km
Altitude of the satellite/radar	$X_{start}$	317.542	Km
Range to target at broadside time $t=0$	$R_0$	635.085	Km
Velocity parameter	$V$	7570	m/sec
Carrier frequency of the pulse	$f_0$	12	Ghz
Period of pulse sampling	$T_s$	$3.33 * 10^{-9}$	sec
Chirp duration	$T_c$	$5 * 10^{-6}$	sec
BandWidth of the pulse	$B$	150	Mhz
Position of the target	$T_p$	$132.1 * 10^{-6}$	sec

Table 5.1: Parameters table used for the generation of the raw data

#### 5.4.4 Results

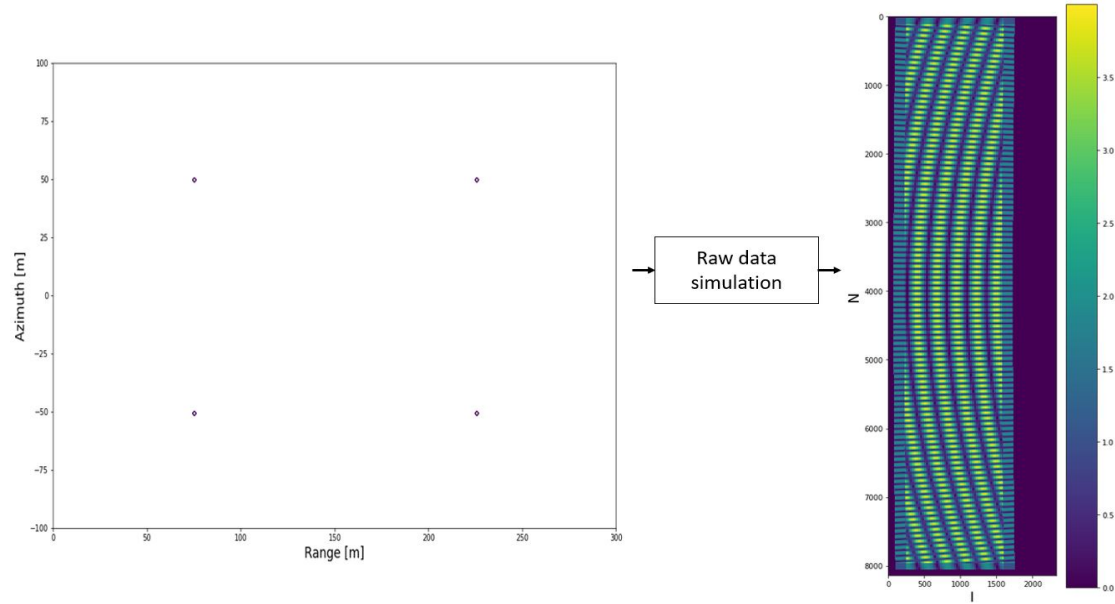


Figure 5.5: Input and output of the Raw data simulation

In the figure 5.5, it is possible to observe the raw data generated by the simulator for a given observed area. (as explained in the section 5.4.2, this does not correspond exactly to real raw data). In this example, the observed area consists of 4 targets forming the corners of a rectangle. The first observation that can be noted is that the dimensions of the output matrix are different from those of the input matrix. This has also been explained and illustrated in the section 5.4.2.

Then, by looking at the obtained raw data matrix, it is possible to distinguish a uniform part in purple color from a part in green and blue color on which appears a pattern (here the colors represent different amplitudes, the purple represents an amplitude equal to 0). The uniform part indicates that at this particular instant the radar receives nothing. In this example, this is explained by the fact that only 4 targets are considered in a large area, so the radar is listening longer than it takes for the signal from the farthest target to reach the radar. If the area considered was completely filled with targets then there would be no uniform areas.

Regarding the non-uniform part, its pattern is the result of the interactions between all the signals received by the radar. Hence, this pattern varies with the number of targets but also with their arrangement.

# Chapter 6

## Image processing algorithms

Once the series of measurements performed by the radar (after the raw data simulation in the case of this thesis) a matrix of size  $N \times I$  is obtained. Each element of this matrix corresponds to a sum of backscatters (amplitude and phase) received at a certain position and at a certain time. Directly observing this matrix does not allow to guess what the observed area looks like, only a pixel cloud can be observed. In order to be able to discover the observed area, a processing must be performed on this matrix. There are different image processing algorithms and all of them present their advantages and disadvantages.

These can be compared on a trade-off line between computational power and image fidelity. Indeed, an algorithm requiring high computational power will provide high fidelity images while a low computational power algorithm will provide low fidelity images.

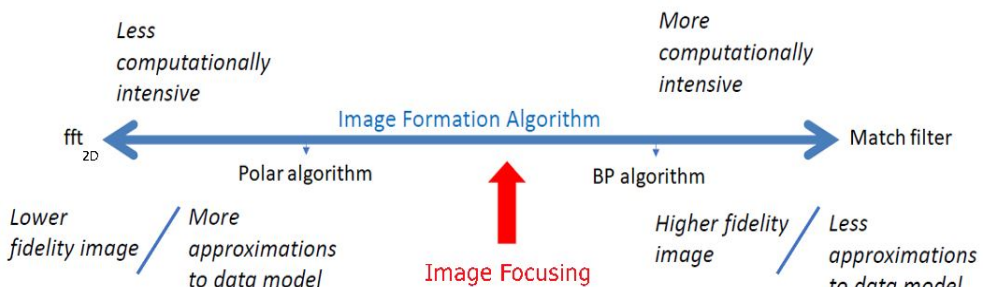


Figure 6.1: Trade-off between the algorithms (modified from [51])

As a reminder in this master thesis the objective is to reach a resolution of  $1m \times 1m$ . It is therefore preferable to study the algorithms allowing to obtain a high fidelity and this is why the Matched Filter will be discussed. However, as explained above, this algorithm requires high computational power. In this chapter we will also study a new algorithm to achieve the desired resolution but at a lower cost.

## 6.1 Matched filter

In signal processing, a matched filter is the result of the correlation between a known template signal and an unknown signal. The goal is to detect the presence of this template signal in the unknown signal. In the presence of Gaussian additive noise, the matched filter is considered as the optimal linear filter to maximize the SNR [52].

Matched filters are therefore frequently used in the radar domain: the signal template corresponds to the transmitted signal whose exact expression is known and the unknown signal corresponds to the received signal. This is because the received signal usually corresponds to the transmitted signal to which a certain delay, amplitude variation and/or frequency variation has been applied.

However, applying a matched filter to raw data is not an easy thing to do. Indeed each element  $(n,i)$  of the matrix corresponds to the sum of an unknown number of distinct signals coming from different targets. The number of possibilities for each element  $(n,i)$  is thus extremely high and testing them all would require tremendous computing power. When the area observed by the radar consists of only one target, then the value of each element  $(n,i)$  depends only on this target and the matched filter provides a very accurate result. Conversely, the more targets there are, the less accurate the matched filter result will be.

As explained above, the number of different possible combinations is huge. However, since the author had limited resources in terms of computing power at the time of writing this master thesis, it was not conceivable to test all the possibilities. Hence, it was decided to consider that the signals coming from different targets were orthogonal and would not interfere with each other. The matched filter operation will then consist in generating the raw data produced independently by each possible target and in computing the norm of the scalar product between each of these  $N \times I$  matrices and the conjugate of the real raw data. The obtained value will then be recorded in a matrix of size  $X \times Y$  where  $X$  and  $Y$  are determined according to the size of the area illuminated by the radar.

In this case, there is not one but several signal templates: one for each target  $c_j$ . The signal template  $T_j$  for a target position  $(x_j, y_j)$  corresponds to the Equation ?? (for one target only):

$$T_j = R_{BB}[n, i] \quad (6.1)$$

The operation of the matched filter is therefore expressed in this way:

$$R_{MF}[x, y] = \langle \text{Vec}^1(T_j), \text{Vec}(\text{RawData}^*) \rangle \quad (6.2)$$

### 6.1.1 Results

When the matched filtering operation is performed on a surface consisting of a single target, the result corresponds exactly to the area observed by the radar (simulated in the case of this thesis). The result can be seen in the figure 6.2.

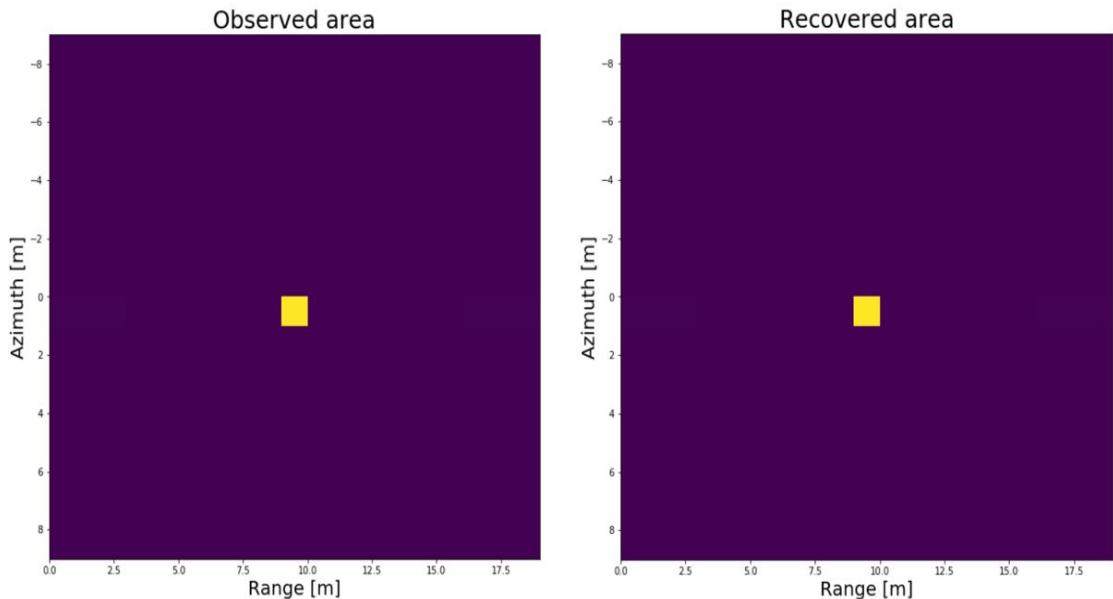


Figure 6.2: Matched filter operation on an area made up of a single target.

---

<sup>1</sup>This operation transforms a matrix into a long vector.

When the matched filtering operation is performed on a surface consisting of several targets, the result also corresponds to the area observed by the radar (the different targets are visible and placed in the right position) but it is possible to observe the appearance of fine lines slightly lighter in colour (the result can be seen in the figure 6.3). The appearance of these lines can be explained by the fact that the signals corresponding to the different targets are not really orthogonal to each other and therefore constructive and destructive zones appear.

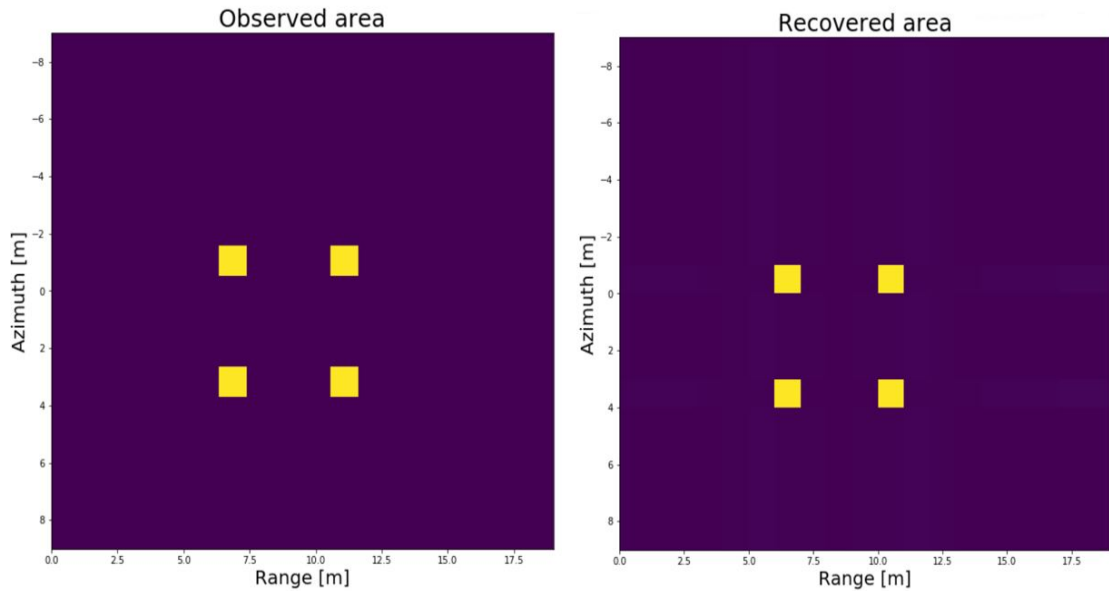


Figure 6.3: Matched filter operation on an area made up of four targets

## 6.2 Image focusing

The previous method does not exploit the 2D structure of the problem. Indeed, a different template must be computed for each point of the matrix and this requires a lot of time and computational power. It would be very interesting to find a method to separate the two dimensions and then perform a correlation in both directions independently. It would then be necessary to find a template signal  $A$  for the azimuth direction and another one  $R$  for the range direction. Knowing that a convolution translates into a product in the frequency domain, the image recovered by this method (known as focused image) would be expressed as:

$$\text{Focused image} = \text{ifft}_{2D} [\text{fft}_{2D}(\text{RawData}) \cdot (\text{fft}(A)_{N \times 1} \otimes \text{fft}(R)_{1 \times I})] \quad (6.3)$$

Here, the operator  $\cdot$  corresponds to a forward product and the operator  $\otimes$  corresponds to a matrix product.

However, to identify these two template signals, it is necessary to find out how the raw data behaves in the two orthogonal directions. All the terms constituting the current expression 6.1 of the received signal depend on both variables  $n$  and  $i$ , so it is not possible to identify these two template signals from this expression. The objective is therefore to succeed in rewriting this expression so that it is composed of a product of two signals, one of which would be solely dependent on variable  $n$  and the other solely on variable  $i$ . These two terms would thus form the two templates required for the implementation of this new solution.

As a reminder, the expression of the delay  $\tau_j$ , which corresponds to the time taken by the pulse to reach the target at position  $(x_j, y_j)$  and then return, is given by :

$$\tau_j[n] = \frac{2}{c} \cdot \sqrt{\underbrace{H^2 + (X_{start} + x_j)^2}_{=t1} + \underbrace{\left(y_j - V \cdot nT_p + \frac{L+Y}{2}\right)^2}_{=t2}} \quad (6.4)$$

It is possible to make an approximation on this time delay. Indeed, given the geometry of the system, the term  $t1$  is much more important than  $t2$ . This is because the slant range from the radar to the target is greater than the distance separating the radar from the target in the azimuth direction. After Taylor's approximation around  $t_2 = 0$ , the expression can be simplified as follows:

$$\tau_j = \frac{2}{c} \cdot \left( \sqrt{H^2 + (X_{start} + x_j)^2} + \frac{\left(y_j - V \cdot nT_p + \frac{L+Y}{2}\right)^2}{2\sqrt{H^2 + (X_{start} + x_j)^2}} \right) \quad (6.5)$$

The model of the received signal is an additive model, i.e. it is the result of the sum of the signals emitted by all the observed targets. For readability reasons, in the further development, only the contribution of a single target will be considered. Then, by replacing the old expression of the delay by this one, the Equation ?? becomes:

$$\begin{aligned}
 R_{BB}[n, i] = & \alpha \cdot \exp \left[ -j \frac{4\pi f_0}{c} \left( \sqrt{H^2 + (X_{start} + x)^2} + \frac{(y - V \cdot nT_p + \frac{L+Y}{2})^2}{2\sqrt{H^2 + (X_{start} + x)^2}} \right) \right] \\
 & \cdot \exp \left[ j \frac{\pi B}{T_c} \left( iT_s + \tau_{min} - \frac{2}{c} \sqrt{H^2 + (X_{start} + x)^2} - \frac{(y - V \cdot nT_p + \frac{L+Y}{2})^2}{c\sqrt{H^2 + (X_{start} + x)^2}} \right)^2 \right] \\
 & \cdot \exp \left[ -j \pi B \left( iT_s + \tau_{min} - \frac{2}{c} \sqrt{H^2 + (X_{start} + x)^2} - \frac{(y - V \cdot nT_p + \frac{L+Y}{2})^2}{c\sqrt{H^2 + (X_{start} + x)^2}} \right) \right] \\
 & \cdot \text{rect} \left[ \frac{iT_s + \tau_{min} - \frac{2}{c} \left( \sqrt{H^2 + (X_{start} + x)^2} + \frac{(y - V \cdot nT_p + \frac{L+Y}{2})^2}{2\sqrt{H^2 + (X_{start} + x)^2}} \right)}{T_c} \right] \\
 & \cdot \text{rect} \left[ \frac{y - V(nT_p + iT_s + \tau_{min}) + L + \frac{Y}{2}}{L} \right]
 \end{aligned} \tag{6.6}$$

The expression  $\tau_{min}$  is known to be equal to  $\frac{2}{c}\sqrt{H^2 + X_{start}^2} = \frac{2}{c}R_0$ . The expression of the difference  $\tau_{min} - \frac{2}{c}\sqrt{H^2 + (X_{start} + x)^2}$  can thus be simplified by carrying out the taylor approximation of order 1 around  $x = 0$ . Thus, the expression of the difference becomes :

$$\tau_{min} - \frac{2}{c}\sqrt{H^2 + (X_{start} + x)^2} = \frac{2}{c}R_0 - \frac{2}{c} \left( R_0 + \frac{X_{start}}{R_0}x \right) = -\frac{2X_{start}}{cR_0}x \tag{6.7}$$

It is consequently also appropriate to approximate  $\sqrt{H^2 + (X_{start} + x)^2}$  to  $R_0$ . Then the Equation 6.6 can be rewritten as:

$$\begin{aligned}
 R_{BB}[n, i] = & \alpha \cdot \exp \left[ -j \frac{4\pi f_0}{c} \left( R_0 + \frac{\left( y - V \cdot nT_p + \frac{L+Y}{2} \right)^2}{2R_0} \right) \right] \\
 & \cdot \exp \left[ j \frac{\pi B}{T_c} \left( iT_s - \frac{2X_{start}}{cR_0} x - \frac{\left( y - V \cdot nT_p + \frac{L+Y}{2} \right)^2}{cR_0} \right)^2 \right] \\
 & \cdot \exp \left[ -j\pi B \left( iT_s - \frac{2X_{start}}{cR_0} x - \frac{\left( y - V \cdot nT_p + \frac{L+Y}{2} \right)^2}{cR_0} \right) \right] \quad (6.8) \\
 & \cdot \text{rect} \left[ \frac{y - V(nT_p + iT_s + \tau_{min}) + L + \frac{Y}{2}}{L} \right] \\
 & \cdot \text{rect} \left[ \frac{iT_s - \frac{2X_{start}}{cR_0} x - \frac{\left( y - V \cdot nT_p + \frac{L+Y}{2} \right)^2}{cR_0}}{T_c} \right]
 \end{aligned}$$

As a reminder, the objective is to obtain a product of two orthogonal exponentials: one of which depends only on the variables  $x$  and  $i$  and the second only on the variables  $y$  and  $n$ . In the first line of the Equation 6.8, it is already possible to observe the exponential depending only on the variables  $y$  and  $n$ . However, the exponentials of the second line still depend on the four variables. The problem can be solved if the following inequality is respected:

$$\frac{2X_{start}}{cR_0} x \gg \frac{\left( y - V \cdot nT_p + \frac{L+Y}{2} \right)^2}{cR_0} \quad (6.9)$$

As explained previously, the term  $\left( y - V \cdot nT_p + \frac{L+Y}{2} \right)$  can reach a maximum absolute value of  $\frac{L}{2}$ . Looking at the values in the Table 5.4, this inequality becomes:

$$x \gg \frac{L^2}{8X_{start}} = 24.8 \quad [\text{m}] \quad (6.10)$$

The value of  $x$  generally exists in ranges such as  $x \in [0, 50km]$ , so it is rather correct to say that this inequality is valid over almost the whole observed area. The Equation 6.8 can be simplified as follows:

$$R_{BB}[n, i] = \alpha \cdot \exp \left[ -j \frac{4\pi f_0}{c} \left( R_0 + \frac{\left( y - V \cdot nT_p + \frac{L+Y}{2} \right)^2}{2R_0} \right) \right] \cdot \text{rect} \left[ \frac{iT_s - \frac{2X_{start}}{cR_0}x}{T_c} \right] \\ \cdot \exp \left[ j\pi B \left( \frac{\left( iT_s - \frac{2X_{start}}{cR_0}x \right)^2}{T_c} - \left( iT_s - \frac{2X_{start}}{cR_0}x \right) \right) \right] \\ \cdot \text{rect} \left[ \frac{y - V(nT_p + iT_s + \tau_{min}) + L + \frac{Y}{2}}{L} \right] \quad (6.11)$$

The expression of the received signal now corresponds to a product of 2 orthogonal exponential: the columns of the matrix vary only with  $y$  and the rows of this matrix vary only with  $x$ . Therefore, it is possible to perform an independent correlation in both directions. In order to center the result on the marker, the template  $Templ[n, i]$  will be chosen for  $x=y=0$ :

$$Templ[n, i] = \exp \left[ -j \frac{4\pi f_0}{c} \left( R_0 + \frac{\left( -V \cdot nT_p + \frac{L+Y}{2} \right)^2}{2R_0} \right) \right] \cdot \exp \left[ j\pi B \left( \frac{(iT_s)^2}{T_c} - iT_s \right) \right] \\ \cdot \text{rect} \left[ \frac{iT_s}{T_c} \right] \cdot \text{rect} \left[ \frac{-V(nT_p + iT_s + \tau_{min}) + L + \frac{Y}{2}}{L} \right] \quad (6.12)$$

From this expression, it is now possible to identify the 2 signal templates that in fact both correspond to a chirp. These will be named Range chirp  $RC[i]$  and Azimuth chirp  $AC[n]$  according to their associated direction:

$$RC[i] = \exp \left[ j\pi B \left( \frac{(iT_s)^2}{T_c} - iT_s \right) \right] \cdot \text{rect} \left[ \frac{iT_s}{T_c} \right] \quad (6.13)$$

$$AC[n] = \exp \left[ -j \frac{4\pi f_0}{c} \left( R_0 + \frac{\left( -V \cdot nT_p + \frac{L+Y}{2} \right)^2}{2R_0} \right) \right] \cdot \text{rect} \left[ \frac{-V(nT_p + iT_s + \tau_{min}) + L + \frac{Y}{2}}{L} \right] \quad (6.14)$$

### 6.2.1 Range Migration

Performing the 2 successive correlations directly on the raw data would not be entirely correct. Indeed, the distance between the radar and any fixed point on the ground is changing within the synthetic aperture time, this property is called Range Cell Migration (RCM) and its effect can be seen in the figure 6.4.

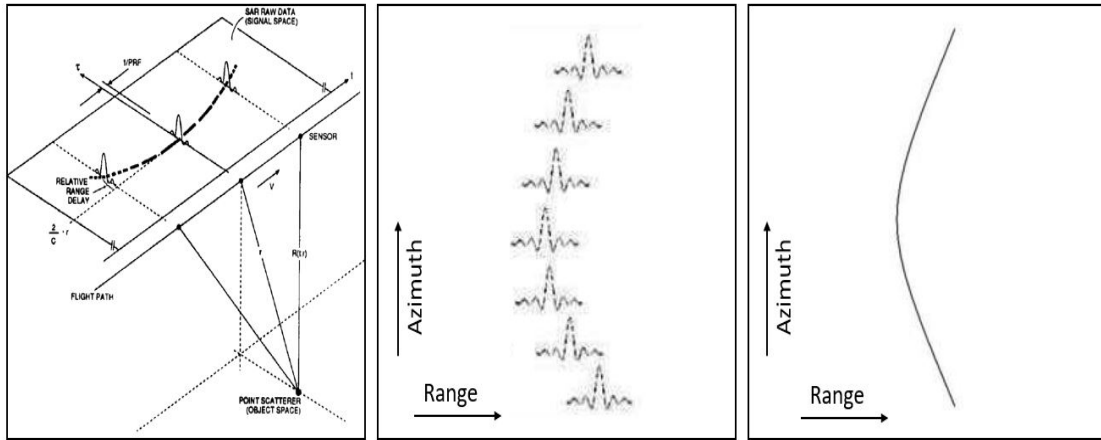


Figure 6.4: Range Cell Migration effect (modified from [53] and [54])

As shown on the illustration on the right, this difference in distance (for a certain target) translates into a curve in the raw data. Data coming from a given target are therefore not aligned on the same column (azimuth direction). However the correlation operation is performed on each column and on each line, if the data are not aligned it will be impossible to perform the focusing in azimuth. It is therefore necessary to straighten the data belonging to the given target on the corresponding column and this operation will be called Range Migration.

In order to perform this operation, a python code has been implemented. The purpose of this code is to calculate for each position  $n$  the difference between the minimum time from which the radar will start receiving signals at this position  $n$  and the minimum time from which the radar will start receiving signals when it is located in the middle of the observed area ( $y=0$  in the figures 5.1 and 5.3). Then the signals received at this position  $n$  are moved by this time difference in the direction of the range. This is why this operation is called range migration, because the signals are migrated in the direction of the range. On the figure 6.5 it is possible to observe the effect of this operation on the raw data.

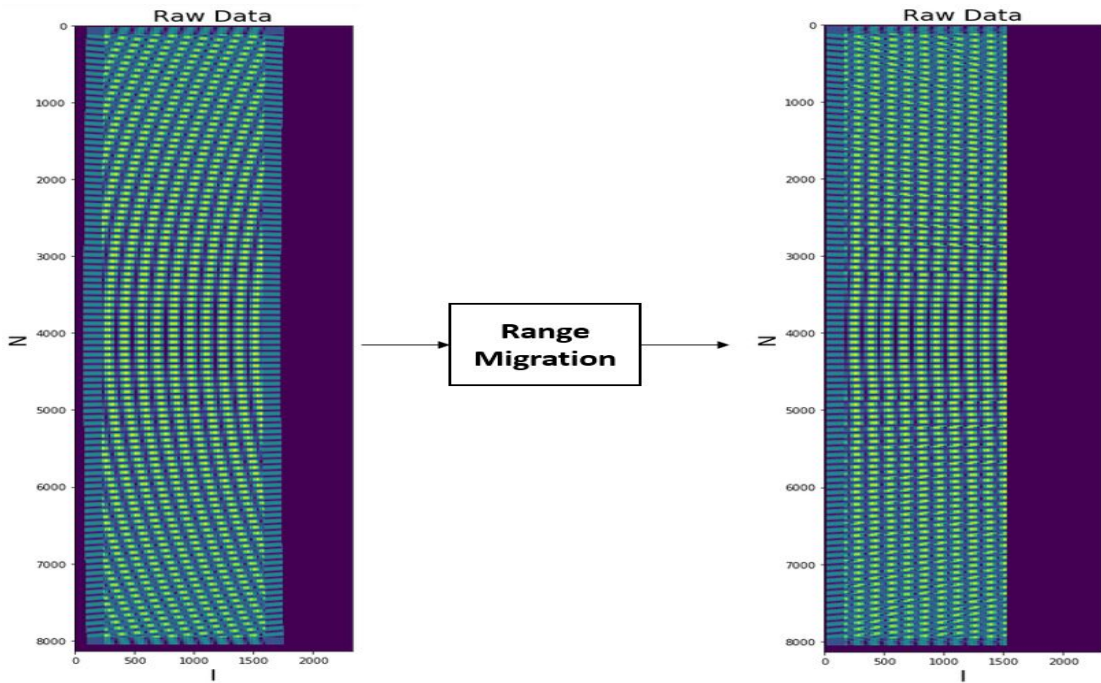


Figure 6.5: Range Migration operation effect

### 6.2.2 Results

In the figure 6.6, it is possible to observe the result obtained by the Image Focusing operation on an area consisting of 4 targets. The targets in the reconstructed image are placed in their correct positions. However, areas of high constructive interference (between the signals corresponding to the different targets) can be observed.

In order to reduce these constructive interference areas, a threshold can be established. After several attempts, the optimal value for this threshold is given by the following relationship:

$$\text{Threshold} = 0.5 \cdot \text{MAXvalue}(\text{RawData}). \quad (6.15)$$

The threshold is therefore half of the largest amplitude in the raw data matrix, so the threshold takes half of the value of the largest backscatter. This choice can be explained by the fact that the difference in amplitude between the interference regions and the areas representing real targets is very large. The result of the Image Focusing operation with threshold is shown in the figure 6.7. It can be seen that the reconstructed image is much less noisy and the targets stand out better.

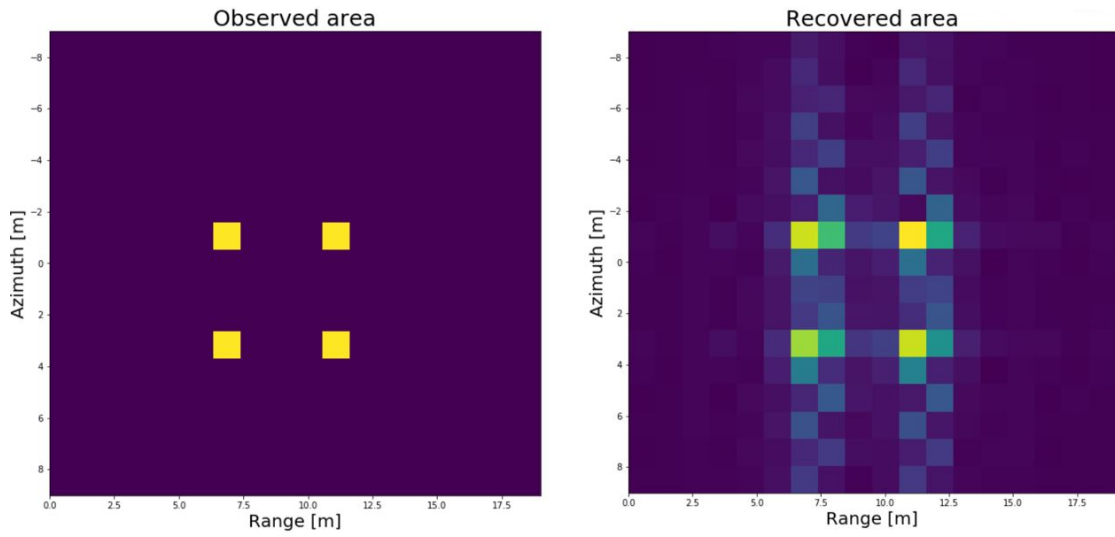


Figure 6.6: Image Focusing operation on an area made up of four targets

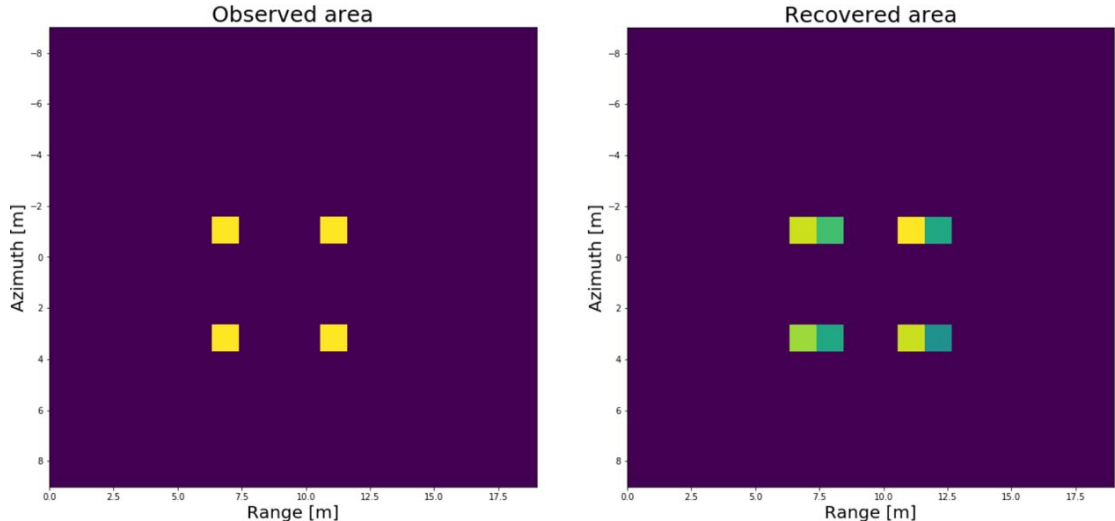


Figure 6.7: Matched filter operation on an area made up of four targets with threshold

It is also interesting to compare the result obtained when the Range Migration operation is performed or not (see figure 6.8). This makes it possible to realize the relevance of this operation. Indeed, on the illustration representing the result obtained without performing the Range Migration operation, a parabolic spread is observable at the targets, which illustrates well the phenomenon of RCM. However, the targets are still well localized.

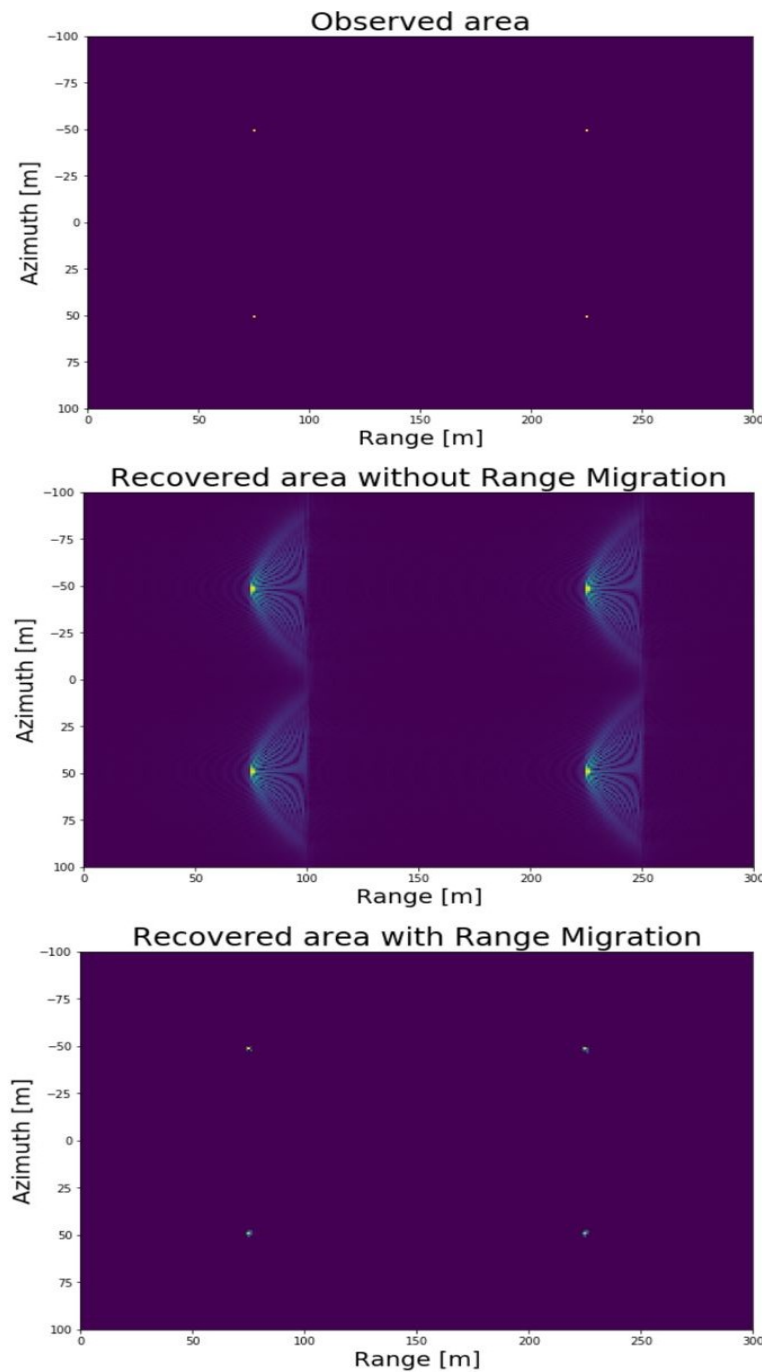


Figure 6.8: Comparison of the result obtained with and without performing the Range Migration operation

## 6.3 Validation and Comparison

It has been shown above that both algorithms allow to recover the targets and to locate them well. Now it is interesting to check if both algorithms allow to reach the 1m x 1m resolution which is one of the main objective of this master thesis.

In order to check if the algorithms allow to reach this resolution, two targets will be located at 1m from each other and the 1m resolution will be validated if it is possible to distinguish the two targets in the reconstructed image. This test will be performed in the direction of the range and azimuth. The two observed areas used for testing can be visualized in the figure 6.9 and 6.10.

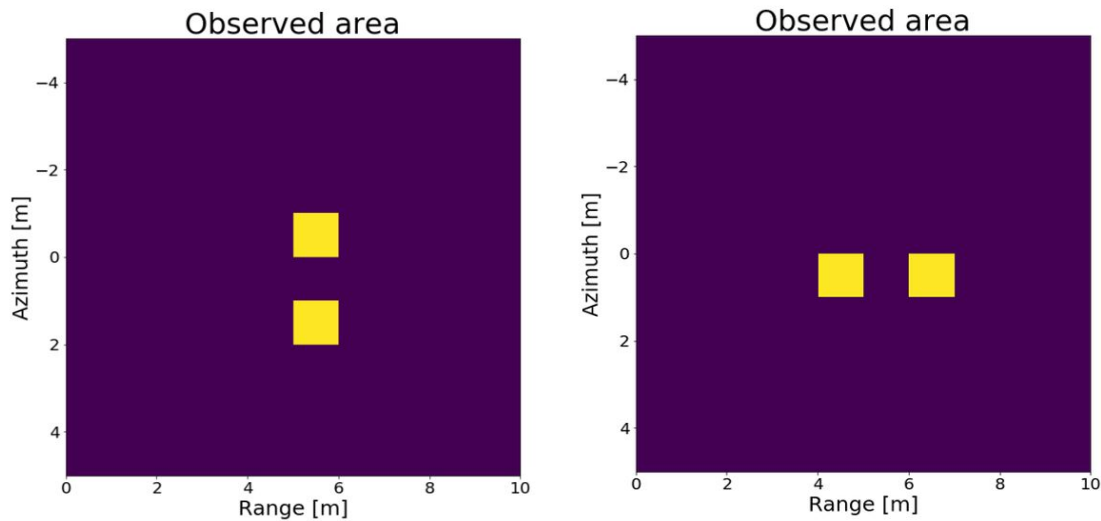


Figure 6.9: Area used for testing the resolution in the azimuth direction

Figure 6.10: Area used for testing the resolution in the range direction

The parameters of the system used to perform these tests are those listed in the Table 5.1.

The results obtained for both directions after performing the Matched Filter operation are available in the figures 6.11 and 6.12 and the results obtained after performing the Image Focusing operation are available in the figures 6.13 and 6.14. As expected, the results obtained by the Matched Filter are better. In the azimuth direction, the two targets are easily distinguishable and well located. In the range direction, the two targets are also distinguishable and well located, but it is possible to observe the appearance of a third target (non-existent in the observed area) of higher intensity between these two targets.

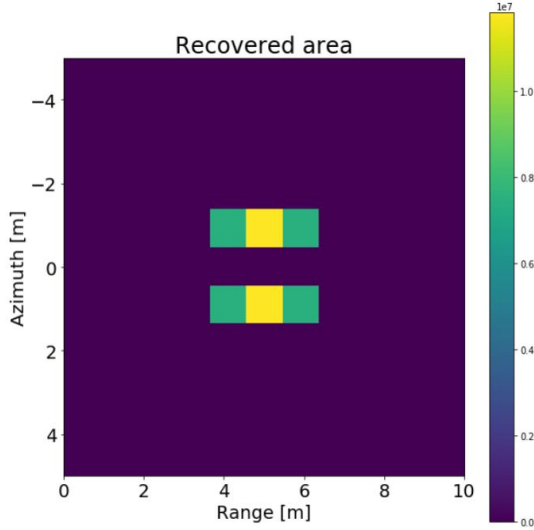


Figure 6.11: Area recovered via Matched filtering operation (azimuth direction)

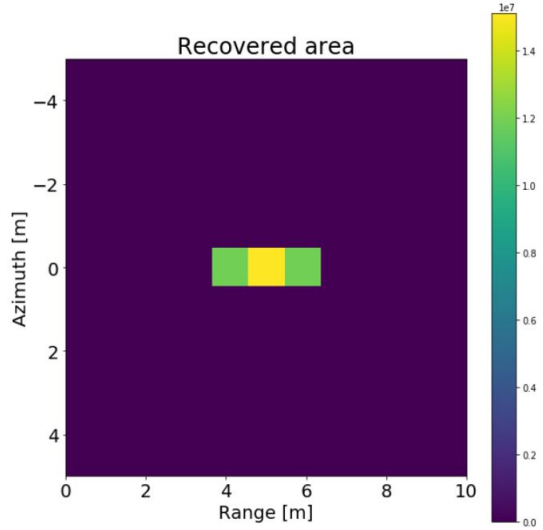


Figure 6.12: Area recovered via Matched filtering operation (range direction)

Regarding the results obtained after Image Focusing, they are less good but far from catastrophic. In the azimuth direction, the two targets are easily distinguishable and well positioned. However, in the range direction, the two targets are not distinguishable and the position of one target is shifted by 1m.

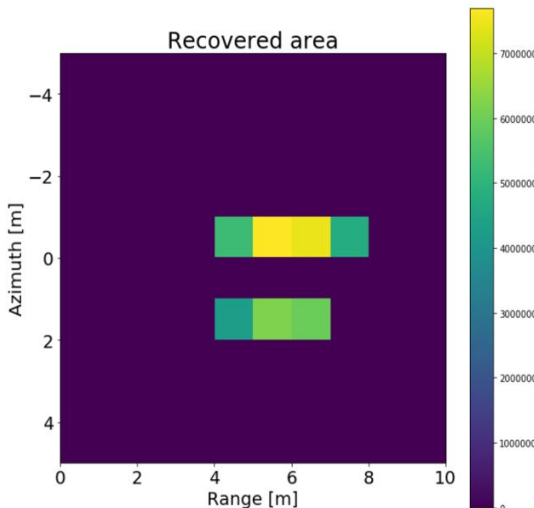


Figure 6.13: Area recovered via Image Focusing operation (azimuth direction)

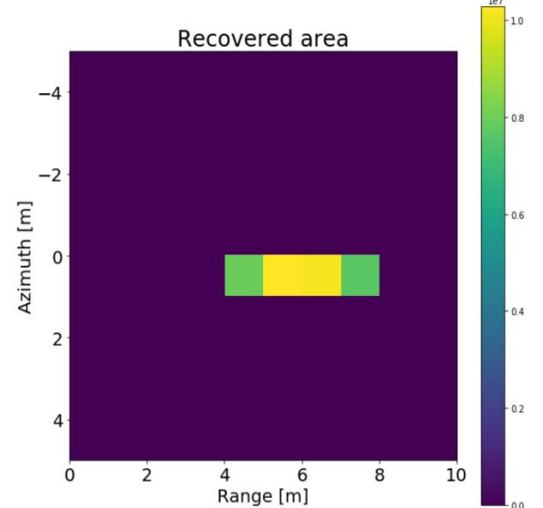


Figure 6.14: Area recovered via Image Focusing operation (range direction)

In these four tests, a spread of information in the range direction can be observed. As a reminder, the parameters were calculated to reach a resolution of 1m, which means that their maximum resolution is also 1m. A second phase of test has been performed with parameters allowing a resolution of  $0.25m$  in the range direction in order to verify if it is indeed the resolution associated with the range that created the spreading in this direction. According to the Equation 4.4, the Bandwidth  $B$  of pulse was multiplied by 4 to obtain this new resolution of  $0.25m$ . The results obtained during this second phase of tests are available in the figures 6.15 and 6.16 for Matched Filtering and in the figures 6.17 and 6.18 for Image Focusing.

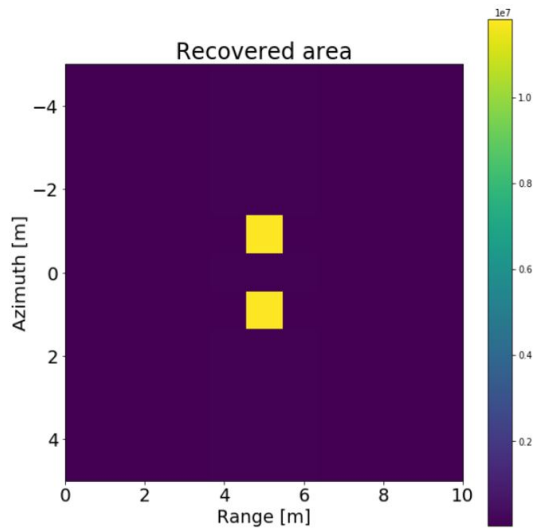


Figure 6.15: Area recovered via Matched filtering operation (azimuth direction)

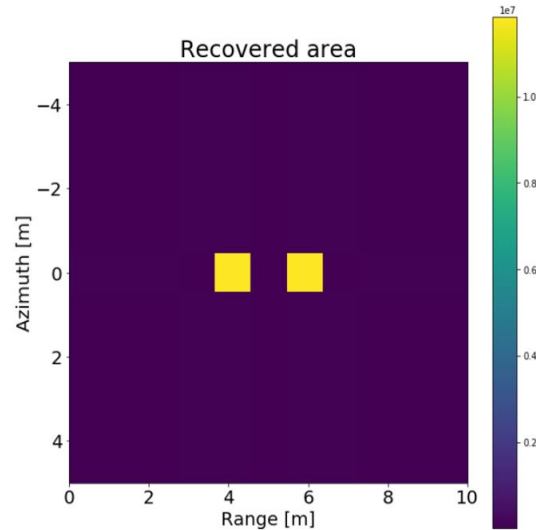


Figure 6.16: Area recovered via Matched filtering operation (range direction)

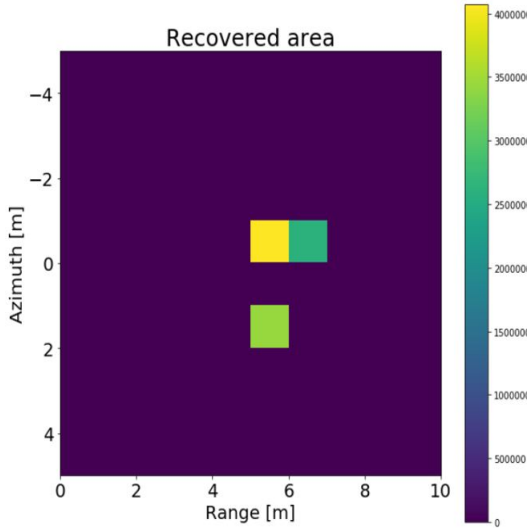


Figure 6.17: Area recovered via Image Focusing operation (azimuth direction)

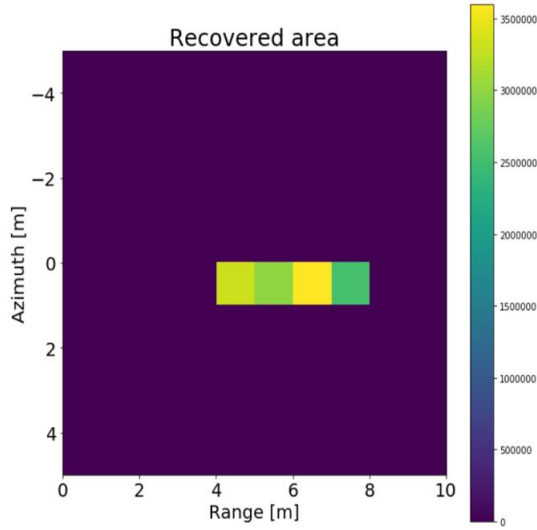


Figure 6.18: Area recovered via Image Focusing operation (range direction)

The results obtained during this second test phase show that the spreading was indeed due to the range resolution. Indeed, now the results obtained after the application of Matched Filtering are perfect: the targets are completely distinguishable and perfectly localized in both directions. The results are also improved after applying Image Focusing because it is now possible to distinguish the two targets in both directions and the targets are well localized but there are still some small traces of interference.

After these tests, it has been demonstrated that the two algorithms achieve a resolution of  $1m \times 1m$  after a small modification of the bandwidth  $B$  of the pulse. It is clear that the Matched Filtering operation produces the best results, but those obtained via Image Focusing meet correctly the  $1m \times 1m$  resolution specification. Considering the difference in computation time the Image Focusing algorithm seems to be extremely interesting.

So far all the tests have been performed on observed areas with a very small number of targets (2 or 4) mainly because generating large area raw data takes a lot of time (several days of simulations with a medium-power computer). Previous tests have therefore allowed to check if the targets were distinguishable and well positioned but these were pretty simple situations with a very limited number of targets. Indeed, an observed area of  $N \times I$  size (in pixels) has  $N \times I$  targets and not only two or four. These tests therefore greatly reduced the possible interactions between the different targets present on the observed area. For these reasons, it was decided to carry out two large simulations. The first one corresponds to a landscape, while the second one corresponds to an airplane cemetery.

The algorithm chosen for these 2 tests is the Image Focusing because it showed that it respected the specification of  $1m \times 1m$  but also because it has a fast execution speed. The computer of the author would not have been able to run the Matched Filtering on such large areas. The results can be seen in the figures 6.19 and 6.20.

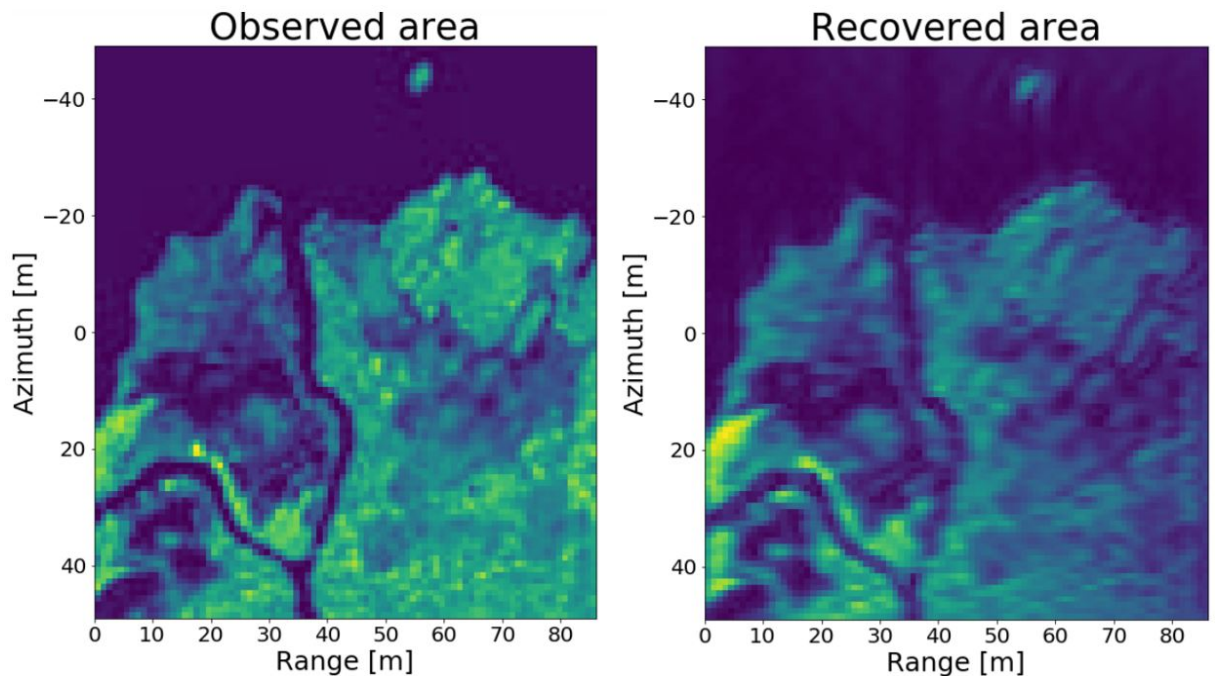


Figure 6.19: Image Focusing test on a landscape (modified from [1])

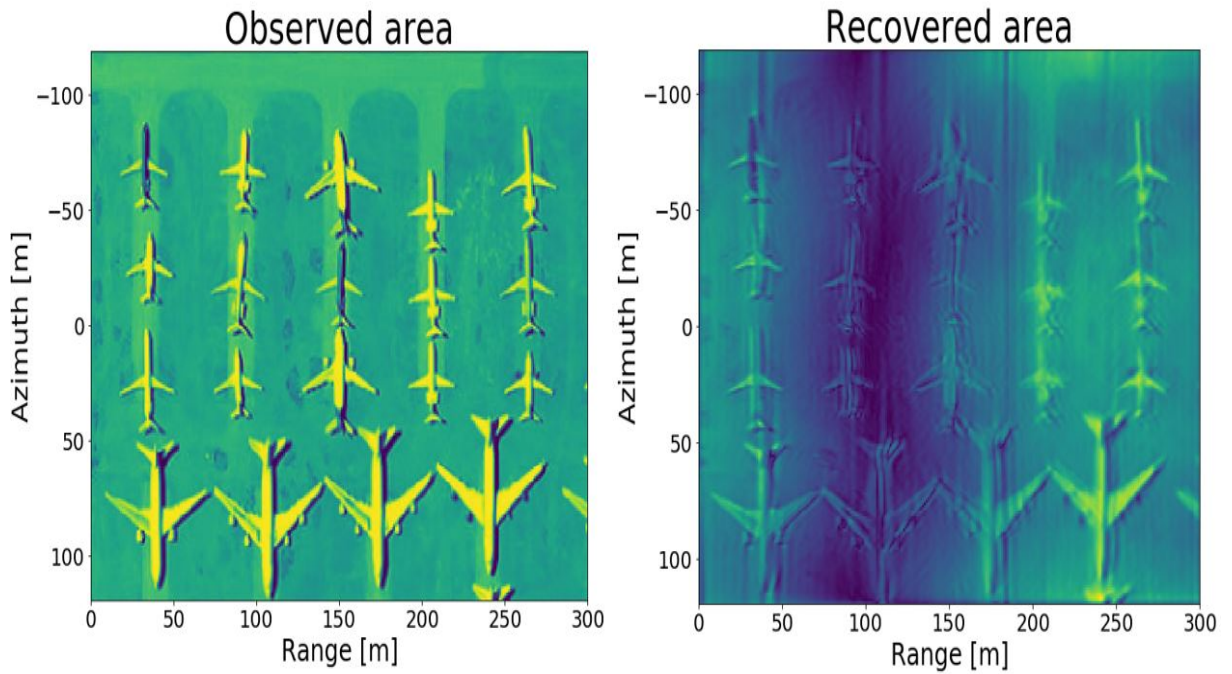


Figure 6.20: Image Focusing test on a airplane graveyard (modified from [55])

The results obtained are very encouraging because the recovered areas strongly resemble the observed areas and on the second figure it is possible to distinguish each aircraft while these are relatively close together. In the figure representing the airplane graveyard, it is also possible to observe areas of lower and higher amplitudes. The exact reason is not known by the author but it could be due to the phenomenon of constructive and destructive interference.

Finally, as already explained in the section 5.4.2, it is important to note that in this master thesis, the raw data are simulated from an image and therefore do not correspond to real radar data. Indeed, the image of the graveyard does not give any information on the fact that the aircraft bodies may reflect the signal better than the ground. As a consequence, the results obtained may not correspond exactly to reality.

# Chapter 7

## Practical design

In this chapter the feasibility of the solution found in this master thesis will be analyzed. The size of the data, the number of operations performed by the algorithms and the choice of physical characteristics will be discussed. This will allow to compare this solution to existing systems. Finally the limitations of the system will also be discussed.

### 7.1 Data size

The size of the data corresponds here to the memory space needed to save the raw data. The memory space is therefore dependent on the size of the raw data matrices. First, it will be necessary to find the expression characterizing the size of the matrices. This one can be found quite easily after reading the section 5.4.2. Indeed, the section indicates that the raw data are of size  $N \times I$  and the expression of these two variables is given as well. The expression of the size of the matrix is thus as follows:

$$\text{Size of the matrix} = N \times I = \frac{L + Y}{VT_p} \cdot \frac{T_c + \tau_{max} - \tau_{min}}{T_s} \quad (7.1)$$

The second step is to translate the size of the matrix in terms of bits. Each element of the matrix is a numpy complex which means that it is represented by 128 bits. Finally, because of readability reasons, the memory space required will be expressed in terms of Go which explains the division by  $8 \cdot 10^9$ . The expression of the required memory space is consequently as follows:

$$\text{Data size} = \frac{\text{Size of the matrix} \cdot 128}{8 \cdot 10^9} \quad (7.2)$$

In order to have a better idea of the memory space required by the system having the characteristics of the Table ?? (and thus a resolution of  $1m \times 1m$ ), the figure

represents the evolution of this value for different area sizes. For example, an area of  $10\text{km} \times 10\text{km}$  requires  $3.38\text{Go}$  of memory while an area of  $100\text{km} \times 100\text{km}$  requires  $219\text{Go}$  of memory. As it is possible to observe in this figure 7.1, for the same resolution, the rate of information received is constant and is  $4.8\text{Go/sec}$ .

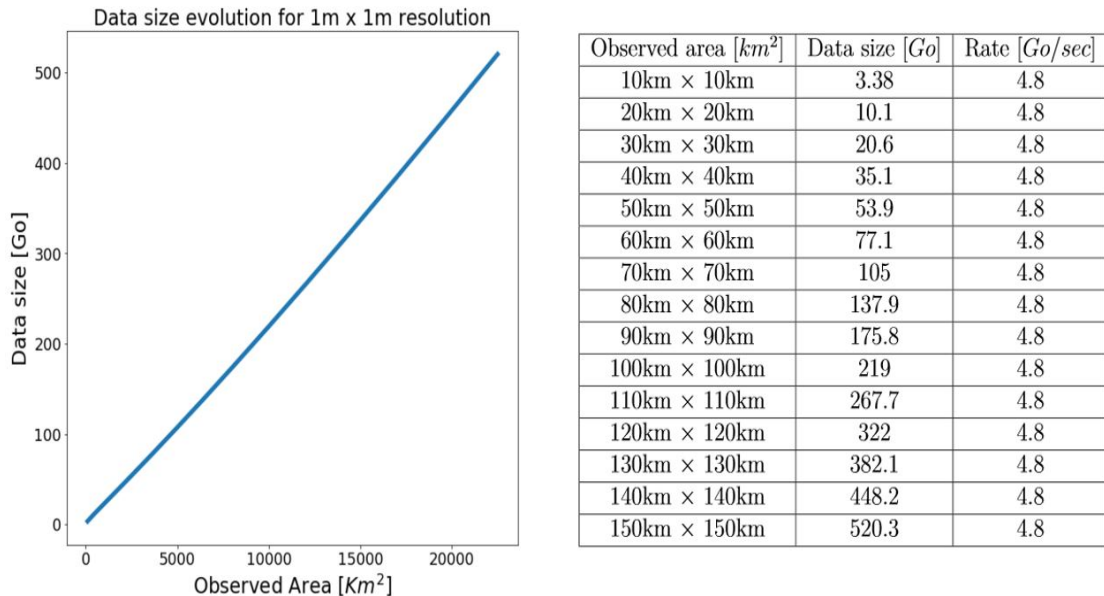


Figure 7.1: Data size evolution for different areas

It is also interesting to know how the required memory space evolves according to the resolution of the system. This can be seen in the figure 7.2 where the calculations have been made for an area of  $100\text{km} \times 100\text{km}$ . The illustration on the left shows that the memory space required increases with the resolution. Indeed, for a resolution of  $15\text{m} \times 15\text{m}$ ,  $1\text{Go}$  is sufficient but for a resolution of  $1\text{m} \times 1\text{m}$   $219\text{Go}$  is required.

## 7.2 Number of operations

The number of operations performed by a system is a very good indicator of computational power and thus makes it possible to characterize the needs of the processor to run such a system. This quantity also makes it possible to determine whether it is possible to carry out the processing directly on board the satellite or whether it is preferable to send the data to a base station in order to benefit from a larger installation and almost unlimited power.

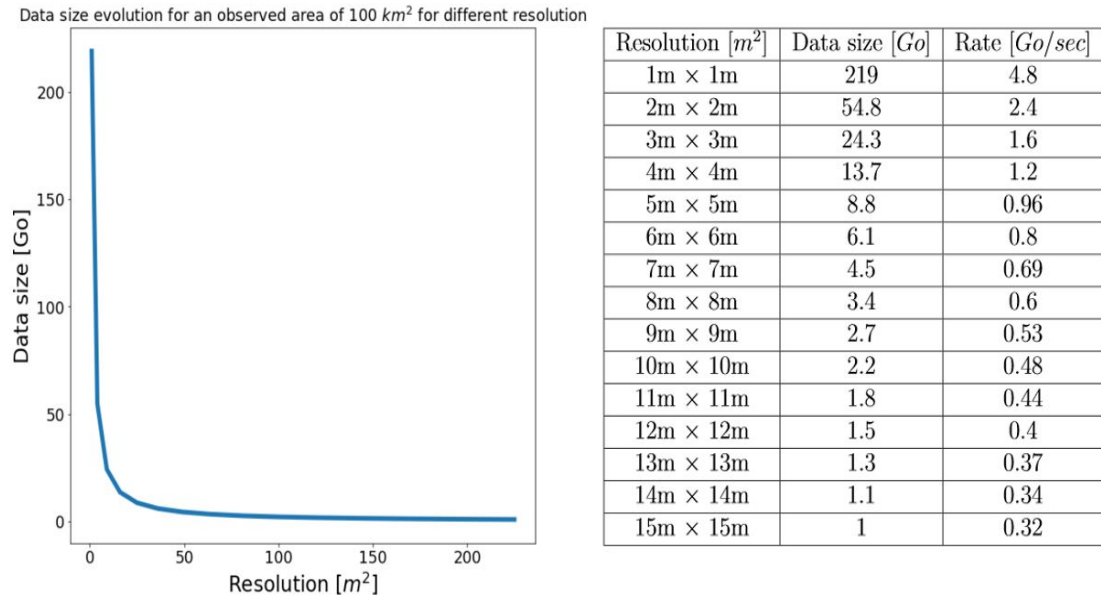


Figure 7.2: Data size evolution for different resolutions

In this section the number of operations performed by the Matched filter and Image Focusing will be studied. This will allow a comparison between them and determine if Image Focusing is really more interesting than the Matched Filter in terms of computational power. Then, it will be interesting to see which ones can be performed or not directly on board the satellite.

In order to determine this number of operations it is necessary to analyse the expression performed by the system. As a reminder, the expression performed by the Matched filter is as follows:

$$\text{Recovered area } [x, y] = |T_{x,y} \cdot \text{RawData}^*| \quad (7.3)$$

where  $T_{x,y}$ 's expression is given by the Equation 6.1. It is therefore possible to notice that for a position  $(x, y)$ , the number of operations is:  $45 \cdot N \cdot I$ .

So, to find the entire observed area, it is necessary to carry out  $X \cdot Y$  times this number of operations. The number of total operations is therefore given by:

$\boxed{\text{Total number of operations for Matched Filter} = 45 \cdot X \cdot Y \cdot N \cdot I} \quad (7.4)$

As a reminder, the expression performed by the Image Focusing algorithm is the following:

$$\text{Focused image} = \text{ifft}_{2D} \left[ \text{fft}_{2D}(\text{RawData}) \cdot \underbrace{(\text{fft}(AC)_{N \times 1} \otimes \text{fft}(RC)_{1 \times I})}_{\text{cst for cst area}} \right] \quad (7.5)$$

The terms  $\text{fft}(RC)$  and  $\text{fft}(AC)$  are uniquely dependent on the size of the observed area (and not on its configuration as is the case for  $\text{rawData}$ ) and on the physical characteristics of the SAR, which are all constant quantities when studying a given system. It is therefore possible to calculate these terms only once and then re-use them for all the areas observed. These two terms can thus be considered as constant and will not affect the number of operations performed by this algorithm.

The operations to be carried out for each different observed surface is therefore the  $\text{ifft}_{2D}$  and the  $\text{fft}_{2D}$ . The number of operations performed by each of these 2 functions is given by the following expressions:

$$\text{fft}_{2D} = N \cdot I \cdot \log(N \cdot I) \text{ operations} \quad (7.6)$$

$$\text{ifft}_{2D} = N \cdot I \cdot \log(N \cdot I) \text{ operations} \quad (7.7)$$

These two operations are carried out successively, the total number of operations is therefore equal to the sum of their respective number of operations.

Hence, the total number of operations performed by the Image Focusing algorithm is given by :

$$\boxed{\text{Total number of operations for Image Focusing} = 2 \cdot N \cdot I \cdot \log(N \cdot I)} \quad (7.8)$$

In order to better realize the difference in computational consumption of the two algorithms, their number of operations performed for a surface identical to that of the figure 6.20 will be compared. For such a surface, the parameters have the following values:

Parameter	Value
N	16117
I	1850
X	300
Y	240

By replacing in the equations 7.4 and 7.8, the number of operations performed is respectively equal to 1026316250 and  $96605.298 \cdot 10^9$ . The Matched Filtering operation therefore requires 94128 times more operations. The interest of the Image Focusing algorithm is thus striking.

### 7.3 Choice of physical parameters

In this section, the Table 7.1 will summarize all the parameters characterizing the system developed during this master thesis. As a reminder, this system has been designed to operate at an orbit of 550km and allow a resolution of 1m x 1m. The algorithm chosen for the processing is Image Focusing for its good resolution, its speed and its reasonable computational power.

Signification	Parameters	Value	Units
Altitude of the satellite	$H$	550	Km
Speed of the satellite	$V$	7570	m/sec
Swath width	$X$	30	Km
Carrier frequency of the pulse	$f_0$	12	Ghz
BandWidth of the pulse	$B$	150	Mhz
Physical antenna length	$l_a$	2	m
Physical antenna height	$h_a$	0.57	m
Angular spread in the azimuth direction	$\phi$	0.0125	radian
Look angle of the radar	$\Theta$	0.52	radian
Period of pulse sampling	$T_s$	$3.33 * 10^{-9}$	sec
Pulse width	$T_c$	$5 * 10^{-6}$	sec
Time duration between 2 chirps	$T_p$	$132.1 * 10^{-6}$	sec
Pulse repetition frequency	$PRF$	7570	Hz
Synthetic aperture	$L$	7938.6	m
Minimal ground range for a target	$X_{start}$	317.542	km
Minimal slant range for a target	$R_0$	635.085	km

Table 7.1: Physical parameters of the system

Looking at the Table 2.2 corresponding to the satellite built by ICeye and situated at more or less the same altitude (570km instead of 550km), it is possible to notice that parameters such as bandwidth  $B$ , PRF, look angle or physical antenna dimensions are in the same range of values. Unfortunately the author has not found any information about the parameters: period of pulse sampling  $T_s$  and pulse width  $T_c$  for this satellite.

These 2 parameters can nevertheless be found in the Table 2.1 corresponding to Sentinel-1. Unlike the previous satellite, the altitude of this satellite is much higher than the one of the model developed during this master thesis. However this does not represent a problem since these parameters are more or less independent of the altitude, they mainly contribute to the choice of the resolution.

Since the resolution is a slightly less good for Sentinel-1, it is still appropriate to compare these parameters between these two satellites. Therefore, it is possible to notice that the period of pulse sampling  $T_s$  is exactly the same and that the pulse width  $T_c$  is in the same order of magnitude.

Following these comparisons, the parameters obtained for the system developed during this master thesis seem to be consistent, which is excellent news.

## 7.4 System limitations

During this master thesis all the different parameters chosen to design the final system were discussed and finally gathered in the Table 7.1.

It is clear that this model is not perfect and that it would have to be modified if it were decided to change the main specificities such as the satellite altitude, the desired resolution or still the frequency used. In this section, it will be discussed the different parameters that present constraints and whose choice should be the result of careful consideration.

### 7.4.1 Optimal Frequency

One of the main characteristics of a SAR is its frequency. As already discussed in the section 3.4, the choice of frequency highlights different properties of the area observed by the radar. Nevertheless, the choice of frequency requires a certain amount of reflection. Indeed, from [56] (Eq 38), it is known that the SNR of the image<sup>1</sup> for constant transmitted power, constant antenna aperture, constant resolution, constant speed and constant system losses is proportional to :

$$\text{SNR}_{\text{image}} \propto f^{n+1} 10^{\frac{-\alpha R}{10}}$$

with  $\alpha$  the atmospheric loss rate and where  $n$  depends on the target type ( $n \in [0, 1]$ ).

From this expression it is easy to see that increasing the frequency increases the SNR. However  $\alpha$  also increases with frequency. Therefore, it is possible to notice that for a given range  $R$ , there exists an optimal frequency to achieve maximum SNR. This means that for a given altitude, a given range and for a given atmosphere, there exists a certain frequency which provides an optimal result.

---

<sup>1</sup>the higher the SNR, the better the image quality achieved

In general, when the range is large and when the weather conditions can be rough, it is preferable to use low frequencies.

It is important to note that criteria other than the SNR can be involved in the choice of frequency, such as the assignment or unavailability of certain hardware.

### 7.4.2 Pulse Repetition Frequency (PRF)

As a reminder, the *PRF* corresponds to the number of pulses emitted per second by the radar. There are two distinct situations: either the radar waits until all echoes have returned before transmitting a second pulse, or the radar emits several pulses before receiving the echo. The second situation is more complex than the first one, as it induces constraints on the range and speed of the radar.

To satisfy the first situation, the following condition must be met:

$$T_c + \frac{2R}{c} \leq \frac{1}{PRF} \quad (7.9)$$

The maximum range that meets this equation is called the unambiguous range [56]. For a constant *PRF* and pulse width  $T_c$ , the first situation is therefore limited in the range. The second situation makes it possible to overcome this limitation and this explains why it is generally preferred in the case of satellite-borne radars.

However, this second option also has limitations. The fact that several pulses are emitted before all the echoes are received leads to ambiguity in the range determination. This ambiguity can be partially resolved by pulse coding. But this does not entirely solve the ambiguity problem, since this problem may also be caused by reflector surfaces that are sufficiently strong to overcome the attenuation of the radar beam.

A reflector that is often troublesome in orbital systems is the nadir point. Since in echo-radar systems the receivers do not listen when the radar is still transmitting, it would be a good idea that when the echo corresponding to the nadir point arrives the radar is still transmitting. This solution enables the pulse width to be increased (in order to increase the SNR and thus improve the image quality) without amplifying the nadir point problem (the echo is always at least longer than the transmitted pulse). However, this last solution creates restrictions in the geometry of the system.

Another condition that the PRF must respect is that it must be equal to or higher than the Doppler bandwidth  $B_D$  in order to limit aliasing. As shown in the section 4.3, the Doppler beam expression is given by:

$$B_D = \frac{2V\phi}{\lambda} \quad (7.10)$$

And during the section 5.2 it was also said that:  $\phi = \frac{\lambda}{l_a}$ . The PRF must also comply with the following equation:

$$PRF \geq \frac{2V}{l_a} \quad (7.11)$$

From this expression, it can be seen that the PRF is independent of the frequency used by the radar and is inversely proportional to the length of the real aperture  $l_a$ . By looking again at the expression 7.9, it can be noticed that an increase of the real aperture length  $l_a$  results in an increase of the unambiguous range.

Finally the PRF also has an impact on the azimuth resolution as shown in the Equation 5.20 where it is possible to notice that the resolution improves as the PRF increases.

### 7.4.3 Sampling frequency

The choice of sampling frequency  $f_s$  is also constrained by certain conditions. The first is that to meet the Nyquist criterion, the sampling frequency must meet the following equation:

$$f_s \geq B_{IF} \quad (7.12)$$

where  $B_{IF}$  is the IF bandwidth of the SAR [56].

Then the Equation 5.18 shows that for a given number of samples  $I$  (for a single pulse), the pulse period is inversely proportional to the sampling rate. As can be seen from the Equations 7.8 and 7.1, the parameter  $I$  could be limited by the power consumption and the memory space available on the SAR. Finally, from the Equation 5.22 it is possible to notice that increasing the sampling frequency improves the range limit resolution.

In order to maximize the resolution in the range, the designer of the SAR might be tempted to choose a very high sampling frequency  $f_s$ . However, this choice would induce a reduction of the pulse period  $T_c$  (for a fixed  $I$ ) which would have the consequence of limiting the range of the SAR.

#### 7.4.4 Extending Range

The range that can be reached by a SAR device is a function of many parameters. In the previous sections some parameters limiting the unambiguous range have already been discussed. But the ability to reach a certain range also depends on the SNR; a range is achievable when the corresponding SNR is sufficiently large. Unfortunately the maximization of the SNR is sometimes done at the expense of the resolution.

Indeed, an effective way to increase the SNR is to increase the average transmitted power. From [56] (Eq 66), it can be seen that, for a given transmission power, the average power increases with *PRF* and pulse width. However, the *PRF* is limited by the range requirement and as explained in the previous section for a fixed *I*, the increase in pulse width induces a decrease in range resolution.

Another way to improve the SNR is to increase the size of the actual antenna. However, from the Equation 4.3 it is quickly noticed that an increase in length would lead to a decrease in range resolution and knowing that  $\alpha = \frac{\lambda}{h_a}$  (as explained in the section 5.2), an increase in height would lead to a decrease in the width of the observable swath.

Average atmospheric losses decrease with altitude. Increasing the satellite altitude would improve the SNR and thereby allow a longer range to be achieved. Combining this solution with an optimal choice of frequency, which would further reduce atmospheric losses, would make it possible to reach a greater range.

Finally, the range can be extended by improving the hardware systems on board the satellite (reduction of radar losses, processing losses or noise reduction), which will improve the SNR significantly.

# Chapter 8

## Conclusion

### 8.1 Summary of contributions

During the course of this master thesis, many topics were discussed to provide a good understanding of the operating principle of SAR.

First, the history of SARs and their performance was discussed in order to set the context (discoveries, events) in which SARs were developed. This allows a clear understanding of the benefits of this system and explains why it is important to further develop it.

In a second step, many topics concerning the operation of radars were discussed in order to provide the reader with a good knowledge basis for understanding how SARs operate. Once this knowledge has been established, it was explained how SAR systems work and how they greatly increase azimuth resolution.

Then the mathematical model of SAR was studied and developed to meet the desired specifications: an altitude of 550km and a resolution of 1m x 1m. In order to validate the results, a python simulator was implemented. The objective of this tool is to generate SAR data from a system whose specifications have been entered into the simulator. This tool is necessary in the development of a SAR system because the desired characteristics are sometimes new and therefore do not correspond to a system already in operation. As a result, it is impossible to test the system on real radar data. It is important to note that the data generated by this simulator does not fully correspond to real SAR data since it is made from 2D images (as explained in the section). However, the data generated does illustrate the SAR operating principle and validates some assumptions.

After the data acquisition, it is obviously the data processing process that has been studied. More precisely two algorithms were developed and then tested. The first one consists in a simple Matched Filtering, the second one, which is more complex, requires several approximations and is called Image Focusing. Both algorithms were tested using the data generated by the simulator. From these tests, it was shown that both algorithms were able to achieve the desired resolution of 1m x 1m. The results of Matched Filtering are obviously better than those obtained using Image Focusing, but the processing time is much longer. Due to the fact that its calculation time is very fast compared to Matched Filtering and that the results obtained are good enough, Image Focusing seems to be a good solution to process images directly on board the satellite.

Finally, the practical implementation has been discussed. The memory space required for data acquisition and the computational power needed to implement both algorithms were studied. A table gathering all the parameters constituting the system developed during the paper is accessible and allows to compare the developed system with existing systems. Finally, the various limitations of such a system have been presented.

To conclude, this work allows the reader to have an overview of the functioning and processing of a SAR system, to make design choices that allow to reach a desired resolution and to become aware of the limits of such a system. Through this work, the author hopes to have convinced of the usefulness of SARs and thus to have promoted their development in order to fight even more effectively against climate change.

## 8.2 Further research directions

The models developed in this paper have only been tested on data generated by the simulator. It would be very interesting to test these models on real radar data in order to test their real performances. Similarly, it would be nice to improve the simulator in order to bring the data closer to reality. A first small improvement could be to add a random phase to the starting 2D image. Then this 2D image could be replaced by a 3D image which would allow to simulate some effects such as shadowing or layover. Finally it would be great to add an interpretation of the image that simulates the backscatter with properties (amplitude, phase, polarization) that correspond to the type of targets displayed on the image.

It would also be interesting to improve the data processing process by adding for example pulse coding, filters, speeckle reduction, etc. and also to implement new applications such as interferometry or new modes such as Spotlight.

On a general note, it is desirable that research and development in this field continue in order to further improve the resolution, coverage and revisit time (by realizing large constellations of small satellites) of SARs. This would allow the emergence of a large number of new applications such as real-time traffic monitoring.

# Bibliography

- [1] College EO. *Echoes in space*. URL: <https://eo-college.org/courses/echoes-in-space/> (visited on 05/02/2020).
- [2] *Space in climate change*. en. Library Catalog: www.esa.int. URL: [https://www.esa.int/Applications/Observing\\_the\\_Earth/Space\\_for\\_our\\_climate/Space\\_in\\_climate\\_change](https://www.esa.int/Applications/Observing_the_Earth/Space_for_our_climate/Space_in_climate_change) (visited on 07/30/2020).
- [3] Hua-Dong Guo, Li Zhang, and Lan-Wei Zhu. “Earth observation big data for climate change research”. en. In: *Advances in Climate Change Research*. Special issue on advances in Future Earth research 6.2 (June 2015), pp. 108–117. ISSN: 1674-9278. DOI: 10.1016/j.accre.2015.09.007. URL: <http://www.sciencedirect.com/science/article/pii/S1674927815000519> (visited on 07/30/2020).
- [4] *Optics or Radars? What is Better for the Earth Observation Purposes?* - Defence24.com. Library Catalog: www.defence24.com. URL: <https://www.defence24.com/optics-or-radars-what-is-better-for-the-earth-observation-purposes> (visited on 07/30/2020).
- [5] Thomas Lillesand, Ralph W. Kiefer, and Jonathan Chipman. *Remote Sensing and Image Interpretation*. en. Google-Books-ID: AFHDCAAAQBAJ. John Wiley & Sons, Feb. 2015. ISBN: 978-1-118-34328-9.
- [6] John F. Vesecky and Robert H. Stewart. “The observation of ocean surface phenomena using imagery from the SEASAT synthetic aperture radar: An assessment”. en. In: *Journal of Geophysical Research* 87.C5 (1982), p. 3397. ISSN: 0148-0227. DOI: 10.1029/JC087iC05p03397. URL: <http://doi.wiley.com/10.1029/JC087iC05p03397> (visited on 05/03/2020).
- [7] *SIR - eoPortal Directory - Satellite Missions*. URL: <https://eoportal.org/web/eoportal/satellite-missions/s/sir> (visited on 05/03/2020).
- [8] *Echoes in space – EO College*. URL: <https://eo-college.org/courses/echoes-in-space/> (visited on 05/01/2020).
- [9] *ERS-1 - eoPortal Directory - Satellite Missions*. URL: <https://eoportal.org/web/eoportal/satellite-missions/e/ers-1> (visited on 05/03/2020).

- [10] *SRTM - eoPortal Directory - Satellite Missions*. URL: <https://eoportal.org/web/eoportal/satellite-missions/s/srtm> (visited on 05/03/2020).
- [11] Fotios Stathopoulos et al. “Evolving the Operations of the TerraSAR-X / TanDEM-X Mission Planning System during the TanDEM-X Science Phase”. en. In: *SpaceOps 2016 Conference*. Daejeon, Korea: American Institute of Aeronautics and Astronautics, May 2016. ISBN: 978-1-62410-426-8. DOI: 10.2514/6.2016-2571. URL: <http://arc.aiaa.org/doi/10.2514/6.2016-2571> (visited on 05/03/2020).
- [12] *Copernicus: Sentinel-1 - Satellite Missions - eoPortal Directory*. URL: <https://directory.eoportal.org/web/eoportal/satellite-missions/c-missions/copernicus-sentinel-1> (visited on 05/03/2020).
- [13] Craig Stringham et al. “The Capella X-band SAR Constellation for Rapid Imaging”. In: *IGARSS 2019 - 2019 IEEE International Geoscience and Remote Sensing Symposium*. Yokohama, Japan: IEEE, July 2019, pp. 9248–9251. ISBN: 978-1-5386-9154-0. DOI: 10.1109/IGARSS.2019.8900410. URL: <https://ieeexplore.ieee.org/document/8900410/> (visited on 08/02/2020).
- [14] Daniel Selva and David Krejci. “A survey and assessment of the capabilities of Cubesats for Earth observation”. en. In: *Acta Astronautica* 74 (May 2012), pp. 50–68. ISSN: 00945765. DOI: 10.1016/j.actaastro.2011.12.014. URL: <https://linkinghub.elsevier.com/retrieve/pii/S0094576511003742> (visited on 08/02/2020).
- [15] *The global race for space radar means this year's satellites need twice the power*. URL: [https://sports.yahoo.com/global-race-space-radar-means-123029381.html?guce\\_referrer=aHR0cHM6Ly93d3cuZ29vZ2x1LmNvbS8&guce\\_referrer\\_sig=AQAAAEx1YXDyV7qx5R-0ea1CeUTJ4ufWFiPwlrvHc2C\\_VNeuzudg27w2VhWD4rJbn\\_gDZSPSh5Bfd2FZdJJim5Y1Az\\_kZpzwtNr\\_oqH503LUU0JAnbHGUAwJWu](https://sports.yahoo.com/global-race-space-radar-means-123029381.html?guce_referrer=aHR0cHM6Ly93d3cuZ29vZ2x1LmNvbS8&guce_referrer_sig=AQAAAEx1YXDyV7qx5R-0ea1CeUTJ4ufWFiPwlrvHc2C_VNeuzudg27w2VhWD4rJbn_gDZSPSh5Bfd2FZdJJim5Y1Az_kZpzwtNr_oqH503LUU0JAnbHGUAwJWu) (visited on 08/02/2020).
- [16] *Congratulations ICEYE & Capella Space!* en-US. Library Catalog: syntheticapertureradar.com. URL: <http://syntheticapertureradar.com/congratulations-iceye-capella-space/> (visited on 08/02/2020).
- [17] *Capella Space gets ready for primetime as constellation operator*. en-US. Library Catalog: spacenews.com. June 2019. URL: <https://spacenews.com/capella-space-gets-ready-for-primetime-as-constellation-operator/> (visited on 08/02/2020).

- [18] *Sentinel-1 Product Specification - Sentinel 1 SAR Document Library - User Guides - Sentinel Online*. URL: [https://sentinel.esa.int/web/sentinel/user-guides/sentinel-1-sar/document-library/-/asset\\_publisher/1d07RF5fJMbd/content/sentinel-1-product-specification](https://sentinel.esa.int/web/sentinel/user-guides/sentinel-1-sar/document-library/-/asset_publisher/1d07RF5fJMbd/content/sentinel-1-product-specification) (visited on 08/01/2020).
- [19] *Download: Product Documents*. URL: <https://www.iceye.com/downloads/product-documents> (visited on 08/01/2020).
- [20] Héloïse Pons. *ICEYE veut déployer « la plus grande constellation de satellites au monde »*. fr. Library Catalog: www.lepoint.fr. Dec. 2018. URL: [https://www.lepoint.fr/sciences-nature/iceye-veut-deployer-la-plus-grande-constellation-de-satellites-au-monde-05-12-2018-2276961\\_1924.php](https://www.lepoint.fr/sciences-nature/iceye-veut-deployer-la-plus-grande-constellation-de-satellites-au-monde-05-12-2018-2276961_1924.php) (visited on 08/03/2020).
- [21] *Capella Space*. en-US. Library Catalog: spaceflight.com. URL: <https://spaceflight.com/sp-customers/customer-2/> (visited on 08/03/2020).
- [22] Encyclopædia Universalis. *RADAR*. fr-FR. Library Catalog: www.universalis.fr. URL: <https://www.universalis.fr/encyclopedie/radar/> (visited on 05/09/2020).
- [23] *Onde électromagnétique*. fr. Page Version ID: 170457900. May 2020. URL: [https://fr.wikipedia.org/w/index.php?title=Onde\\_%C3%A9lectromagn%C3%A9tique&oldid=170457900](https://fr.wikipedia.org/w/index.php?title=Onde_%C3%A9lectromagn%C3%A9tique&oldid=170457900) (visited on 05/10/2020).
- [24] Ruhani Walia. *Curtain Call for Cables*. en. Library Catalog: medium.com. Mar. 2020. URL: <https://medium.com/@ruhani.walia/curtain-call-for-cables-bcb38bdfc56> (visited on 07/23/2020).
- [25] nccacoatnotes. *UV Light—Slicing and Dicing the Light That Can't Be Seen*. en. Library Catalog: nccacoatnotes.com. Mar. 2018. URL: <https://nccacoatnotes.com/2018/03/19/uv-light-slicing-and-dicing-the-light-that-cant-be-seen/> (visited on 07/23/2020).
- [26] *Radar*. fr. Page Version ID: 169906259. Apr. 2020. URL: <https://fr.wikipedia.org/w/index.php?title=Radar&oldid=169906259> (visited on 05/11/2020).
- [27] *Radar Tutoriel - Ondes et bandes de fréquences*. fr. Library Catalog: www.radartutorial.eu. Publisher: Dipl.-Ing. (FH) Christian Wolff. URL: <https://www.radartutorial.eu/07.waves/Ondes%20et%20bandes%20de%20fr%C3%A9quences.fr.html> (visited on 05/11/2020).

- [28] (*PDF*) *Early Warning Against Stealth Aircraft, Missiles and Unmanned Aerial Vehicles*. en. Library Catalog: www.researchgate.net. URL: [https://www.researchgate.net/publication/321082973\\_Early\\_Warning\\_Against\\_Stealth\\_Aircraft\\_Missiles\\_and\\_Unmanned\\_Aerial\\_Vehicles](https://www.researchgate.net/publication/321082973_Early_Warning_Against_Stealth_Aircraft_Missiles_and_Unmanned_Aerial_Vehicles) (visited on 07/23/2020).
- [29] *Radar Systems - an overview / ScienceDirect Topics*. URL: <https://www.sciencedirect.com/topics/engineering/radar-systems> (visited on 05/12/2020).
- [30] Jonah Gamba. *Radar Signal Processing for Autonomous Driving*. en. Signals and Communication Technology. Singapore: Springer Singapore, 2020. ISBN: 9789811391927 9789811391934. DOI: 10.1007/978-981-13-9193-4. URL: <http://link.springer.com/10.1007/978-981-13-9193-4> (visited on 05/15/2020).
- [31] *Radar Tutoriel - L'Equation du Radar*. fr. Library Catalog: www.radartutorial.eu Publisher: Dipl.-Ing. (FH) Christian Wolff. URL: <https://www.radartutorial.eu/01.basics/L%27Equation%20du%20Radar.fr.html> (visited on 05/15/2020).
- [32] *Radar Tutoriel - Effet Doppler-Fizeau*. fr. Library Catalog: www.radartutorial.eu Publisher: Dipl.-Ing. (FH) Christian Wolff. URL: <https://www.radartutorial.eu/11.coherent/co06.fr.html> (visited on 05/16/2020).
- [33] *Imaging radar*. en. Page Version ID: 943642148. Mar. 2020. URL: [https://en.wikipedia.org/w/index.php?title=Imaging\\_radar&oldid=943642148](https://en.wikipedia.org/w/index.php?title=Imaging_radar&oldid=943642148) (visited on 05/16/2020).
- [34] *remote sensing - What are the differences between down-looking and side looking radar?* Library Catalog: earthscience.stackexchange.com. URL: <https://earthscience.stackexchange.com/questions/19028/what-are-the-differences-between-down-looking-and-side-looking-radar> (visited on 07/23/2020).
- [35] *Bestand:Zenith-Nadir-Horizon.svg - Wikibooks*. URL: <https://nl.m.wikibooks.org/wiki/Bestand:Zenith-Nadir-Horizon.svg> (visited on 07/23/2020).
- [36] *Geometry Glossary*. URL: <https://earth.esa.int/handbooks/asar/CNTR5-5.html> (visited on 07/23/2020).
- [37] Natural Resources Canada. *Radar Image Distortions*. eng. Last Modified: 2015-11-20 Library Catalog: www.nrcan.gc.ca Publisher: Natural Resources Canada. Jan. 2008. URL: <https://www.nrcan.gc.ca/maps-tools-publications/satellite-imagery-air-photos/remote-sensing-tutorials/microwave-remote-sensing/radar-image-distortions/9325> (visited on 05/20/2020).

- [38] *Radar Course 3 - Real Aperture Radar - ERS Radar Course 3 - ESA Operational EO Missions - Earth Online - ESA*. URL: [https://earth.esa.int/web/guest/missions/esa-operational-eo-missions/ers/instruments/sar/applications/radar-courses/content-3/-/asset\\_publisher/mQ9R7ZVkKg5P/content/radar-course-3-real-aperture-radar](https://earth.esa.int/web/guest/missions/esa-operational-eo-missions/ers/instruments/sar/applications/radar-courses/content-3/-/asset_publisher/mQ9R7ZVkKg5P/content/radar-course-3-real-aperture-radar) (visited on 05/17/2020).
- [39] *Radar Course 2 - Real Aperture Radar - Course 2 - ERS Radar Courses - ESA Operational EO Missions - Earth Online - ESA*. URL: [https://earth.esa.int/web/guest/missions/esa-operational-eo-missions/ers/instruments/sar/applications/radar-courses/content-2/-/asset\\_publisher/qIBc6NYRXfnG/content/radar-course-2-real-aperture-radar](https://earth.esa.int/web/guest/missions/esa-operational-eo-missions/ers/instruments/sar/applications/radar-courses/content-2/-/asset_publisher/qIBc6NYRXfnG/content/radar-course-2-real-aperture-radar) (visited on 07/23/2020).
- [40] Ya-Qiu Jin and Feng Xu. *Polarimetric scattering and SAR information retrieval*. en. Singapore: IEEE / Wiley, 2013. ISBN: 978-1-118-18816-3 978-1-118-18815-6 978-1-118-18817-0.
- [41] *Level 1B Products*. URL: <https://earth.esa.int/handbooks/asar/CNTR2-6.html> (visited on 07/23/2020).
- [42] *Radar Tutoriel - Affinement Doppler du faisceau*. fr. Library Catalog: www.radartutorial.eu Publisher: Dipl.-Ing. (FH) Christian Wolff. URL: <https://www.radartutorial.eu/20.airborne/ab05.fr.html> (visited on 07/23/2020).
- [43] Bastian Wahyudi. "SIMULASI ANTENA MIKROSTRIP POLARISASI MELINGKAR UNTUK CIRCULARLY POLARIZED - SYNTHETIC APERATURE RADAR (CP -SAR) PROGRAM STUDI FISIKA FMIPA UNP". id. In: (), p. 8.
- [44] (*PDF*) *Satellite Oceanography from the ERS Synthetic Aperture Radar and Radar Altimeter: A Brief Review*. en. Library Catalog: www.researchgate.net. URL: [https://www.researchgate.net/publication/312878984\\_Satellite\\_Oceanography\\_from\\_the\\_ERS\\_Synthetic\\_Aperture\\_Radar\\_and\\_Radar\\_Altimeter\\_A\\_Brief\\_Review](https://www.researchgate.net/publication/312878984_Satellite_Oceanography_from_the_ERS_Synthetic_Aperture_Radar_and_Radar_Altimeter_A_Brief_Review) (visited on 07/23/2020).
- [45] J.A. Johannessen and F. Collard. *3rd ESA Advanced Training Course on Ocean Remote Sensing 2013*. en-US. Library Catalog: eo4society.esa.int. URL: <https://eo4society.esa.int/event/3rd-esr-advanced-training-on-ocean-remote-sensing-2013/> (visited on 05/19/2020).
- [46] *Introduction to Microwave Remote sensing - ppt video online download*. Library Catalog: slideplayer.com. URL: <https://slideplayer.com/slide/6866701/> (visited on 05/20/2020).
- [47] *Synthetic Aperture Radar - Wikiwand*. URL: [https://www.wikiwand.com/de/Synthetic\\_Aperture\\_Radar](https://www.wikiwand.com/de/Synthetic_Aperture_Radar) (visited on 07/23/2020).

- [48] Alberto Moreira et al. “A tutorial on synthetic aperture radar”. en. In: *IEEE Geoscience and Remote Sensing Magazine* 1.1 (Mar. 2013), pp. 6–43. ISSN: 2168-6831. DOI: 10.1109/MGRS.2013.2248301. URL: <http://ieeexplore.ieee.org/document/6504845/> (visited on 05/20/2020).
- [49] *Synthetic-aperture radar*. en. Page Version ID: 954977354. May 2020. URL: [https://en.wikipedia.org/w/index.php?title=Synthetic-aperture\\_radar&oldid=954977354](https://en.wikipedia.org/w/index.php?title=Synthetic-aperture_radar&oldid=954977354) (visited on 05/22/2020).
- [50] Michael Foumelis. *Amatrice Earthquake - Sentinel-1 TOPS Ascending - Differential Interferogram (S1A\_20160815-S1A\_20160827)*. type: dataset. Oct. 2016. DOI: 10.5281/zenodo.165497. URL: <https://zenodo.org/record/165497#.XxmxDuc69PY> (visited on 07/23/2020).
- [51] Dr Armin Doerry. “Introduction to Synthetic Aperture Radar”. en. In: (), p. 81.
- [52] *Matched filter*. en. Page Version ID: 959188940. May 2020. URL: [https://en.wikipedia.org/w/index.php?title=Matched\\_filter&oldid=959188940](https://en.wikipedia.org/w/index.php?title=Matched_filter&oldid=959188940) (visited on 07/03/2020).
- [53] Samiur Rahman. “Focusing Moving Targets Using Range Migration Algorithm in Ultra Wideband Low Frequency Synthetic Aperture Radar”. en. In: (), p. 52.
- [54] R. Keith Raney et al. *Precision SAR processing using chirp scaling*. en. Library Catalog: www.semanticscholar.org. 1994. URL: /paper/Precision-SAR-processing-using-chirp-scaling-Raney-Runge/7204441181b74ece91f442291c74fc76e7figure/0 (visited on 07/23/2020).
- [55] *Aircraft Boneyard in Victorville Airport, California / Pictures From Above*. en-US. Library Catalog: fromabove.altervista.org. Dec. 2018. URL: <https://fromabove.altervista.org/picture-229/> (visited on 07/24/2020).
- [56] A W Doerry. *Performance Limits for Synthetic Aperture Radar*. en. Tech. rep. SAND2001-0044, 773988. Jan. 2001, SAND2001-0044, 773988. DOI: 10.2172/773988. URL: <http://www.osti.gov/servlets/purl/773988/> (visited on 08/08/2020).

**UNIVERSITÉ CATHOLIQUE DE LOUVAIN**  
**École polytechnique de Louvain**  
Rue Archimède, 1 bte L6.11.01, 1348 Louvain-la-Neuve, Belgique | [www.uclouvain.be/epl](http://www.uclouvain.be/epl)